LECTURE NOTES ON TURBULENCE

B. MUTLU SUMER

Technical University of Denmark
DTU Mekanik, Section for Fluid Mechanics, Coastal & Maritime Engineering
Building 403, 2800 Lyngby, Denmark, bms@mek.dtu.dk

Revised 2013

Contents

1 Basic equations **7**

1.1 Method of averaging and Reynolds decomposition 7
1.2 Continuity equation 8
1.3 Equations of motion 9
1.4 Energy equation 11
1.4.1 Energy equation for laminar flows 11
1.4.2 Energy equation for the mean flow 12
1.4.3 Energy equation for the fluctuating flow 13
1.5 References 15

2 Steady boundary layers **17**

2.1 Flow close to a wall 17
2.1.1 Idealized flow in half space y>0 17
2.1.2 Mean and turbulence characteristics of flow close to a smooth wall 23
2.1.3 Mean and turbulence characteristics of flow close to a rough wall 31
2.2 Flow across the entire section 43
2.3 Turbulence-modelling approach 48
2.3.1 Turbulence modelling of flow close to a wall 49
2.3.2 Turbulence modelling of flow across the entire section . 57
2.4 Flow resistance 59
2.5 Bursting process 61
2.6 Appendix. Dimensional analysis 66
2.7 References 69

3 Statistical analysis **73**

3.1 Probability density function 73

3.2 Correlation analysis 76
3.2.1 Space correlations 76
3.2.2 Time correlations 81
3.3 Spectrum analysis 84
3.3.1 General considerations 85
3.3.2 Energy balance in wave number space 87
3.3.3 Kolmogoroff's theory. Universal equilibrium range and inertial subrange 91
3.3.4 One-dimensional spectrum 94
3.4 References 98

4 Diffusion and dispersion **99**
4.1 One-Particle analysis 99
4.1.1 Diffusion for small times 103
4.1.2 Diffusion for large times 104
4.2 Longitudinal dispersion 113
4.2.1 Mechanism of longitudinal dispersion 113
4.2.2 Application of one-particle analysis 114
4.3 Calculation of dispersion coefficient 118
4.3.1 Formulation 119
4.3.2 Zeroth moment of concentration 121
4.3.3 Mean particle velocity 123
4.3.4 Longitudinal dispersion coefficient 124
4.4 Longitudinal dispersion in rivers 126
4.5 References 129

5 Wave boundary layers **131**
5.1 Laminar wave boundary layers 132
5.1.1 Velocity distribution across the boundary layer depth . 132
5.1.2 Flow resistance 135
5.2 Laminar-to-turbulent transition 136
5.3 Turbulent wave boundary layers 140
5.3.1 Ensemble averaging 140
5.3.2 Mean flow velocity 141
5.3.3 Flow resistance 144
5.3.4 Turbulence quantities 144
5.3.5 Effect of Reynolds number 144
5.3.6 Boundary layer thickness 146

5.3.7 Turbulent wave boundary layers over rough walls . . . 148
5.4 Other aspects . . . 151
5.5 References . . . 152

6 Turbulence modelling **155**
6.1 The closure problem . . . 155
6.2 Turbulence models . . . 156
6.3 Mixing-length model . . . 157
6.3.1 Turbulent transport of momentum . . . 157
6.3.2 Mixing length . . . 160

6.4 k-omega model . . . 169
6.4.1 Model equations . . . 169
6.4.2 Model constants . . . 171
6.4.3 Blending function F_1 . . . 171

6.4.4 Eddy viscosity and Blending function F_2 . . . 172
6.4.5 Boundary conditions . . . 172
6.4.6 Numerical computation . . . 174
6.4.7 An application example . . . 175
6.5 Large Eddy Simulation (LES) . . . 181
6.5.1 Model equations . . . 181
6.5.2 An application example . . . 183
6.6 References . . . 189

Chapter 1

Basic equations

1.1 Method of averaging and Reynolds decomposition

The *mean value* of a hydrodynamic quantity, for example, the x_i- component of the velocity, u_i, is defined by

$$\overline{u_i} = \frac{1}{T}\int_{t_0}^{t_0+T} u_i \, dt \tag{1.1}$$

in which t_0 is any arbitrary time, and T is the time over which the mean is taken. Clearly T should be sufficiently large to give a reliable mean value.

This is called time averaging. There are also other kinds of averaging, such as ensemble averaging, or moving averaging. We shall adopt the ensemble

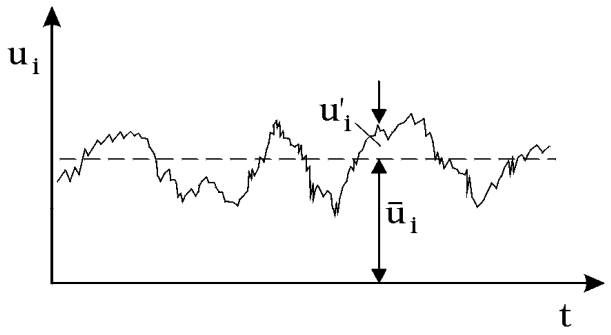

Figure 1.1: Time series of u_i.

averaging in the case of wave boundary layers, as will be detailed in Chapter 5.

The instantaneous value of the velocity u_i may be written (see Fig. 1.1)

$$u_i = \overline{u_i} + u_i' \tag{1.2}$$

in which u_i' is called the *fluctuating part* (or *fluctuation*) of u_i, and $\overline{u_i}$ is its mean. This is called the *Reynolds decomposition*. The Reynolds decomposition can be applied to any hydrodynamic quantity.

Let f and g be any such quantities (any velocity component, pressure, etc.). The following relations are known as the Reynolds conditions (here, the overbar denotes the time averaging, Eq. 1.1):

$$\begin{aligned}
\overline{f+g} &= \overline{f} + \overline{g} \\
\overline{af} &= a\overline{f} \\
\overline{a} &= a \\
\overline{\frac{\partial f}{\partial s}} &= \frac{\partial \overline{f}}{\partial s} \\
\overline{\overline{f}g} &= \overline{f}\,\overline{g} \\
\overline{\overline{f}} &= \overline{f} \\
\overline{f'} &= 0 \\
\overline{\overline{f}\overline{g}} &= \overline{f}\,\overline{g} \\
\overline{\overline{f}h'} &= \overline{f}\quad \overline{h'} = 0
\end{aligned} \tag{1.3}$$

in which a = constant, and $s = x_1, x_2, x_3, t$.

1.2 Continuity equation

For an incompressible fluid (such as water), the continuity equation is (from the conservation of mass)

$$\overline{\frac{\partial u_i}{\partial x_i}} = 0 \tag{1.4}$$

where Einstein's summation convention is used, namely there is summation over the repeated indices:

$$\frac{\partial u_1}{\partial x_1} + \frac{\partial u_2}{\partial x_2} + \frac{\partial u_3}{\partial x_3} = 0 \tag{1.5}$$

in which u_i is the $i-$component of the velocity.

Averaging (Eq. 1.1) gives:

$$\overline{\frac{\partial u_i}{\partial x_i}} = \frac{\partial \overline{u_i}}{\partial x_i} = 0 \tag{1.6}$$

Subtracting the preceding equation from Eq. 1.4 gives

$$\frac{\partial u_i'}{\partial x_i} = 0 \tag{1.7}$$

To sum up, Eq. 1.6 is the continuity equation for the mean velocity and Eq. 1.7 is the continuity equation for its fluctuating part.

1.3 Equations of motion

For a Newtonian fluid (such as water) the *Navier-Stokes (N.-S.) equation* is

$$\rho(\frac{\partial u_i}{\partial t} + u_j \frac{\partial u_i}{\partial x_j}) = \rho g_i + \frac{\partial \sigma_{ij}}{\partial x_j} \tag{1.8}$$

in which t is the time, g_i is the volume force (such as the gravity force) and x_i is the Cartesian coordinates. The quantity σ_{ij} is the stress on the fluid, and given as

$$\sigma_{ij} = -p\delta_{ij} + \mu(\frac{\partial u_i}{\partial x_j} + \frac{\partial u_j}{\partial x_i}) \tag{1.9}$$

The preceding relation is the constitutive equation for a Newtonian fluid. Here, p is the pressure, and μ is the viscosity, and δ_{ij} is the Kronecker delta defined as

$$\begin{aligned} \delta_{ij} &= 1 \text{ for } i = j, \\ \delta_{ij} &= 0 \text{ for } i \neq j \end{aligned} \tag{1.10}$$

From the continuity equation (Eq. 1.4), the N.-S. equation becomes

$$\rho\frac{\partial u_i}{\partial t} + \frac{\partial}{\partial x_j}(\rho u_i u_j) = \rho g_i + \frac{\partial \sigma_{ij}}{\partial x_j} \tag{1.11}$$

and averaging each term

$$\rho\frac{\partial \overline{u_i}}{\partial t} + \frac{\partial}{\partial x_j}(\rho\overline{u_i u_j}) = \rho\overline{g}_i + \frac{\partial \overline{\sigma}_{ij}}{\partial x_j} \tag{1.12}$$

Now, the second term on the left hand side of the preceding equation (using the Reynolds decomposition)

$$\frac{\partial}{\partial x_j}(\rho\overline{u_i u_j}) = \rho\overline{u}_j\frac{\partial\overline{u}_i}{\partial x_j} + \frac{\partial}{\partial x_j}(\rho\overline{u_i' u_j'}) \tag{1.13}$$

Inserting the preceding equation in Eq. 1.12

$$\rho(\frac{\partial\overline{u}_i}{\partial t} + \overline{u}_j\frac{\partial\overline{u}_i}{\partial x_j}) = \rho\overline{g}_i + \frac{\partial}{\partial x_j}(\overline{\sigma}_{ij} - \rho\overline{u_i' u_j'}) \tag{1.14}$$

This equation is known as the *Reynolds equation*.

As seen, the equation of motion for the mean flow in the case of the turbulent flow (Eq. 1.14) is quite similar to that in the case of the laminar flow (Eq. 1.8). Comparison of the two equations indicates that, in the case of the turbulent flow, there is an additional stress, namely $-\rho\overline{u_i' u_j'}$. This additional stress is called the *Reynolds stress*. There are nine such stresses

$$-\rho\overline{u_i' u_j'} = \begin{bmatrix} -\rho\overline{u_1' u_1'} & -\rho\overline{u_1' u_2'} & -\rho\overline{u_1' u_3'} \\ -\rho\overline{u_2' u_1'} & -\rho\overline{u_2' u_2'} & -\rho\overline{u_2' u_3'} \\ -\rho\overline{u_3' u_1'} & -\rho\overline{u_3' u_2'} & -\rho\overline{u_3' u_3'} \end{bmatrix} \tag{1.15}$$

As seen, these stresses form a symmetrical second order tensor (the Reynolds stress tensor).

To summarize at this point, there are four equations for the mean flow. These are

1. the continuity equation (Eq. 1.6) and
2. three equations of motion (Eq. 1.14),

and there are ten unknowns (namely, three components of the velocity, $\overline{u}_i$, and the pressure, $\overline{p}$, and six components of the Reynolds stress, $-\rho\overline{u_i' u_j'}$). Therefore the system is not closed. This problem is known as the *closure problem of turbulence*. We shall return to this problem later.

(In the case of laminar flow, there are four unknowns (namely, three components of the velocity, u_i, and the pressure, p) and four equations, namely the continuity equation (Eq. 1.4) and three N.-S. equation (Eqs. 1.8 and 1.9). Therefore, the system is closed.)

1.4 Energy equation

1.4.1 Energy equation for laminar flows

N.-S. equation:

$$\frac{\partial u_i}{\partial t} + u_\alpha \frac{\partial u_i}{\partial x_\alpha} = g_i - \frac{1}{\rho}\frac{\partial p}{\partial x_i} + \nu \frac{\partial^2 u_i}{\partial x_\alpha \partial x_\alpha} \tag{1.16}$$

Multiplying both sides of the equation by u_j

$$u_j \frac{\partial u_i}{\partial t} + u_j u_\alpha \frac{\partial u_i}{\partial x_\alpha} = u_j g_i - u_j \frac{1}{\rho}\frac{\partial p}{\partial x_i} + \nu u_j \frac{\partial^2 u_i}{\partial x_\alpha \partial x_\alpha} \tag{1.17}$$

The first term on the left hand side is

$$u_j \frac{\partial u_i}{\partial t} = \frac{\partial}{\partial t}(u_i u_j) - u_i \frac{\partial u_j}{\partial t} \tag{1.18}$$

and solving $\frac{\partial u_j}{\partial t}$ from Eq. 1.16, and inserting it into the preceding equation gives

$$u_j \frac{\partial u_i}{\partial t} = \frac{\partial}{\partial t}(u_i u_j) - u_i(g_j - \frac{1}{\rho}\frac{\partial p}{\partial x_j} + \nu \frac{\partial^2 u_j}{\partial x_\alpha \partial x_\alpha} - u_\alpha \frac{\partial u_j}{\partial x_\alpha}) \tag{1.19}$$

Substituting the latter equation in Eq. 1.17, and setting $i = j$,

$$\frac{\partial}{\partial t}(\frac{1}{2}\rho u_i u_i) + u_i \frac{\partial p}{\partial x_i} + \rho u_i u_\alpha \frac{\partial u_i}{\partial x_\alpha} = \rho u_i g_i + \mu u_i \frac{\partial^2 u_i}{\partial x_\alpha \partial x_\alpha} \tag{1.20}$$

Adding the term

$$-\mu(\frac{\partial u_i}{\partial x_\alpha} + \frac{\partial u_\alpha}{\partial x_i})\frac{\partial u_i}{\partial x_\alpha}$$

on both sides of the equation and also the term

$$\mu u_i \frac{\partial^2 u_\alpha}{\partial x_i \partial x_\alpha}$$

on the right hand side of the equation (this term is actually zero due to continuity), and after some algebra, the following equation is obtained

$$\frac{\partial K}{\partial t} + \frac{\partial}{\partial x_\alpha}[K u_\alpha + p u_\alpha - u_i \mu(\frac{\partial u_i}{\partial x_\alpha} + \frac{\partial u_\alpha}{\partial x_i})] = \rho u_\alpha g_\alpha - \Phi \tag{1.21}$$

in which K is the kinetic energy per unit volume of fluid

$$K = \frac{1}{2}\rho u_i u_i = \frac{1}{2}\rho(u^2 + v^2 + w^2) \tag{1.22}$$

and Φ is the energy dissipation per unit volume of fluid and per unit time

$$\Phi = \mu(\frac{\partial u_i}{\partial x_\alpha} + \frac{\partial u_\alpha}{\partial x_i})\frac{\partial u_i}{\partial x_\alpha} \tag{1.23}$$

1.4.2 Energy equation for the mean flow

The equation of motion for the mean flow (the Reynolds equation, Eq.1.14):

$$\rho\frac{\partial \overline{u}_i}{\partial t} + \rho u_\alpha \frac{\partial \overline{u}_i}{\partial x_\alpha} = \rho\overline{g}_i - \frac{\partial \overline{p}}{\partial x_j} + \mu\frac{\partial^2 \overline{u}_i}{\partial x_\alpha \partial x_\alpha} + \frac{\partial}{\partial x_\alpha}(-\rho\overline{u_i' u_\alpha'}) \tag{1.24}$$

Now, in the preceding subsection, the energy equation, Eq. 1.21, is obtained from the equation of motion, Eq. 1.16. In a similar manner, the energy equation for the mean flow can be obtained from the equation of motion for the mean flow (i.e., from Eq. 1.24). The result is

$$\frac{\partial K_0}{\partial t} + \frac{\partial}{\partial x_\alpha}[K_0\overline{u}_\alpha + \rho\overline{u_i' u_\alpha'}\,\overline{u}_i + \overline{p}\;\overline{u}_\alpha - \overline{u}_i\mu(\frac{\partial \overline{u}_i}{\partial x_\alpha} + \frac{\partial \overline{u}_\alpha}{\partial x_i})] = \rho\overline{u}_\alpha\overline{g}_\alpha - \Phi_0 - (-\rho\overline{u_i' u_\alpha'})\frac{\partial \overline{u}_i}{\partial x_\alpha} \tag{1.25}$$

in which K_0 is the kinetic energy per unit volume of fluid for the mean flow

$$K_0 = \frac{1}{2}\rho\overline{u}_i\overline{u}_i = \frac{1}{2}\rho(\overline{u}^2 + \overline{v}^2 + \overline{w}^2) \tag{1.26}$$

and Φ_0 is the energy dissipation per unit volume of fluid and per unit time, again, for the mean flow

$$\Phi_0 = \mu(\frac{\partial \overline{u}_i}{\partial x_\alpha} + \frac{\partial \overline{u}_\alpha}{\partial x_i})\frac{\partial \overline{u}_i}{\partial x_\alpha} \tag{1.27}$$

Now, note the last term on the right hand side of Eq. 1.25. We shall return to this term in the next subsection.

1.4.3 Energy equation for the fluctuating flow

Averaging Eq. 1.21 gives

$$\frac{\partial}{\partial t}(\frac{1}{2}\rho\overline{u_i u_i}) + \frac{\partial}{\partial x_\alpha}[\frac{1}{2}\rho\overline{u_i u_i u_\alpha} + \overline{p u_\alpha} - \overline{u_i \mu(\frac{\partial u_i}{\partial x_\alpha} + \frac{\partial u_\alpha}{\partial x_i})}] = \rho\overline{u_\alpha g_\alpha} - \overline{\Phi} \quad (1.28)$$

Furthermore, Eq. 1.25:

$$\frac{\partial}{\partial t}(\frac{1}{2}\rho\overline{u}_i\overline{u}_i) + \frac{\partial}{\partial x_\alpha}[\frac{1}{2}\rho\overline{u}_i\overline{u}_\alpha\overline{u}_i + \rho\overline{u'_i u'_\alpha}\overline{u}_i + \overline{p}\ \overline{u}_\alpha - \overline{u}_i\mu(\frac{\partial\overline{u}_i}{\partial x_\alpha} + \frac{\partial\overline{u}_\alpha}{\partial x_i})] =$$

$$= \rho\overline{u}_\alpha\overline{g}_\alpha - \Phi_0 - (-\rho\overline{u'_i u'_\alpha})\frac{\partial\overline{u}_i}{\partial x_\alpha} \quad (1.29)$$

Subtracting Eq. 1.29 from Eq. 1.28 gives

$$\frac{\partial K_t}{\partial t} + \frac{\partial}{\partial x_\alpha}[K_t\overline{u}_\alpha + \frac{1}{2}\rho\overline{u'_i u'_i u'_\alpha} + \overline{p' u'_\alpha} - \overline{u'_i\mu(\frac{\partial u'_i}{\partial x_\alpha} + \frac{\partial u'_\alpha}{\partial x_i})}] = \rho\overline{u'_\alpha g'_\alpha} - \Phi_t + (-\rho\overline{u'_i u'_\alpha})\frac{\partial\overline{u}_i}{\partial x_\alpha} \quad (1.30)$$

in which K_t is the kinetic energy per unit volume of fluid for the fluctuating flow (i.e., the kinetic energy of turbulence)

$$K_t = \frac{1}{2}\rho\overline{u'_i u'_i} = \frac{1}{2}\rho(\overline{u'^2} + \overline{v'^2} + \overline{w'^2}) \quad (1.31)$$

and Φ_t is the viscous dissipation of the turbulent energy per unit volume of fluid and per unit time

$$\Phi_t = \overline{\mu(\frac{\partial u'_i}{\partial x_\alpha} + \frac{\partial u'_\alpha}{\partial x_i})\frac{\partial u'_i}{\partial x_\alpha}} \quad (1.32)$$

Eq. 1.25 is the energy equation for the mean flow, and Eq.1.30 is that for turbulence. As seen, the term $(-\rho\overline{u'_i u'_\alpha})\frac{\partial\overline{u}_i}{\partial x_\alpha}$ is common in both equations, but with opposite signs. This implies that if this term is an energy gain for turbulence, then it will be an energy loss for the mean flow, or vice versa. Now, we shall show that this term is an energy gain for turbulence.

Integrating Eq.1.30 over a volume V gives

$$\frac{\partial}{\partial t}\int_V K_t\ dV + \int_S F_\alpha n_\alpha\ dS = \int_V \rho\overline{u'_\alpha g'_\alpha}\ dV - \int_V \Phi_t\ dV + \int_V\ (-\rho\overline{u'_i u'_\alpha})\frac{\partial\overline{u}_i}{\partial x_\alpha}\ dV \quad (1.33)$$

in which

$$F_\alpha = K_t \overline{u}_\alpha + \frac{1}{2}\rho\overline{u'_i u'_i u'_\alpha} + \overline{p' u'_\alpha} - \overline{u'_i \mu(\frac{\partial u'_i}{\partial x_\alpha} + \frac{\partial u'_\alpha}{\partial x_i})} \tag{1.34}$$

and S is the surface encircling the volume V. Here, the volume integral in the second term on the left hand side of Eq. 1.33 is converted to a surface integral, using the Green-Gauss theorem. The first term on the right hand side of Eq. 1.33 drops when the volume force is taken as the gravity force, since $g'_\alpha = 0$. The second term on the left hand side of Eq. 1.33, on the other hand, is the energy flux at the surface S. Therefore, it is not a source term. Now, consider a situation where there is no influx of turbulent energy. In this case, the maintenance of turbulence (i.e., $\frac{\partial}{\partial t}\int_V K_t \, dV \geq 0$ in Eq. 1.33) is only possible when $\int_V (-\rho\overline{u'_i u'_\alpha})\frac{\partial \overline{u}_i}{\partial x_\alpha} \, dV$ in Eq. 1.33 is positive, meaning that the term $(-\rho\overline{u'_i u'_\alpha})\frac{\partial \overline{u}_i}{\partial x_\alpha}$ in the turbulence energy equation (Eq. 1.30) should be positive. In other words, this term is an energy gain for turbulence, and therefore it is an energy loss for the mean flow. This is an important result, because it implies that turbulence extracts its energy from the mean flow, and the rate at which the energy is extracted from the mean flow is $(-\rho\overline{u'_i u'_\alpha})\frac{\partial \overline{u}_i}{\partial x_\alpha}$.

An important implication of the above result is that turbulence is generated only when there exists a velocity gradient in the flow $\frac{\partial \overline{u}_i}{\partial x_\alpha}$. When there is no velocity gradient, no turbulence will be generated. In this case, any field of turbulence introduced into the flow will be dissipated (the decay of turbulence). See Monin and Yaglom (1973, pp. 373-388) for further discussion.

Example 1 *Find the turbulence energy generation and the total energy dissipation (per unit volume of fluid and per unit time) for a turbulent boundary flow in an open channel (Fig. 1.2).*

The energy extracted from the mean flow is $(-\rho\overline{u'_i u'_\alpha})\frac{\partial \overline{u}_i}{\partial x_\alpha}$. For the present flow, this will be

$$(-\rho\overline{u'v'})\frac{\partial \overline{u}}{\partial y}$$

This is the energy extracted from the mean flow per unit time and per unit volume of fluid (Fig. 1.2 c). As seen from the figure, the energy "generation" for turbulence is zero at the free surface while it increases tremendously as the wall is approached.

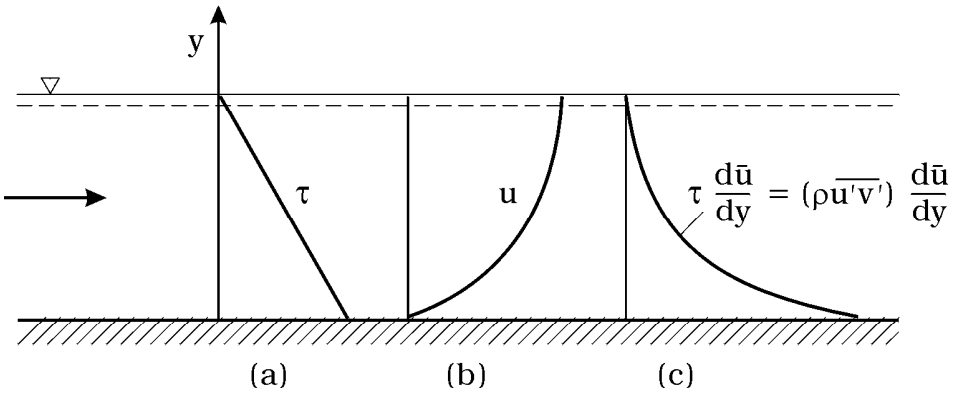

Figure 1.2: (a) Shear stress, (b) velocity and (c) turbulent energy extracted from the mean flow.

From Eq. 1.25, the total energy dissipation, on the other hand, is

$$\Phi_0 + (-\rho\overline{u_i' u_\alpha'})\frac{\partial \overline{u}_i}{\partial x_\alpha}$$

in which Φ_0 is given in Eq. 1.27. The total energy dissipation will therefore be

$$(\mu\frac{\partial \overline{u}}{\partial y})\frac{\partial \overline{u}}{\partial y} + (-\rho\overline{u'v'})\frac{\partial \overline{u}}{\partial y}$$

From the preceding relation, it is seen that the energy dissipation is very large near the wall, and it decreases with the distance from the wall, similar to the variation of the turbulent energy generation (Fig. 1.2 c).

1.5 References

1. Monin, A.S. and Yaglom, A.M. (1973). Statistical Fluid Mechanics: Mechanics of Turbulence, vol. 1, MIT Press. Cambridge, Mass.

Chapter 2

Steady boundary layers

In this chapter, we will study steady, turbulent boundary layers over a wall, in a channel, or in a pipe. (Examples of turbulent boundary layers over a wall may be: flow over a flat plate, flow over the seabed, the atmospheric boundary-layer flow over the earth surface, etc.).

We will first concentrate on the flow close to a wall (a general analysis), and then we will study the flow close to a smooth wall, and subsequently that close to a rough wall. (The latter will include the flow near the bed of a channel, and that near the wall of a pipe, etc.). Finally, we will turn our attention to flows in channels/pipes, considering the entire channel/pipe cross section.

2.1 Flow close to a wall

2.1.1 Idealized flow in half space y>0

First, consider the following idealized case.

The flow is steady, and takes place in the half space $y > 0$ (Fig. 2.1), and there is no pressure gradient in the horizontal direction, i.e., no pressure gradient in the $x-$ direction.

Shear stress.

The basic equations are the continuity equation and the two components of the Reynolds equation. The continuity equation is automatically satisfied. The $y-$ component of the Reynolds equation gives an equation for the

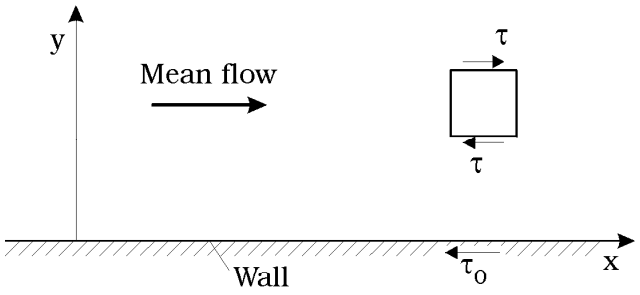

Figure 2.1: Shear stress in the idealized half space $y > 0$.

Reynolds stress $-\rho\overline{v'^2}$. The $x-$ component of the Reynolds equation (Eq. 1.14), on the other hand, reads

$$\rho(\frac{\partial\overline{u}}{\partial t}+\overline{u}\frac{\partial\overline{u}}{\partial x}+\overline{v}\frac{\partial\overline{u}}{\partial y})=\rho\overline{g}_x-\frac{\partial\overline{p}}{\partial x}+\mu(\frac{\partial^2\overline{u}}{\partial x^2}+\frac{\partial^2\overline{u}}{\partial y^2})+\frac{\partial}{\partial x}(-\rho\overline{u'^2})+\frac{\partial}{\partial y}(-\rho\overline{u'v'}) \tag{2.1}$$

Since $\frac{\partial\overline{u}}{\partial t}=0$, $\overline{v}=0$, $\overline{g}_x=0$, $\frac{\partial\overline{p}}{\partial x}=0$, $\overline{u}$ is a function of only y, and the flow is uniform in the $x-$ direction (i.e., $\frac{\partial\overline{u}}{\partial x}=0$), then the Reynolds equation will be

$$\mu\frac{d^2\overline{u}}{dy^2}+\frac{d}{dy}(-\rho\overline{u'v'})=0 \tag{2.2}$$

or,

$$\frac{d}{dy}(\mu\frac{d\overline{u}}{dy}+(-\rho\overline{u'v'}))=\frac{d\tau}{dy}=0 \tag{2.3}$$

in which τ is the total shear stress:

$$\tau=\mu\frac{d\overline{u}}{dy}+(-\rho\overline{u'v'}) \tag{2.4}$$

which is composed of two parts, namely the viscous part (the first term), and the part induced by turbulence (the Reynolds stress, the second term).

Integrating 2.3 gives

$$\tau=c; \qquad c=\text{ constant} \tag{2.5}$$

The boundary condition at the wall:

$$y=0: \qquad \tau=\tau_0 \tag{2.6}$$

in which τ_0 is the wall shear stress. From Eqs. 2.4 and 2.6, one obtains

$$\tau(= \mu\frac{d\overline{u}}{dy} + (-\rho\overline{u'v'})) = \tau_0 \tag{2.7}$$

This is an important result. It shows that the shear stress is constant over the entire depth, and equal to the wall shear stress, τ_0.

Mean velocity.

Our objective is to determine the velocity $\overline{u}$ as a function of y. To this end, we resort to dimensional analysis (see Appendix at the end of this chapter for a brief account of the dimensional analysis).

Now, the mean properties of the flow (such as $\overline{u}$) depend on the following quantities

$$\tau_0,\ y,\ \mu,\ \rho \tag{2.8}$$

Here we consider a smooth wall, therefore no parameter representing the wall roughness is included.

The flow depends on τ_0 because the shear stress determines the flow velocity; the larger the shear stress, the larger the flow velocity. (Also, it must be stressed that the shear stress in this idealized case remains unchanged across the depth, as shown in the preceding paragraphs).

Likewise, the flow depends on the distance from the wall, y, because the closer to the wall, the smaller the velocity (just at the wall, obviously the velocity will be zero due to the no-slip condition).

Clearly, the flow should also depend on the fluid properties, namely μ, and ρ.

Hence

$$\overline{u} = F(\tau_0,\ y,\ \mu,\ \rho) \tag{2.9}$$

or

$$\Phi(\overline{u},\ \tau_0,\ y,\ \mu,\ \rho) = 0 \tag{2.10}$$

From dimensional analysis, the preceding dimensional function Φ can be converted to a nondimensional function ϕ

$$\phi(\frac{\overline{u}}{U_f},\ \frac{yU_f}{\nu}) = 0 \tag{2.11}$$

in which $\frac{\overline{u}}{U_f}$, and $\frac{yU_f}{\nu}$ are two nondimensional quantities, U_f is the friction velocity defined by

$$U_f = \sqrt{\frac{\tau_0}{\rho}} \tag{2.12}$$

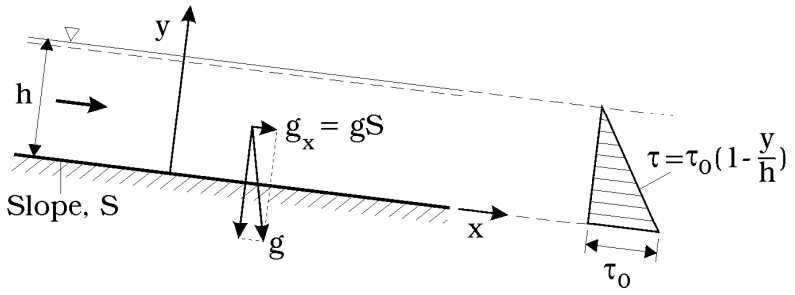

Figure 2.2: Flow in an open channel.

and ν is the kinematic viscosity

$$\nu = \frac{\mu}{\rho} \tag{2.13}$$

Solving $\frac{\overline{u}}{U_f}$ from Eq. 2.11

$$\frac{\overline{u}}{U_f} = f(y^+) \tag{2.14}$$

in which

$$y^+ = \frac{yU_f}{\nu} \tag{2.15}$$

Eq. 2.14 is known as *the law of the wall.* The quantities U_f and ν are called the *inner flow parameters,* or *wall parameters.*

Example 2 *Boundary layer in an open channel. Flow close to the bed of the channel.*

Now, consider a real-life flow, namely the flow in an open channel (Fig. 2.2). The flow in the channel is driven by gravity, with the volume force $g_x = gS$ in which S is the slope of the channel. The $x-$ component of the Reynolds equation, Eq. 2.3, will in the present case read

$$\frac{d}{dy}(\mu\frac{d\overline{u}}{dy} + (-\rho\overline{u'v'})) = \frac{d\tau}{dy} = -\rho g_x = -\rho gS = -\gamma S \tag{2.16}$$

in which γ is the specific weight of the fluid. Integrating gives

$$\tau = -\gamma Sy + c; \qquad c\text{: constant} \tag{2.17}$$

The boundary condition at the free surface:

$$y = h : \qquad \tau = 0 \tag{2.18}$$

which gives $c = \gamma Sh$ where h is the depth. Then the shear stress

$$\tau = \gamma Sh(1 - \frac{y}{h}) \tag{2.19}$$

The wall shear stress (the bed shear stress) will then be

$$\tau_0 = \gamma Sh \tag{2.20}$$

Hence, the shear stress

$$\tau = \tau_0(1 - \frac{y}{h}) \tag{2.21}$$

(see sketch in Fig. 2.2).

Our main concern in this section is the flow close to the wall. Close to the wall, i.e., $y \ll h$, the wall shear stress

$$\tau = \tau_0(1 - \frac{y}{h}) \simeq \tau_0 \tag{2.22}$$

i.e., near the wall, the shear stress can be assumed to be constant and equal to the wall shear stress, $\tau \simeq \tau_0$. This thin layer of fluid is called the *constant stress layer*.

As seen, the flow in the constant stress layer is similar to the idealized flow considered in the preceding section; in both flows, the shear stress is constant across the depth. The immediate implication of this result is that, the velocity distribution close to the wall in the present case (i.e., in the constant stress layer) is given by the law of the wall (Eq. 2.14):

$$\frac{\overline{u}}{U_f} = f(y^+) \tag{2.23}$$

Example 3 *Boundary layer in a pipe. Flow close to the wall of the pipe.*

Now, consider a fully developed turbulent boundary layer in a pipe (Fig. 2.3).

Similar to the previous example, the $x-$ component of the Reynolds equation in the present case:

$$\frac{1}{r}\frac{\partial}{\partial r}(r\tau) = \frac{\partial \overline{p}}{\partial x} \tag{2.24}$$

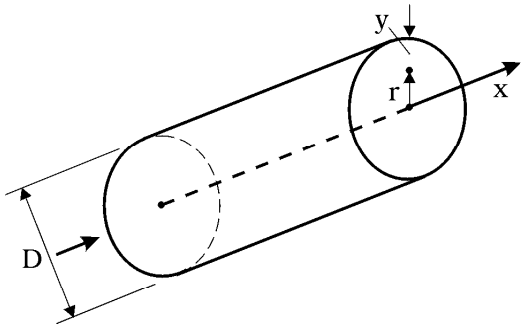

Figure 2.3: Flow in a pipe.

Here, the gravity term is included in the pressure gradient term for convenience. The flow is driven by the pressure gradient $\frac{\partial \overline{p}}{\partial x}$.

Integrating Eq.2.24 gives

$$r\tau = \frac{\partial \overline{p}}{\partial x}\frac{r^2}{2} + c \tag{2.25}$$

in which c is a constant.

The boundary condition at the center line of the pipe

$$r = 0: \qquad \tau = 0 \tag{2.26}$$

which gives $c = 0$. The boundary condition at the wall of the pipe

$$r = \frac{D}{2}: \qquad \tau = \tau_0 \tag{2.27}$$

From Eqs.2.25 and 2.27, one gets

$$\tau = 2\tau_0\frac{r}{D} \text{ or } \qquad \tau = \tau_0(1 - \frac{2y}{D}) \tag{2.28}$$

in which $y = \frac{D}{2} - r$ is the distance from the pipe wall.

Again, similar to the previous example, for $y \ll \frac{D}{2}$, i.e., close to the wall, the shear stress can be assumed to be constant and approximately equal to the wall shear stress $\tau \simeq \tau_0$, the constant stress layer. Similar to the boundary layer in an open channel, in this thin layer of fluid near the wall of the pipe, the velocity is given by the law of the wall

$$\frac{\overline{u}}{U_f} = f(y^+) \tag{2.29}$$

2.1.2 Mean and turbulence characteristics of flow close to a smooth wall

In this subsection, mean and turbulence characteristics of the boundary layer flow close to a wall will be studied in greater detail. As seen in the previous examples, the shear stress near the wall is approximately constant, and can be taken equal to the wall shear stress (the constant stress layer). This subsection is concerned with the flow in the constant stress layer. The analysis regarding the mean velocity will be undertaken for two extreme cases: namely, for small values of y^+, and for large values of y^+.

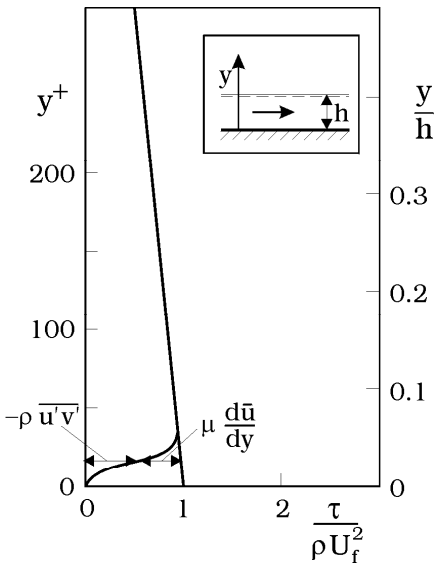

Figure 2.4: Shear stress distribution in open channel. Grass (1971).

Mean velocity for small values of y^+. Viscous sublayer.

As seen in the preceding paragraphs, the total shear stress is composed of two parts, the viscous part and the turbulent part (Reynolds stress) (Eq. 2.4). Fig. 2.4 shows the contribution of each part to the total shear stress as a function of the distance from the wall. The figure indicates that, very near the wall, the turbulent part is small compared with the viscous part, $(-\rho\overline{u'v'}) \ll \mu\frac{d\overline{u}}{dy}$. Hence

$$\tau = \tau_0 = \mu\frac{d\overline{u}}{dy} + (-\rho\overline{u'v'}) \simeq \mu\frac{d\overline{u}}{dy} \tag{2.30}$$

or

$$\tau_0 \simeq \mu \frac{d\overline{u}}{dy} \tag{2.31}$$

Integrating gives

$$\overline{u} = \frac{U_f^2}{\nu} y + c \tag{2.32}$$

The no-slip condition at the wall:

$$y = 0 : \qquad \overline{u} = 0 \tag{2.33}$$

This gives $c = 0$. Therefore, the mean velocity distribution will be

$$\overline{u} = \frac{U_f^2}{\nu} y \tag{2.34}$$

or in terms of the law of the wall (Eq.2.14 and Eq.2.15)

$$\frac{\overline{u}}{U_f} = y^+ \tag{2.35}$$

The velocity varies linearly with the distance from the wall. This analytical expression agrees well with the experiments for $y^+ < 5$. Beyond $y^+ = 5$, the data begins to deviate from the analytical expression (Fig. 2.5). The layer in which the analytical expression agrees with the experimental data is called the *viscous sublayer:*

$$\delta_v = 5\frac{\nu}{U_f}, \text{or alternatively } \delta_v^+ = 5 \tag{2.36}$$

It must be mentioned that, although this very thin layer of fluid is called viscous sublayer, turbulence from the main body of the flow does penetrate into this layer. This can be seen in the velocity signal in the viscous sublayer, and also in the wall shear stress signal in the form of turbulent fluctuations.

To get a feel of how thin this layer is, for example, for $U_f = O(1 \text{ cm/s})$, $\delta_v = 5\frac{\nu}{U_f} = 5 \times 10^{-2} \times O(1) = O(0.05 \text{ cm}) = O(0.5 \text{ mm})$.

Mean velocity for large values of y^+. Logarithmic layer.

Fig. 2.4 shows that, for large values of y^+, the viscous part of the total shear stress is small compared with the turbulent part, $\mu\frac{d\overline{u}}{dy} \ll (-\rho\overline{u'v'})$. (It

should be noted that, although y^+ is large, yet y is still small compared with h so that $\tau \simeq \tau_0$, namely y is in the constant stress layer).

Now, the shear stress generates the velocity variation over the depth; i.e., the cause-and-effect relationship between the shear stress τ and the velocity variation $\frac{d\overline{u}}{dy}$ is such that τ generates $\frac{d\overline{u}}{dy}$.

Since the shear stress for large values of y^+ is practically uninfluenced by the viscosity, the velocity variation $\frac{d\overline{u}}{dy}$ should also be uninfluenced by the viscosity; therefore, dropping the viscosity μ, from Eq. 2.9,

$$\frac{d\overline{u}}{dy} = \frac{d}{dy} F(\tau_0,\ y,\ \rho) \tag{2.37}$$

or

$$\Psi(\frac{d\overline{u}}{dy},\ \tau_0,\ y,\ \rho) = 0 \tag{2.38}$$

From dimensional analysis, this dimensional equation is converted to the following nondimensional equation:

$$\psi(\frac{d\overline{u}}{dy}\frac{1}{\frac{U_f}{y}}) = 0 \tag{2.39}$$

This equation has a single variable, namely

$$\frac{d\overline{u}}{dy}\frac{1}{\frac{U_f}{y}}$$

Solving this variable from Eq. 2.39 will give

$$\frac{d\overline{u}}{dy}\frac{1}{\frac{U_f}{y}} = A \tag{2.40}$$

in which A is a constant (the solution).

Integrating Eq. 2.40 gives

$$\overline{u} = AU_f\ \ln y\ +\ B_1 \tag{2.41}$$

or in terms of the law of the wall (Eq.2.14 and Eq.2.15):

$$\overline{u} = U_f\ (A \ln y^+\ +\ B) \tag{2.42}$$

in which B is another constant. This expression is known as the *logarithmic law.*

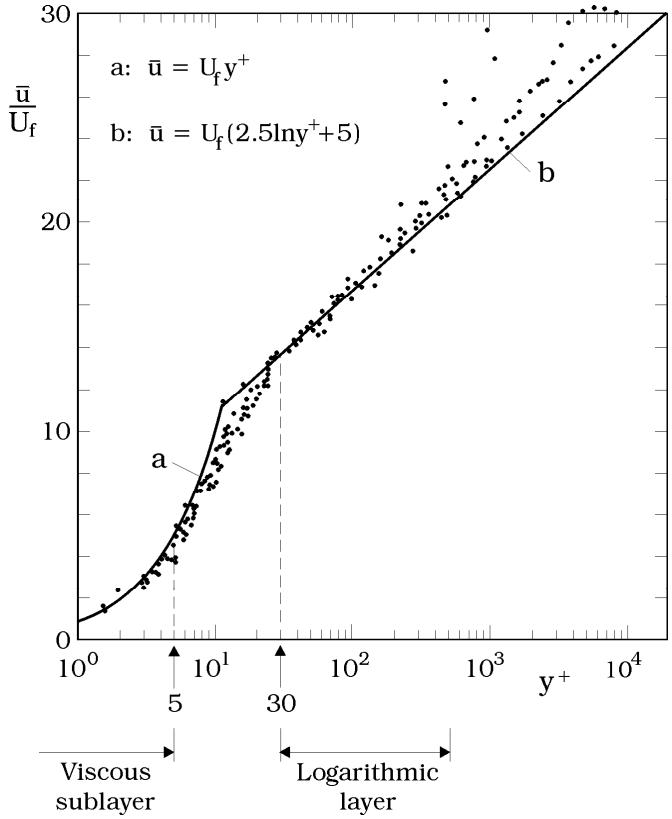

Figure 2.5: Velocity distribution. Taken from Monin and Yaglom (1973).

1. Experiments done in pipe flows, in channel flows, and in boundary layer flows over walls, etc. have all confirmed the logarithmic law with

$$A = 2.5, \quad B = 5.1 \tag{2.43}$$

Constant A is also written in the literature in the form of $1/\varkappa$, in which $\varkappa$ is called von Karman constant, $\varkappa = 0.4$. Apparently, A is a universal constant; no matter what the category of the wall is (smooth, rough, transitional), this constant always assumes the same value, i.e., $A = 2.5$, as will be demonstrated later in the section.

2. Fig. 2.5 compares the logarithmic law with the experimental data. It is seen that the logarithmic law agrees quite well with the data in the range $30 < y^+ < 500$. (It may be noted, however, that the upper

bound of the latter interval is related to the flow-depth (boundary-layer thickness) effect; Obviously, this bound is determined by the condition $y \ll h$, or alternatively $y^+ \ll \frac{hU_f}{\nu}$. Hence, depending on the Reynolds number $\frac{hU_f}{\nu}$, the numerical value of the upper bound may change).

3. The layer in which the logarithmic law is satisfied is called the *logarithmic layer.*

4. The lower bound of the logarithmic layer is often taken as $y^+ = 70$ in the literature. The layer of fluid which lies between the viscous sublayer and the logarithmic layer is called the *buffer layer,* $5 < y^+ < 70$. Clearly, in this layer, both the viscous effects and the turbulence effects are equally important.

The above analysis implies that, for the velocity distribution to satisfy the logarithmic law, the following two conditions have to be met:

1. y should be in the constant stress layer, $\tau \simeq \tau_0$, and for this

$$y \ll h$$

in which h is the flow depth in the case of the open channel flow, or it is the radius in the case of the pipe flow, or the boundary-layer thickness in the case of the boundary layer over a wall. (The above condition can be taken as $y < 0.1h$. However, the data given in Monin & Yaglom (1971, p. 288-289) implies that it can be relaxed even to $y < (0.2 - 0.3)h$);

2. y should be sufficiently large so that the variation of the velocity, $\frac{d\overline{u}}{dy}$, is independent of the viscosity. For this, y^+ should be

$$y^+ > 30 - 70$$

These conditions are to be observed when fitting the logarithmic law (Eq. 2.42) to a measured velocity distribution.

Turbulence quantities.
By "turbulence quantities", we mean the Reynolds stresses, namely

$$-\rho\overline{u_i'u_j'} = \begin{bmatrix} -\rho\overline{u'^2} & -\rho\overline{u'v'} & -\rho\overline{u'w'} \\ -\rho\overline{v'u'} & -\rho\overline{v'^2} & -\rho\overline{v'w'} \\ -\rho\overline{w'u'} & -\rho\overline{w'v'} & -\rho\overline{w'^2} \end{bmatrix} \tag{2.44}$$

For the present flow, $-\rho\overline{u'w'}$ should be zero because there is no variation of the velocity in the $z-$ direction (see Fig. 2.6). Also, $-\rho\overline{v'w'}$ should be zero because there is no mean flow in the $y, z-$ plane (no secondary currents). Furthermore, the Reynolds stress tensor is symmetric with respect to the diagonal. Therefore, there are only four independent Reynolds stresses. These are the three diagonal components, and one off-diagonal component, namely, $-\rho\overline{u'v'}$, or, for convenience, dropping -ρ in the diagonal components, and ρ in the off-diagonal components:

$$\overline{u'^2},\ \overline{v'^2},\ \overline{w'^2},\ \text{and}\ -\overline{u'v'} \tag{2.45}$$

Now, close to the wall, these quantities should depend on the same independent quantities as in the case of the mean velocity (Eq. 2.9), namely

$$\tau_0,\ y,\ \mu,\ \rho \tag{2.46}$$

From dimensional analysis, we get the following nondimensional relations

$$\sqrt{\overline{u'^2}} = U_f\ f_1(y^+),\ \sqrt{\overline{v'^2}} = U_f\ f_2(y^+),\ \sqrt{\overline{w'^2}} = U_f\ f_3(y^+),\ -\overline{u'v'} = U_f^2\ f_4(y^+) \tag{2.47}$$

The functions $f_1, ..f_4$ are universal functions, and their explicit forms are to be determined from experiments.

For large values of y^+, we know that the variation of the velocity with y, i.e., $\frac{d\overline{u}}{dy}$, is independent of the viscosity (see the argument in conjunction with Eq. 2.37). Since the turbulence is generated by the velocity gradient $\frac{d\overline{u}}{dy}$, and since $\frac{d\overline{u}}{dy}$ is independent of the viscosity, then the turbulence should also be independent of the viscosity. Therefore, for large values of y^+, the viscosity

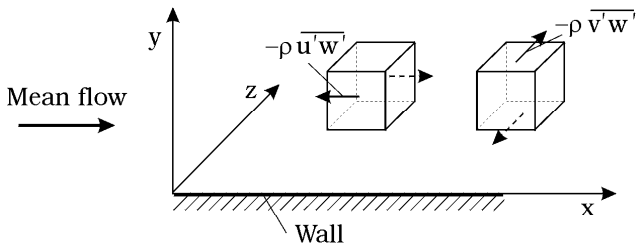

Figure 2.6: Zero components of the Reynolds stresses.

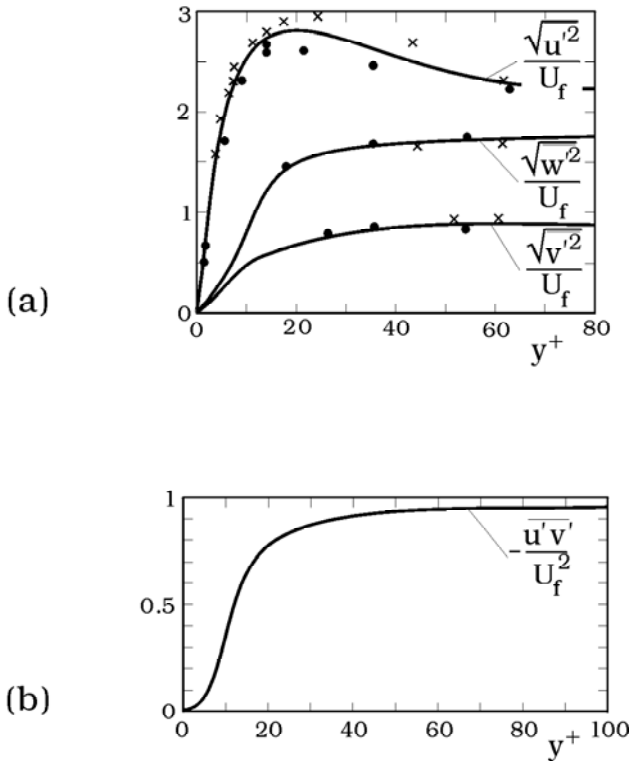

Figure 2.7: Turbulence quantities. Taken from Monin and Yaglom (1973).

should drop out in the expressions in Eq. 2.47, meaning that the turbulence quantities in Eq. 2.47 should tend to constant values:

$$\begin{aligned}
\frac{\sqrt{\overline{u'^2}}}{U_f} &= f_1(y^+) \to A_1, \qquad (2.48)\\
\frac{\sqrt{\overline{v'^2}}}{U_f} &= f_2(y^+) \to A_2,\\
\frac{\sqrt{\overline{w'^2}}}{U_f} &= f_3(y^+) \to A_3,\\
\frac{-\overline{u'v'}}{U_f^2} &= f_4(y^+) \to A_4
\end{aligned}$$

Fig. 2.7 shows the experimental results. As expected, the universal func-

tions $f_1, ..f_4$ approach zero, as y^+ goes to zero, and also, in conformity with Eqs. 2.48, they tend to constant values as y^+ takes very large values. From the figure, the latter constant values are

$$A_1 \simeq 2.3,\ A_2 \simeq 0.9,\ A_3 \simeq 1.7,\ \text{and}\ A_4 \simeq 1 \tag{2.49}$$

Example 4 *Turbulent energy budget*

From Eq. 1.30, the turbulent energy equation for a steady boundary-layer flow

$$\frac{\partial F_\alpha}{\partial x_\alpha} - (-\rho\overline{u_i' u_\alpha'})\frac{\partial \overline{u}_i}{\partial x_\alpha} + \Phi_t = 0 \tag{2.50}$$

in which Φ_t is given in Eq. 1.32, and F_α

$$F_\alpha = K_t \overline{u}_\alpha + \frac{1}{2}\rho\overline{u_i' u_i' u_\alpha'} + \overline{p' u_\alpha'} - \overline{u_i' \mu(\frac{\partial u_i'}{\partial x_\alpha} + \frac{\partial u_\alpha'}{\partial x_i})} \tag{2.51}$$

The second term in Eq. 2.50 represents the turbulence production, and the third term the viscous dissipation of turbulent energy.

The first term, on the other hand, represents the flux of turbulent energy; it consists of four parts:

1. $K_t \overline{u}_\alpha$ represents the transport of turbulent energy by convection;
2. $\frac{1}{2}\rho\overline{u_i' u_i' u_\alpha'}$ represents the transport due to turbulent diffusion;
3. $\overline{p' u_\alpha'}$ represents the transport due to pressure fluctuations; and
4. $-\overline{u_i' \mu(\frac{\partial u_i'}{\partial x_\alpha} + \frac{\partial u_\alpha'}{\partial x_i})}$ represents the transport due to viscous dissipation.

For the present boundary-layer flow, the "turbulent energy budget", Eq. 2.50, reduces to

$$\frac{\partial F_\alpha}{\partial x_\alpha} - (-\rho\overline{u'v'})\frac{\partial \overline{u}}{\partial y} + \Phi_t = 0 \tag{2.52}$$

It can easily be seen that F_α in the present case consists of only items 2, 3 and 4 above.

Fig. 2.8 shows the contributions to the turbulent energy budget of the previously mentioned effects plotted versus the distance from the wall y^+. It is seen that most of the energy production and energy dissipation takes place near the wall in the buffer layer, namely $5 < y^+ < 70$.

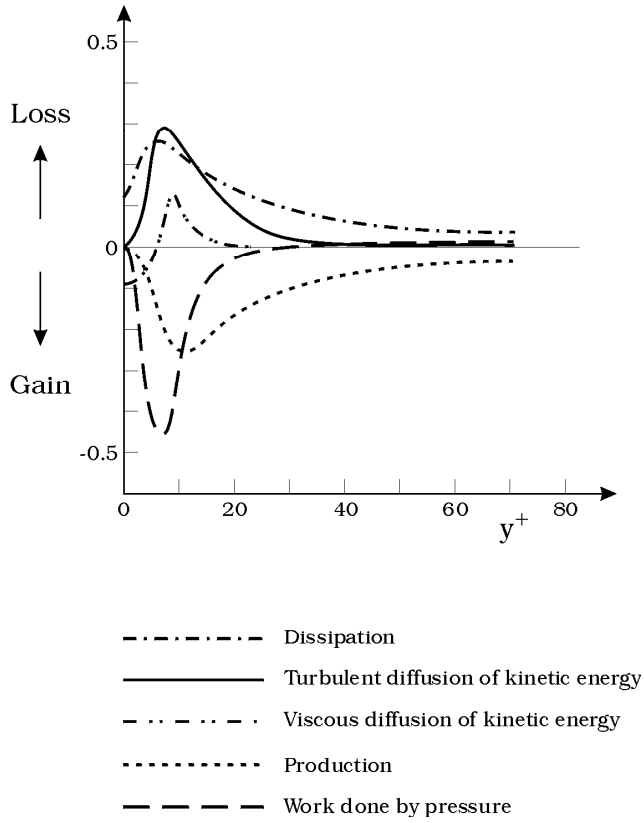

Figure 2.8: Turbulent energy budget. Laufer (1954).

2.1.3 Mean and turbulence characteristics of flow close to a rough wall

Mean velocity.

Consider that the wall is now covered with roughness elements (Fig. 2.9). Let the height of the roughness elements be k. Assume that k is sufficiently large (larger than the thickness of the viscous sublayer) so that it influences the flow.

In this case, there is one additional parameter to describe the flow, namely the roughness height, k. Therefore, Eq. 2.9 will read

$$\overline{u} = F(\tau_0,\ y,\ \mu,\ \rho,\ k) \tag{2.53}$$

Now, the total shear stress is given as in the case of the smooth wall (Eq.

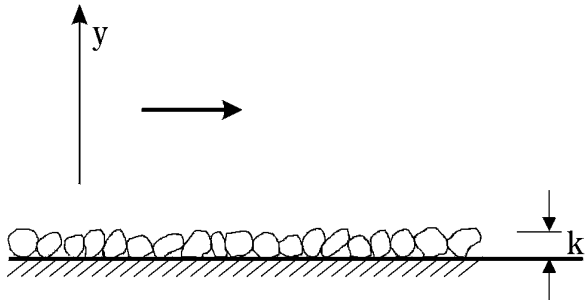

Figure 2.9: Rough wall.

2.4), namely

$$\tau = \mu \frac{d\overline{u}}{dy} + (-\rho \overline{u'v'}) \tag{2.54}$$

However, the turbulent part of the total shear stress, $-\rho\overline{u'v'}$, will in the present case, consist of two parts:

1. one is induced by the mean velocity gradient, $\frac{d\overline{u}}{dy}$, (in the same way as in the case of the smooth wall); and

2. the other is caused by the vortex shedding from the roughness elements. (Observations show that lee-wake vortices are shed from the roughness elements into the main body of the flow in a continuous manner, Sumer et al., 2001).

Clearly, for large distances from the wall, (1) the viscous part $\mu\frac{d\overline{u}}{dy}$ in the total shear stress (Eq. 2.54) is negligible, as discussed in the previous section, and (2) the vortex-shedding-induced part of $-\rho\overline{u'v'}$ is also negligible, because the vortices shed into the flow cannot penetrate to large distances due to their limited life time. This means that, for large distances from the wall, the shear stress is practically independent of the viscosity and the wall roughness.

Now, as discussed in the previous section, in the cause-and-effect relationship between the shear stress and the velocity variation, the shear stress is the cause and the velocity variation $\frac{d\overline{u}}{dy}$ is the effect. Since the shear stress for large distances from the wall is independent of the viscosity and the wall

roughness, then the velocity variation $\frac{d\overline{u}}{dy}$ should also be independent of these effects. Hence, dropping out these quantities (i.e., μ and k) in Eq. 2.53,

$$\frac{d\overline{u}}{dy} = \frac{d}{dy}F(\tau_0,\ y,\ \rho) \tag{2.55}$$

This is precisely the same equation as in the case of the smooth wall (Eq. 2.37). Therefore, the result obtained in conjunction with Eq. 2.37 is directly applicable (Eq. 2.41), i.e.,

$$\overline{u} = AU_f\ \ln y\ +\ B_1 \tag{2.56}$$

Here, A is the same constant as that in the case of the smooth wall, $A = 2.5$. Our analysis implies that this constant has the same value, irrespective of the category of the wall (smooth, or rough). Therefore, A must be a *universal constant*.

In the present context, the preceding expression may be written as

$$\overline{u} = AU_f\ \ln(\frac{y}{y_0}) \tag{2.57}$$

in which y_0 is called the *roughness length* (not to be confused with the roughness height k). Eq. 2.53 suggests that this new quantity should be a function of μ, k, τ_0 and ρ,

$$y_0 = y_0(\mu,\ k,\ \tau_0,\ \rho) \tag{2.58}$$

and from dimensional analysis,

$$y_0 = k\ g(\frac{kU_f}{\nu}) \tag{2.59}$$

The explicit form of the function $g(\frac{kU_f}{\nu})$ can be found from experiments. Nikuradse carried out such experiments (see Schlichting, 1979); He coated the walls of circular pipes with sand grains of given size. The sand grains were glued on the wall in a densely packed manner. The height of Nikuradse's sand roughness will be denoted by k_s.

Changing k by k_s, Eq. 2.59 will be

$$y_0 = k_s\ g(\frac{k_sU_f}{\nu}) \tag{2.60}$$

According to Nikuradse's experiments, there are three categories of wall:

1. Hydraulically smooth wall when $\frac{k_s U_f}{\nu} < 5$. (This is when the roughness height is smaller than the thickness of the viscous sublayer, Eq. 2.36. Clearly, in this case, the roughness elements are covered by the viscous sublayer, and therefore not directly exposed to the main body of the flow. Hence, the wall, although it is rough, acts as a smooth wall);

2. Completely rough wall when $\frac{k_s U_f}{\nu} > 70$. (In this case, the viscous sublayer is completely destructed, and the roughness elements are completely exposed to the main body of the flow); and

3. Transitional wall when $5 < \frac{k_s U_f}{\nu} < 70$.

Now, in the case of the **hydraulically smooth wall**, the function g takes the following form

$$g(\frac{k_s U_f}{\nu}) = \frac{a}{\frac{k_s U_f}{\nu}} \tag{2.61}$$

This is because k_s will drop out only when g is given in the form depicted in the preceding equation. Here a is a constant. Inserting the preceding expression into Eq. 2.60

$$y_0 = k_s \frac{a}{\frac{k_s U_f}{\nu}}$$

and from Eq. 2.57

$$\overline{u} = AU_f \ \ln(\frac{y}{y_0}) = AU_f \ \ln(\frac{y}{\frac{a}{\frac{U_f}{\nu}}}) = AU_f \ \ln(\frac{1}{a}\frac{yU_f}{\nu})$$

Comparing the preceding equation with Eqs. 2.42 and 2.43 gives the constant a as $1/9$.

In the case of the **completely rough wall**, on the other hand, the function g is given as

$$g(\frac{k_s U_f}{\nu}) = b \tag{2.62}$$

This is because the viscosity does not play any role, and therefore should drop out of formulation; and this is possible only when g is given as in the preceding form. Here, b is another constant. Nikuradse's experiments show that this constant is

$$g(\frac{k_s U_f}{\nu}) = b = \frac{1}{30} \tag{2.63}$$

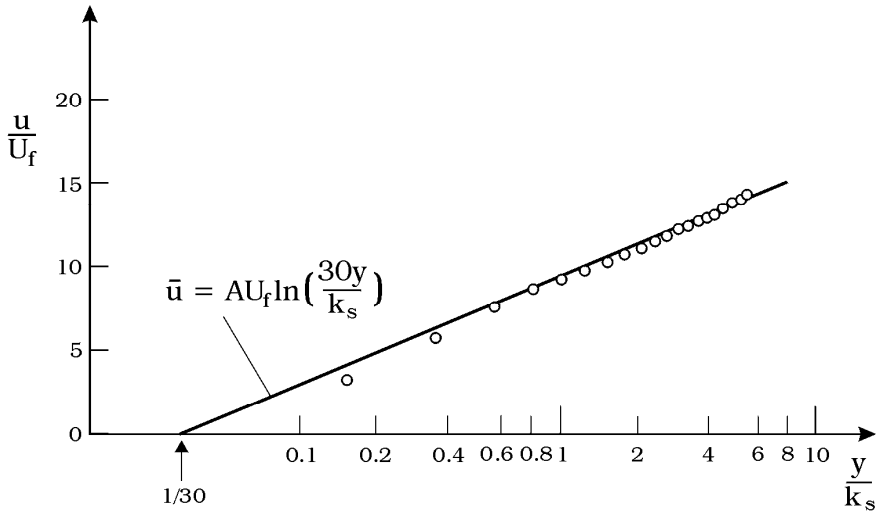

Figure 2.10: Velocity distribution. Rough wall. Grass (1971).

Substituting this into Eq. 2.60, the roughness length will be found

$$y_0 = \frac{k_s}{30} \tag{2.64}$$

and from Eq. 2.57

$$\overline{u} = AU_f \ \ln(\frac{30y}{k_s}) \tag{2.65}$$

This is the *logarithmic law for flow over a completely rough wall.* Fig. 2.10 compares the above expression with the experimental data (Grass, 1971, Fig. 4). As seen, the logarithmic law begins to deviate from the measured velocity profile for $y \lesssim 0.2k_s$. This is not unexpected, because it has been seen that, for the velocity profile to satisfy the logarithmic law, y should be sufficiently large, so large that the variation of the velocity $\frac{d\overline{u}}{dy}$ is independent of the wall roughness; otherwise, the velocity distribution will clearly not satisfy the logarithmic law, as revealed by Fig. 2.10.

In the case of the **transitional wall**, the function g is given in Fig. 2.11. The data can be represented by the following empirical expression:

$$g(k_s^+) = \frac{1/9}{k_s^+} + \frac{1}{30}\exp[-140(k_s^+ + 6)^{-1.7}]$$

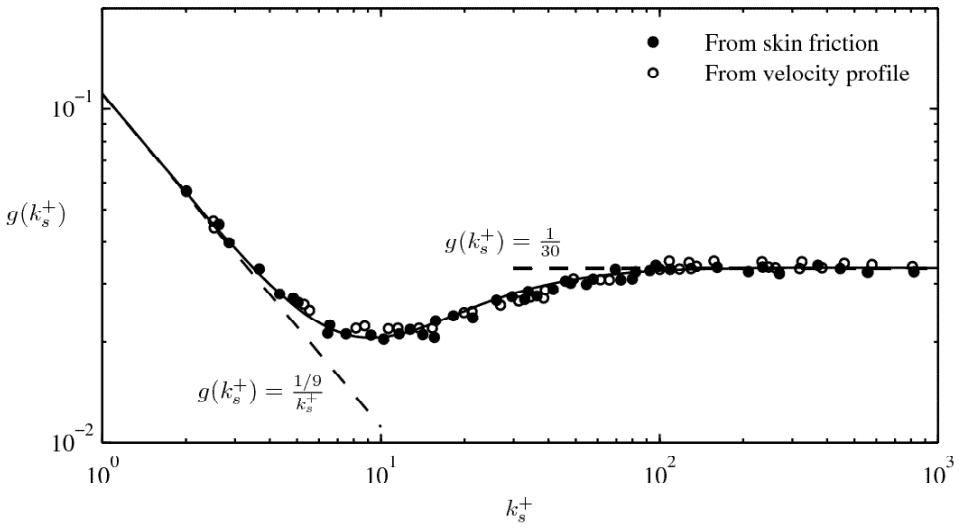

Figure 2.11: Variation of function $g(k_s^+)$. Data: Nikuradse (1933), reproduced from Monin and Yaglom (1973). Solid curve: $g(k_s^+) = \frac{1/9}{k_s^+} + \frac{1}{30}\exp[-140(k_s^+ + 6)^{-1.7}]$

Nikuradse's equivalent sand roughness.

The wall roughness is influenced by various factors such as the height of the roughness elements, the shape of the roughness elements, and the packing pattern. Therefore, it will differ from that in Nikuradse's experiments. To be able to compare the results obtained with different wall roughnesses, we need a common "base line". The concept Nikuradse's equivalent sand roughness facilitates this.

The idea is to find Nikuradse's equivalent sand roughness for any wall roughness. Nikuradse's equivalent sand roughness, k_s, is defined such that the velocity distribution across the depth is given by Eq. 2.65. In practice, it is easy to find k_s; the measured velocity distribution is plotted on a semi-logarithmic diagram, and the $y-$ intercept of the line which represents the logarithmic law (Eq. 2.65) will be $\frac{k_s}{30}$.

The values of Nikuradse's equivalent sand roughness are reported in the literature for various wall roughnesses, and they are generally in the range $k_s \widetilde{=} (2-4)k$ (Kamphuis, 1974, and the review in the paper by Bayazit, 1983). It may be noted that the upper bound of the previously mentioned range can

sometimes reach values as much as $5k$ and even more, depending on the shape of the roughness elements, the packing pattern as well as the roughness-height-to-flow-depth ratio (the latter is for large values of this ratio such as $> O(0.3)$) (Bayazit, 1983). In particular, $k_s \widetilde{=} 2k$ for walls covered by sand, pebbles, or stones the size in the range 0.54-46 mm (Kamphuis, 1974); and $k_s \widetilde{=} (3-6)k$ for the ground covered with ordinary grass or agricultural crops (Monin and Yaglom, 1973). Bayazit (1983) reports the following values for the equivalent sand roughness for various boundaries:

Author	Roughness	k_s
Leopold et al. (1964)	Gravel	$3.5D_{84}$
Limerinos (1970)	Gravel	$3.5D_{84}$
Bayazit (1976)	Closely packed spheres	$2.5D$
Charlton et al. (1978)	Gravel	$3.5D_{90}$
Hey (1979)	Gravel	$3.5D_{84}$
Thompson and Campbell (1979)	Gravel	$4.5D_{90}$
Gladki (1979)	Gravel	$2.5D_{80}$
Denker (1980)	Closely-packed cylinders	$2D$
Bray (1980)	Gravel	$3.5D_{84}$ $(3.1D_{90})$
Griffths (1981)	Gravel	$5D_{50}$

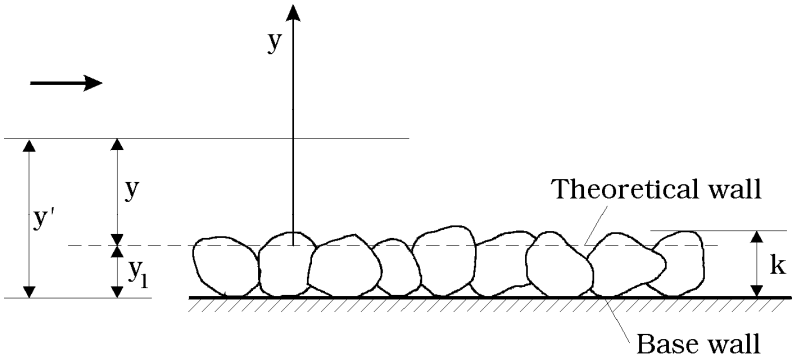

Figure 2.12: Theoretical wall.

Finally, $k_s \widetilde{=} 2.5k$ for a river bed where the sediment grains are in motion (k being the grain size). This is when the bed remains plane (i.e., no bed forms are developed) (Engelund and Hansen, 1967). This corresponds to a weak sediment transport, and before bed ripples emerge. When the bed is

covered with ripples, k_s is found to be $k_s \widetilde{=} (2-3)k$ with 2-D ripples (Fredsøe et al., 2000), k being the ripple height. In the case of 3-D ripples, the previous relation can, to a first approximation, be used. For very high velocities, ripples are washed away and the bed becomes plane again; This sediment-transport regime is called the sheet-flow regime (Sumer et al., 1996). In this case, the k_s value can be calculated from the following empirical relations (Sumer et al., 1996):

1. No-suspension sediment transport ($w/U_f > 0.8 - 1$):

$$\frac{k_s}{k} = 2 + 0.6\theta^{2.5}; \qquad 0 < \theta \lesssim 2 \tag{2.66}$$

2. Suspension sediment transport ($w/U_f < 0.8 - 1$):

$$\frac{k_s}{k} = 4.5 + \frac{1}{8}\exp\left[0.6(\frac{w}{U_f})^4\theta^2\right]\theta^{2.5} \tag{2.67}$$

in which k is the sediment grain size, w the fall velocity of sediment grains and θ the Shields parameter defined by

$$\theta = \frac{U_f^2}{g(s-1)k} \tag{2.68}$$

in which s is the specific gravity of sediment grains and g the acceleration due to gravity.

Theoretical wall.

In the case of the rough wall, the exact location of the wall is not well defined. Does it lie at the top of the roughness elements, or does it lie at the base bottom, or does it lie somewhere between? This issue brings in the concept of the theoretical wall.

Formally, *the theoretical wall is defined as the location from which the y distances in* Eq. 2.65 *are measured* (Fig. 2.12).

Now, for convenience, change the coordinate to y', the distance from the base wall. Now suppose that the theoretical bed lies at the distance y_1 from the wall (Fig. 2.12), then the relationship between y and y':

$$y = y' - y_1 \tag{2.69}$$

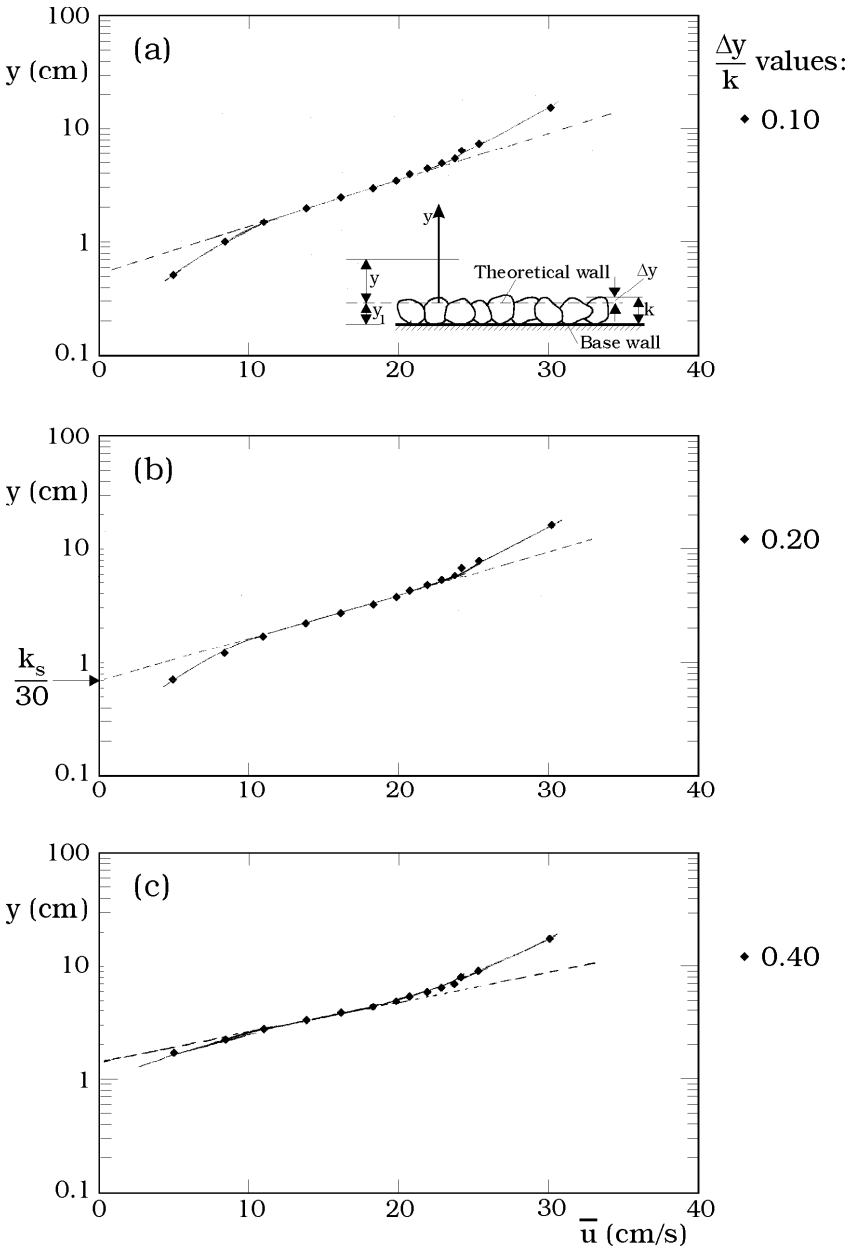

Figure 2.13: Semilog plots of the velocity distribution for three different theoretical-wall locations.

Hence the logarithmic law (Eq. 2.65) will read

$$\overline{u} = AU_f \ \ln(\frac{30(y' - y_1)}{k_s}) \tag{2.70}$$

For a given measured velocity profile $\overline{u}(y')$, and taking $A = 2.5$, the quantities U_f, k_s and y_1 (i.e., the location of the theoretical wall) can be determined from Eq. 2.70. The procedure may possibly be best described by reference to the following example:

In the laboratory, time-averaged velocity profiles are measured with a Laser Doppler Anemometer over a stone-covered bed in an open channel (the stones the size of $k = 3.8$ cm, and the flow depth $h = 40$ cm from the top of the stones). The measurements are made at four, equally spaced, vertical sections between the crests of two neigbouring stones. Then, the space-averaged velocity profile is obtained from the measured, four velocity distributions. Subsequently, the following procedure is adopted to get the location of the theoretical wall (namely, y_1, or alternatively Δy, see the definition sketch in Fig. 2.13), U_f and k_s.

1. Plot $\overline{u}$ (here, $\overline{u}$ denotes the time- and space-averaged velocity) in a semi-log graph for various values of y_1 (or alternatively for various values of Δy). (The measured velocity profiles are plotted for eight values of Δy, namely $\Delta y/k = 0$; 0.1; 0.15; 0.2; 0.25; 0.3; 0.35; 0.4. Only three profiles are displayed here, in Fig. 2.13, to keep the figure relatively simple).

2. Identify the straight line portion of each curve in Fig. 2.13.

3. For this, look at the interval $0.2k_s \lesssim y \lesssim 0.1h$ to start with. (The latter interval can be taken as $0.2k_s \lesssim y \lesssim (0.2 - 0.3)h$ with the upper bound relaxed if necessary). This is the interval where the *logarithmic layer* is supposed to lie. Here the upper boundary $0.1h$ (or $(0.2 - 0.3)h$ in the relaxed case), ensures that the y levels lie in the constant stress layer, while the lower boundary, $0.2k_s$, ensures that the variation of $\overline{u}$ with respect to y is not influenced by the boundary roughness, two conditions necessary for the velocity distribution to satisfy the logarithmic law.

4. Identify the case where the thickness of the logarithmic layer (where the velocity is represented with a straight line) is largest. The previously

mentioned eight velocity profiles, when analyzed, reveals the following result:

$\frac{\Delta y}{k}$	Logarithmic layer	Thickness of the logarithmic layer
0	$1.5 < y(cm) < 5$	3.5 cm
0.1	$1.5 < y(cm) < 5$	3.5 cm
0.15	$1.5 < y(cm) < 5$	3.5 cm
0.2	$1.5 < y(cm) < 6$	4.5 cm
0.25	$1.5 < y(cm) < 5$	3.5 cm
0.3	$2.5 < y(cm) < 5.5$	3.0 cm
0.35	$2.5 < y(cm) < 5$	2.5 cm
0.4	$2.5 < y(cm) < 5$	2.5 cm

5. As seen from the preceding table, the case where $\Delta y/k = 0.2$ gives the thickest logarithmic layer. Therefore, adopt this location as the location of the theoretical wall (Fig. 2.13 b).

6. The straight line portion of this velocity profile (corresponding to $\Delta y/k = 0.2$, Fig. 2.13 b) has a slope equal to AU_f, Eq. 2.70. From this information, find U_f.

7. Extend the straight line portion of the velocity profile (corresponding to $\Delta y/k = 0.2$) to find its y-intercept; this is equal to $\frac{k_s}{30}$ (Fig. 2.13 b).

Returning to the theoretical wall, research shows that the origin of the distance $y(= y' - y_1)$, namely the level of the theoretical bed, lies $(0.15\text{-}0.35)k$ below the top of the roughness elements (Bayazit, 1976, and 1983).

Turbulence quantities.

The turbulence quantities given in Eq. 2.45 in the case of the rough wall should depend on the same independent quantities as in the case of the smooth wall (Eq. 2.46) except that (1) μ will drop out (no influence of viscosity) and (2) k_s will be added to the list of the independent quantities:

$$\tau_0,\ y,\ \rho,\ k_s \tag{2.71}$$

From dimensional analysis, we get the following nondimensional relations

$$\sqrt{\overline{u'^2}} = U_f\ g_1(\frac{y}{k_s}),\ \sqrt{\overline{v'^2}} = U_f\ g_2(\frac{y}{k_s}),\ \sqrt{\overline{w'^2}} = U_f\ g_3(\frac{y}{k_s}),\ -\overline{u'v'} = U_f^2\ g_4(\frac{y}{k_s}) \tag{2.72}$$

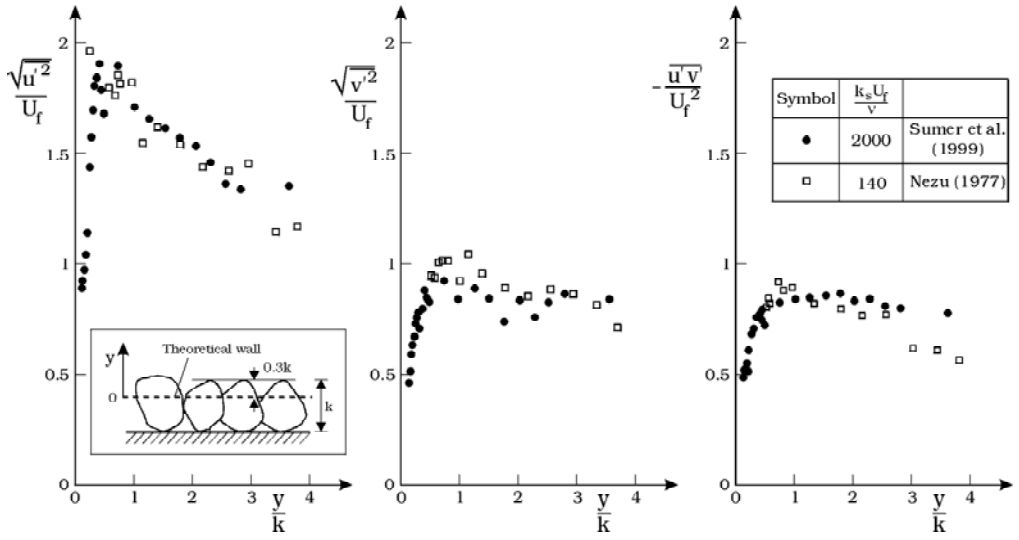

Figure 2.14: Turbulence quantities. Rough wall. Averaging over both time and space. Sumer et al. (2001).

Fig. 2.14 shows data regarding $\sqrt{\overline{u'^2}}$, $\sqrt{\overline{v'^2}}$, and $-\overline{u'v'}$. The data are plotted in a format slightly different from that in the above equation, namely, the actual roughness height is used to normalize y, rather than Nikuradse's equivalent sand roughness. Notice the large difference in the roughness Reynolds numbers of the two sets of data. Despite this, the good agreement between these two data may imply that the functions $g_1,..,g_4$ are universal.

Fig. 2.15 compares the turbulence quantities obtained in another study; in these tests, everything else is maintained unchanged, but the wall roughness is changed, to see the influence of the wall roughness on the end results. From the figure, the following two points are worth emphasizing:

1. The influence of the wall roughness disappears with the distance from the wall, as expected.

2. The distribution of turbulence across the depth is more uniform in the case of the rough wall than in the case of the smooth wall.

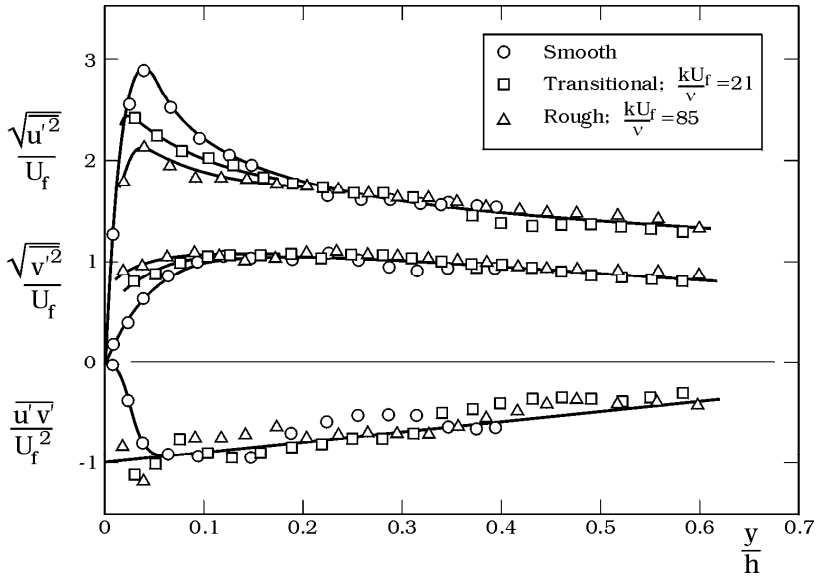

Figure 2.15: Turbulence quantities. Grass (1971).

2.2 Flow across the entire section

In the preceding section, we have been concerned with the flow close to a wall (a wall of an open channel, that of a pipe, etc.). In this section we will turn our attention to the flow across the entire section of the channel/pipe. Clearly, in this case, there will be an additional parameter, namely the flow depth in the case of the channel-flow (or the pipe radius in the case of the pipe flow, or the boundary-layer thickness in the case of the boundary-layer flow).

Mean flow.

In the analysis developed for flows close to a wall, the mean flow velocity has been written as a function of four quantities, τ_0, y, μ, ρ (Eq. 2.9). When we consider the flow across the entire section, however, two changes will take place:

1. There will be one additional parameter, namely the flow depth (or the pipe radius, or the boundary-layer thickness) affecting the flow, as mentioned in the preceding paragraph (Fig. 2.2); and

2. The shear stress τ (Fig. 2.2),

$$\tau = \tau_0(1 - \frac{y}{h}) \tag{2.73}$$

will replace the wall shear stress τ_0 .

Hence, the velocity is now dependent of the following five parameters

$$\overline{u} = F(\tau,\ y,\ \mu,\ \rho,\ h) \tag{2.74}$$

However, from Eqs. 2.73 and 2.74, the preceding equation may be written as

$$\overline{u} = F(\tau_0,\ y,\ \mu,\ \rho,\ h) \tag{2.75}$$

From dimensional analysis, the following nondimensional function may be obtained

$$\overline{u} = U_f\ \varphi(\frac{U_f h}{\nu},\ \frac{y}{h}) \tag{2.76}$$

Now, we will follow the same line of thought as in the preceding sections; namely, the variation of the velocity $\frac{d\overline{u}}{dy}$ at large distances from the wall is independent of the viscosity. Dropping out the viscosity in Eq. 2.75,

$$\frac{d\overline{u}}{dy} = \frac{d}{dy}F(\tau_0,\ y,\ \rho,\ h)$$

or

$$\Psi_1(\frac{d\overline{u}}{dy},\ \tau_0,\ y,\ \rho,\ h) = 0 \tag{2.77}$$

and from dimensional analysis one obtains

$$\frac{d\overline{u}}{dy} = \frac{U_f}{h}\ \varphi_1(\frac{y}{h}) \tag{2.78}$$

Integrating gives

$$\overline{u} = U_f \int \varphi_1(\frac{y}{h})\ d(\frac{y}{h}) + c$$

and using the boundary condition

$$y = h: \qquad \overline{u} = U_0$$

one obtains

$$\overline{u} - U_0 = U_f \int_{y=h}^{y} \varphi_1(\frac{y}{h})\ d(\frac{y}{h})$$

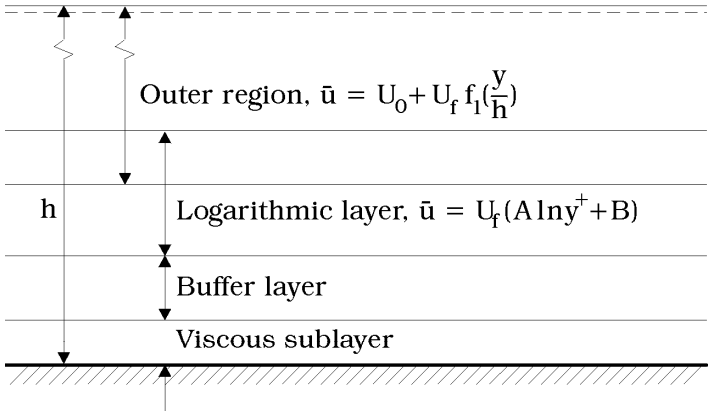

Figure 2.16: Flow regions in a turbulent boundary layer.

or denoting the integral by another function, $f_1(\frac{y}{h})$,

$$\overline{u} - U_0 = U_f \ f_1(\frac{y}{h}) \tag{2.79}$$

in which U_0 is the velocity at the free surface in the case of the open-channel flow, and the center line velocity in the case of the pipe flow. The preceding equation is known as the *velocity-defect law*. This velocity distribution is satisfied in the outer-flow region, Fig. 2.16.

The explicit form of the function $f_1(\frac{y}{h})$ can be found in the following way.

As sketched in Fig. 2.16, the outer region and the logarithmic layer is expected to overlap over a certain y interval. Therefore, in the overlapping region, the two velocity distributions, namely the logarithmic law (Eq. 2.42) and the velocity-defect law (Eq. 2.79), should be identical; therefore from Eqs. 2.42 and 2.79,

$$AU_f \ \ln(\frac{yU_f}{\nu}) \ + \ BU_f \equiv U_0 + U_f \ f_1(\frac{y}{h}) \tag{2.80}$$

and solving the function f_1

$$f_1(\frac{y}{h}) = A \ln(\frac{y}{h}) + B' \tag{2.81}$$

Therefore, the velocity-defect law

$$\overline{u} - U_0 = U_f \ (A \ln(\frac{y}{h}) + B') \tag{2.82}$$

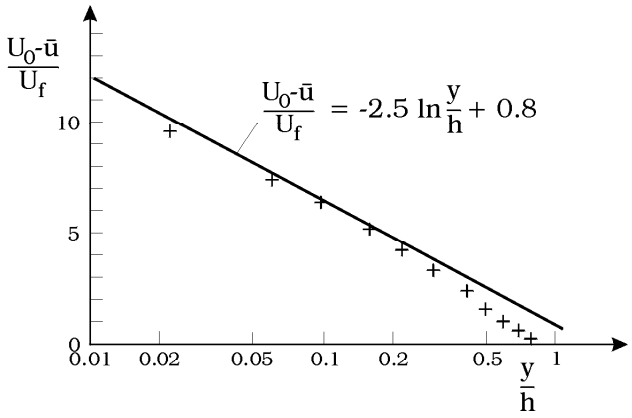

Figure 2.17: Velocity distribution over the entire section of the pipe.

1. A is the same universal constant as in the analysis for the near-wall flow, i.e., $A = 2.5$.

2. B', on the other hand, is found from experiments as $B' = -0.8$ for pipe flows (Monin and Yaglom, 1971). However, if Eq. 2.82 is assumed to be applicable for the entire cross section, then B' has to be $B' = 0$.

3. Experiments show that the velocity-defect law begins to deviate from the measured velocity profiles (not very significantly, however) for $\frac{y}{h} > 0.2 - 0.3$ (Fig. 2.17).

4. When the general form of the equation for the velocity is considered (Eq. 2.76), it will be seen that U_0 is a function of the Reynolds number. From Eq. 2.80,

$$U_0 = AU_f \ \ln(\frac{hU_f}{\nu}) + \ U_f(B - B') \tag{2.83}$$

5. The velocity-defect law is also given in terms of the cross-sectional average velocity. In the case of the *open-channel flow*

$$V = \frac{1}{h}\int_{y=0}^{h} \overline{u}(y)\ dy$$

and

$$V = U_0 - U_f(A - B') \tag{2.84}$$

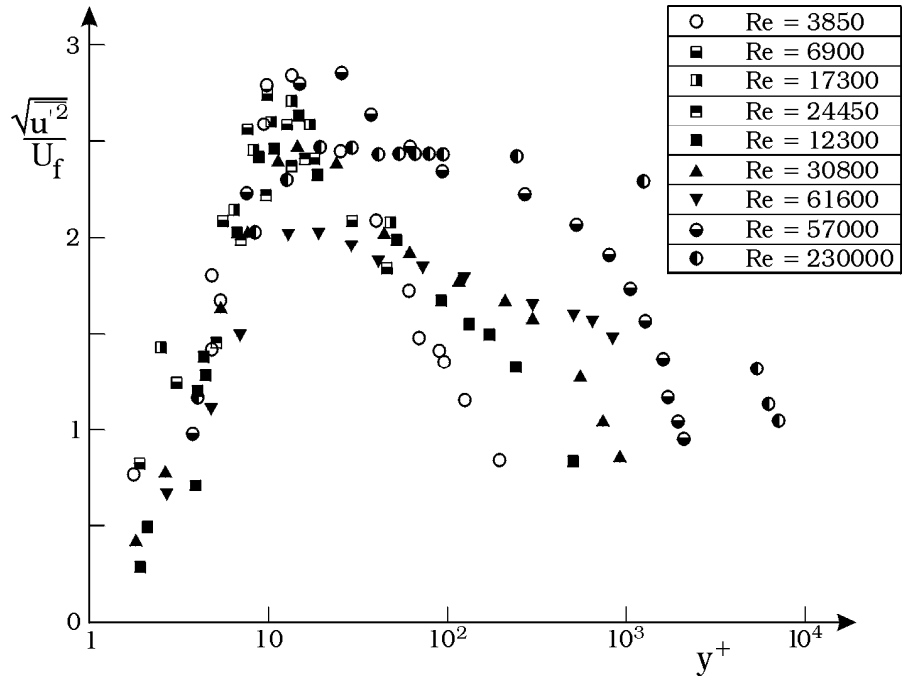

Figure 2.18: Streamwise turbulence intensity distributions. Compiled by Wei and Willmarth (1989).

In this case, the velocity-defect law (from Eqs. 2.82 and 2.84) will read as

$$\overline{u} - V = AU_f \ (\ln(\frac{y}{h}) + 1) \tag{2.85}$$

Note that, from the preceding equation, the velocity $\overline{u}$ is equal to the mean flow velocity, $\overline{u} = V$, when $y = 0.37h$.

6. Finally, it can readily be seen that the velocity-defect law in its form in Eq. 2.82 is equally valid for the case of the rough wall as well. However, the velocity U_0 in this case will be different from that in Eq. 2.83:

$$U_0 = AU_f \ln(\frac{30h}{k_s}) - U_f B' \tag{2.86}$$

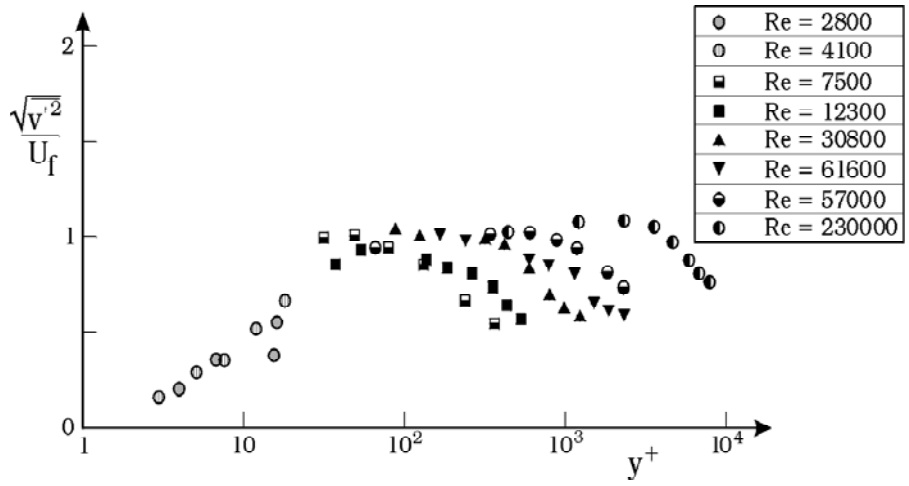

Figure 2.19: Transverse turbulence intensity distributions. Compiled by Wei and Willmarth (1989).

Turbulence quantities.

The functional forms of the turbulence quantities depicted in Eq. 2.47 will include one additional parameter in the present case, namely $\frac{hU_f}{\nu}$, or alternatively $\frac{hV}{\nu}$, the Reynolds number.

Figs. 2.18 and 2.19 illustrates how this latter parameter influences the turbulence quantities $\sqrt{\overline{u'^2}}$ and $\sqrt{\overline{v'^2}}$ (Wei and Willmarth, 1989). As seen, near the wall, the effect of Re disappears, as expected (see Section 2.1.2). However, away from the wall, the Reynolds number significantly influences the turbulence quantities. As Re increases, $\frac{\sqrt{\overline{u'^2}}}{U_f}$, and $\frac{\sqrt{\overline{v'^2}}}{U_f}$ increase. This is basically due to the increase in the flow depth when Re increases; indeed, the flow depth in terms of the wall parameters is like $h^+ \sim Re^p$, $p > 0$ in which $h^+ (= \frac{hU_f}{\nu})$. (As Re increases, the turbulence generated near the wall will be diffused to larger and larger h^+, as revealed by Figs. 2.18 and 2.19).

2.3 Turbulence-modelling approach

The preceding sections give a considerable insight into the process of turbulent boundary layers in channels/pipes, and over walls. However, the method used for the analysis does not enable us to do a parametric study, a study

where the influence of various parameters on the boundary layer process can be studied in a systematic manner. This can be achieved with the aid of *turbulence modelling*. A detailed account of turbulence modelling is given in Chapter 6. We restrict ourselves here only with the so-called mixing-length model and use it to address the problem of determining the mean velocity distribution as function of the distance from the wall.

2.3.1 Turbulence modelling of flow close to a wall

Smooth wall.

Our objective is to obtain the velocity distribution, $\overline{u}$, near the wall (in the constant-stress layer). The $x-$ component of the Reynolds equation leads to the following equation (Eq. 2.7):

$$\tau(= \mu\frac{d\overline{u}}{dy} + (-\rho\overline{u'v'})) = \tau_0 \tag{2.87}$$

in which there are two unknowns, namely $\overline{u}$, and $-\rho\overline{u'v'}$. To close the system, we need a second equation. Drawing an analogy to Newton's friction law

$$\tau = \mu\frac{du}{dy} \tag{2.88}$$

the turbulence-induced shear stress can be written as

$$-\rho\overline{u'v'} = \mu_t\frac{d\overline{u}}{dy} \tag{2.89}$$

in which μ_t is called turbulence viscosity. This is the simplest turbulence model, and was suggested by Boussinesq in 1877.

The second step is to determine the turbulence viscosity in the above equation. Making an analogy, this time, to the kinetic theory of gases, μ_t is written as

$$\mu_t = \rho\ell_m V_t \tag{2.90}$$

in which ℓ_m is what is called the *mixing length* (interpreted as the length of "penetration" of fluid particles, or the length over which fluid particles/parcels keep their coherence), and V_t is the turbulence velocity (a characteristic velocity of the turbulent motion, for example, $V_t \sim \sqrt{\overline{v'^2}}$). The hypothesis leading to Eq. 2.90 is known as Prandtl's mixing-length hypothesis. The preceding equation is obtained in a different way in Chapter 6, Section 6.3.2.

There are two quantities to be ascribed in the preceding equation to determine the turbulence viscosity: ℓ_m and V_t. According to Prandtl's second hypothesis, these two quantities are related in the following way (see Chapter 6, Section 6.3.2):

$$V_t = \ell_m \left| \frac{d\overline{u}}{dy} \right| \tag{2.91}$$

Clearly, it is expected that (1) the larger the mixing length, the larger the turbulence velocity; and also (2) the larger the velocity gradient $\left|\frac{d\overline{u}}{dy}\right|$, the larger the turbulence generation (Section 1.4.3), and therefore the larger the turbulence velocity, revealing Eq. 2.91.

From Eqs. 2.90 and 2.91, the turbulence viscosity

$$\mu_t = \rho \ell_m^2 \left| \frac{d\overline{u}}{dy} \right| \tag{2.92}$$

The third step is to determine the mixing length in the preceding equation. van Driest (1956) gives the mixing length as follows

$$\ell_m = \varkappa y[1 - \exp(-\frac{y^+}{A_d})] \tag{2.93}$$

in which $\varkappa$ is the von Karman constant (=0.4), and A_d is called the damping coefficient, and taken as 25. As seen,

$$\ell_m \to \varkappa y, \text{ for large values of } y^+ \tag{2.94}$$

while

$$\ell_m \to 0, \text{ as } y^+ \to 0 \tag{2.95}$$

The latter implies that there will be no turbulence mixing as the wall is approached.

Eqs. 2.89, 2.92 and 2.93 are the model equations (three equations); so, there are four equations altogether (along with the Reynolds equation, Eq. 2.87), and four unknowns, namely, $\overline{u}$, $-\rho\overline{u'v'}$, μ_t, and ℓ_m (the latter already given by Eq. 2.93). Hence, the system is closed. Therefore the unknowns can be determined. Let us focus on $\overline{u}$.

From Eqs. 2.87, 2.89 and 2.92, one gets

$$\rho \ell_m^2 (\frac{d\overline{u}}{dy})^2 + \mu \frac{d\overline{u}}{dy} = \tau_0 \tag{2.96}$$

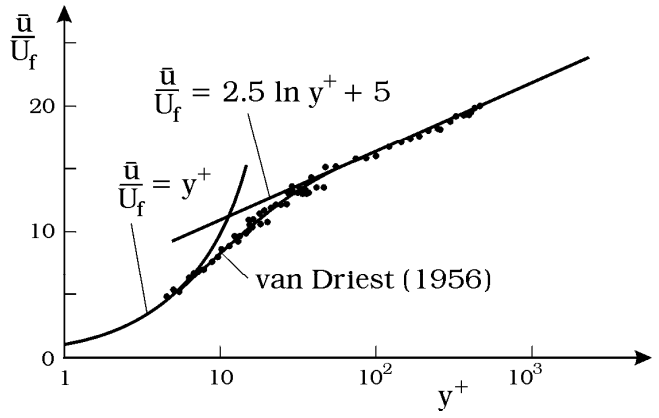

Figure 2.20: Velocity distribution. Nezu and Rodi (1986).

Solving $\frac{d\overline{u}}{dy}$ from the preceding equation, and then substituting Eq. 2.93 into the solution, and subsequently integrating gives

$$\overline{u} = 2U_f \int_0^{y^+} \frac{dy^+}{1 + \left\{1 + 4\varkappa^2 y^{+2}[1 - \exp(-\frac{y^+}{A_d})]^2\right\}^{1/2}} \tag{2.97}$$

The velocity distribution described by this expression is known as the *van Driest velocity profile,* Fig. 2.20.

1. As seen from the figure, for small values of y^+, the van Driest profile goes to the linear velocity distribution in the viscous sublayer (Eq. 2.35),

$$\frac{\overline{u}}{U_f} = y^+ \tag{2.98}$$

while, for large values of y^+, it goes to the logarithmic velocity distribution in the logarithmic layer (Eq. 2.42),

$$\overline{u} = U_f \ (A \ln y^+ + B) \tag{2.99}$$

2. Furthermore, the van Driest profile agrees remarkably well with the measured velocity profile including the buffer layer ($5 < y^+ < 70$).

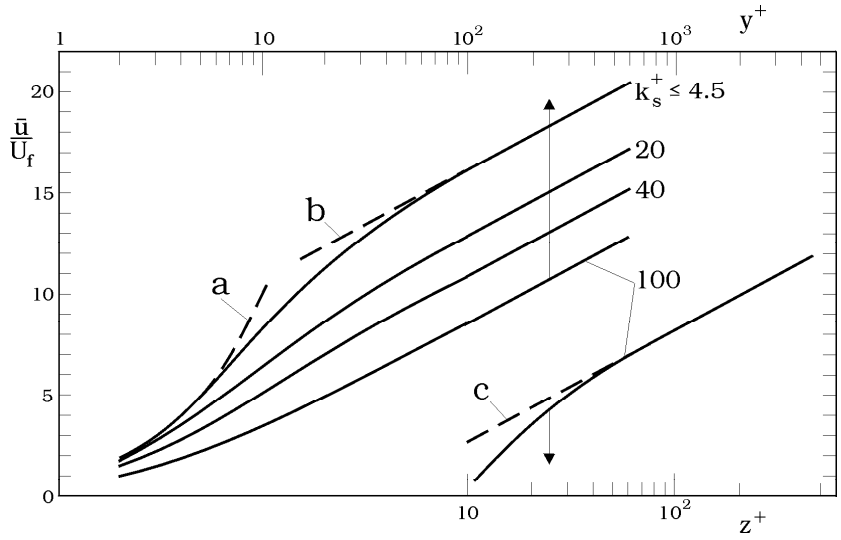

Figure 2.21: van Driest velocity profiles for different values of roughness.

Regarding the other two unknowns, $-\rho\overline{u'v'}$ and μ_t, inserting Eqs. 2.93 and 2.97 in Eq.2.92, μ_t is obtained, and from this and Eqs. 2.97 and 2.89, $-\rho\overline{u'v'}$ is obtained.

Transitional and rough walls.
In this case, the mixing length may be given as (Cebeci and Chang, 1978)

$$\ell_m = \varkappa(y + \Delta y)[1 - \exp(-\frac{(y^+ + \Delta y^+)}{A_d})] \tag{2.100}$$

1. y in the above equation is the distance from the wall; it is measured from the level where the velocity $\overline{u}$ is zero. This level lies almost at the top of the roughness elements. (y here should not be confused with the distance measured from the theoretical wall. As will be pointed out later (Item 3 below), apparently $y + \Delta y$ is the distance measured from the theoretical wall).

2. Δy is the so-called coordinate displacement, or the coordinate shift (see Example 5 below), and given by Cebeci and Chang (1978)

$$\Delta y^+ = 0.9[\sqrt{k_s^+} - k_s^+ \ \exp(-\frac{k_s^+}{6})]; \qquad 5 < k_s^+ < 2000 \tag{2.101}$$

in which k_s^+ is the roughness Reynolds number (k_s being Nikuradse's equivalent sand roughness):

$$k_s^+ = \frac{k_s U_f}{\nu} \tag{2.102}$$

3. Apparently, the distance $y + \Delta y$ is the distance measured from the theoretical wall, as will be shown in Example 5.

Similar to the case of the smooth wall, $\overline{u}$ can be obtained from the model equations, with ℓ_m given in Eq. 2.100:

$$\overline{u} = 2U_f \int_0^{y^+} \frac{dy^+}{1 + \left\{1 + 4\varkappa^2(y^+ + \Delta y^+)^2[1 - \exp(-\frac{(y^+ + \Delta y^+)}{A_d})]^2\right\}^{1/2}} \tag{2.103}$$

Fig. 2.21 displays the velocity profiles obtained from Eq. 2.103 including the smooth-wall profile. In Fig. 2.21, a represents the linear profile in the viscous sublayer (Eq. 2.98), b the logarithmic profile in the case of the hydraulically smooth wall (Eq. 2.99), and c the logarithmic profile in the case of the completely rough wall (Eq. 2.65), namely, by putting $z = y + \Delta y$,

$$\overline{u} = AU_f \ \ln(\frac{30z}{k_s}) \tag{2.104}$$

z being measured from the theoretical wall.

Example 5 *Rotta's (1962) theory about the coordinate shift* Δy.

The velocity distribution *for large* y^+ *values* is written in the following form:

$$\overline{u} = U_f \ [\frac{1}{\varkappa} \ln y^+ + c(k_s^+)] \tag{2.105}$$

in which y is measured from the level where the velocity $\overline{u} = 0$ (not to be confused with y measured from the theoretical wall). The function $c(k_s^+)$ in the above equation is determined from Nikuradse's experiments (Fig. 2.22). Note that $1 < k_s^+ < 1000$ (see the figure).

For the smooth-wall case, the preceding equation reduces to

$$\overline{u} = U_f \ [\frac{1}{\varkappa} \ln y^+ + c(0)] \tag{2.106}$$

Now, in the case of the smooth wall, we know that there are three distinct regions, namely,

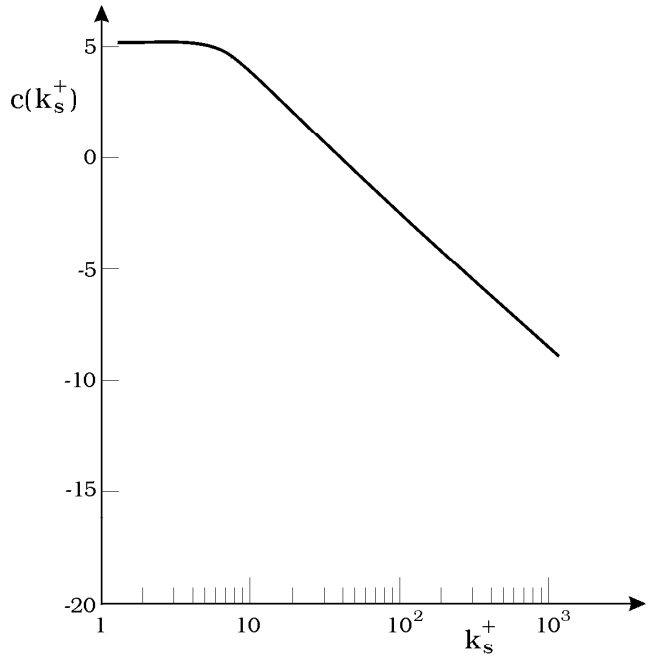

Figure 2.22: Function $c(k_s^+)$ in Rotta's (1962) theory.

1. $y^+ < 5$ where the momentum transfer across the depth is due to viscosity (Region 1, Fig. 2.23);

2. $5 < y^+ < 70$ where this transfer is due to both viscosity and turbulence (Region 2, Fig. 2.23); and

3. $y^+ > 70$ where it is practically due to turbulence alone (Region 3, Fig. 2.23).

In the case of the transitional/rough wall, Region 2 and Region 3 are still present (Fig. 2.24 a). However, Region 1 is practically not existent. Now, we imagine a fictitious region (Region 1) just beneath Region 2, where a fictitious momentum transfer takes place. Let us assume that this momentum transfer is due to viscosity. Let the thickness of this layer be Δy. So, with the addition of this fictitious layer, the flow over the rough wall will be "identical" to that over the smooth wall. Therefore, we can implement the smooth-wall velocity distribution (Eq. 2.106) for the present case (with the wall coordinate $y+\Delta y$,

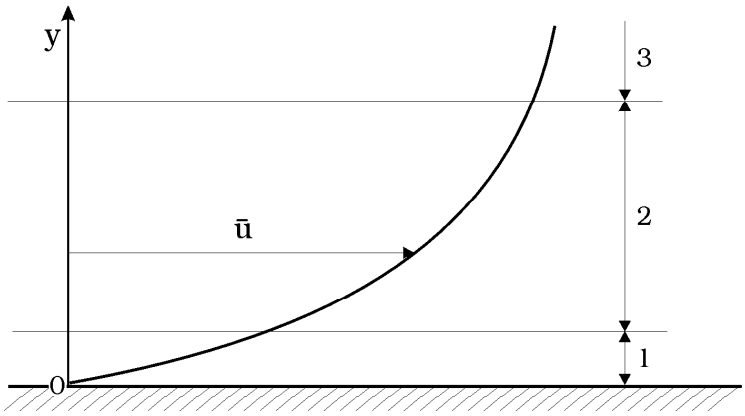

Figure 2.23: Three regions in the flow over a smooth wall.

Fig. 2.24 b):

$$\overline{u} + U'(\Delta y) = U_f \, [\frac{1}{\varkappa} \ln(y^+ + \Delta y^+) + c(0)] \tag{2.107}$$

in which $\overline{u}$ is the actual velocity and $U'(\Delta y)$ is the fictitious velocity that is to be added to $\overline{u}$, to get the fictitious smooth-wall velocity (see the figure). Considering large values of y^+, therefore $y^+ + \Delta y^+ \simeq y^+$, the above equation becomes

$$\overline{u} + U'(\Delta y) \simeq U_f \, [\frac{1}{\varkappa} \ln(y^+) + c(0)] \tag{2.108}$$

The fictitious velocity $U'(\Delta y)$ can be calculated from, for example, Eq. 2.97, replacing y^+ in Eq. 2.97 by Δy^+ (Δy^+ cannot be calculated from Eq. 2.106 because the latter equation is valid only for large values of y^+). Therefore, from Eqs. 2.108 and 2.97, the actual velocity is obtained as

$$\overline{u} = U_f \, [\frac{1}{\varkappa} \ln(y^+) + c(0)] - U'(\Delta y^+) \tag{2.109}$$

On the other hand, this velocity is given independently in Eq. 2.105. So, setting these two equations equal,

$$U_f \, [\frac{1}{\varkappa} \ln(y^+) + c(0)] - U'(\Delta y^+) \equiv U_f \, [\frac{1}{\varkappa} \ln y^+ + c(k_s^+)] \tag{2.110}$$

one gets

$$c(k_s^+) - c(0) + \frac{U'(\Delta y^+)}{U_f} = 0 \tag{2.111}$$

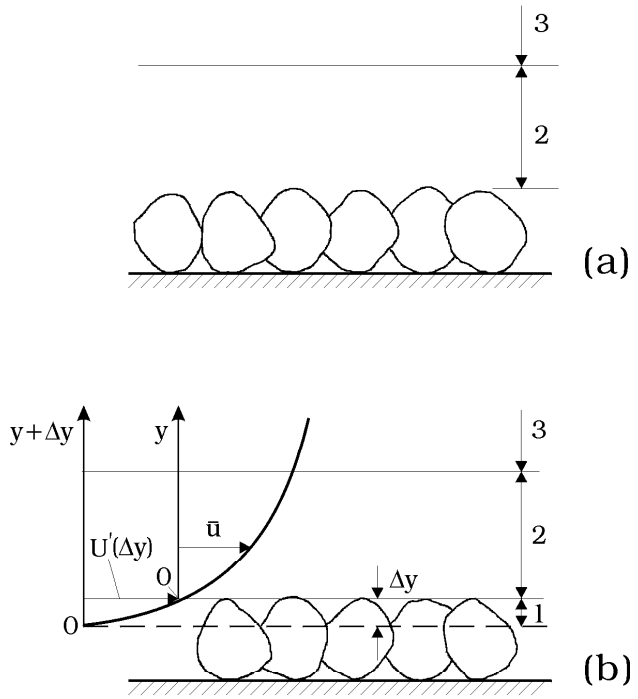

Figure 2.24: Flow over a rough wall in Rotta's (1962) theory.

Given the function $c(k_s^+)$ (Fig. 2.22), and $U'(\Delta y^+)$ from Eq. 2.97,

$$U'(\Delta y^+) = 2U_f \int_0^{\Delta y^+} \frac{dy^+}{1 + \left\{1 + 4\kappa^2 \Delta y^{+2} [1 - \exp(-\frac{\Delta y^+}{A_d})]^2\right\}^{1/2}}$$

the coordinate shift Δy^+ can be calculated from Eq. 2.111. Rotta (1962) carried out this calculation. Fig. 2.25 shows the result.

It may be noted that the variation depicted in Fig. 2.25 agrees fairly well with the expression given by Cebeci and Chang (1978) in Eq. 2.101.

As a final remark, the coordinate shift normalized by the roughness height, $\frac{\Delta y}{k}$, can be found from Eq. 2.101 (where k_s may be taken as $2k$). The result of this exercise is plotted in Fig. 2.26. As seen, the $\frac{\Delta y}{k}$ values exhibited in the figure agree rather well with the experimental observations that the level of the theoretical bed lies (0.15-0.35)k below the top of the roughness elements, given in conjunction with the theoretical bed in Section

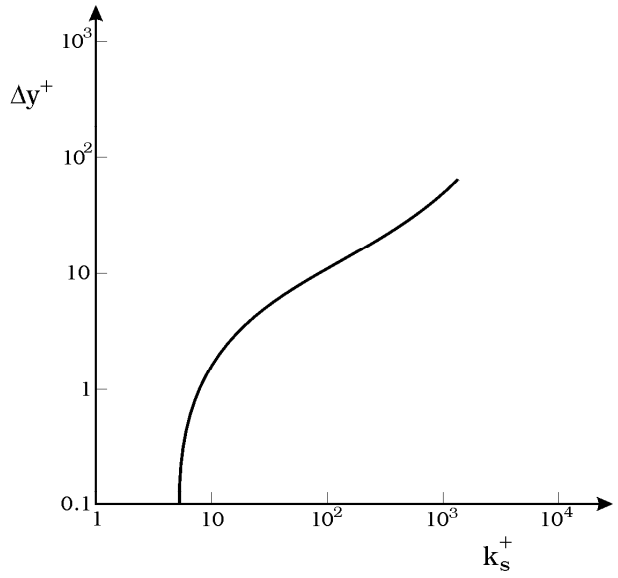

Figure 2.25: Coordinate shift in Rotta's (1962) theory.

2.1.3. This implies that the coordinate shift Δy may be interpreted as the distance of the theoretical wall from the top of the roughness elements.

2.3.2 Turbulence modelling of flow across the entire section

The velocity distribution given in Eq. 2.103 is obviously valid near the wall. When applied for the entire depth, the velocities predicted from this equation are apparently smaller than the measured velocities. This difference is corrected by the so-called Coles' wake function (see Coleman and Alanso, 1983)

$$(\frac{\Pi}{\varkappa})\ \omega(\frac{y^+}{h^+}) = (\frac{\Pi}{\varkappa})\ 2\ \sin^2(\frac{\pi}{2}\frac{y^+}{h^+}) \tag{2.112}$$

in which Π is a wake strength coefficient, h is the flow-depth/pipe-radius, or the boundary-layer thickness.

When this equation is used together with Eq. 2.103, it does not produce a profile with a derivative $\frac{d\overline{u}}{dy}$ equal to zero at the center line of a pipe, or at the free-stream edge of the boundary layer over a wall (clearly, in the case of

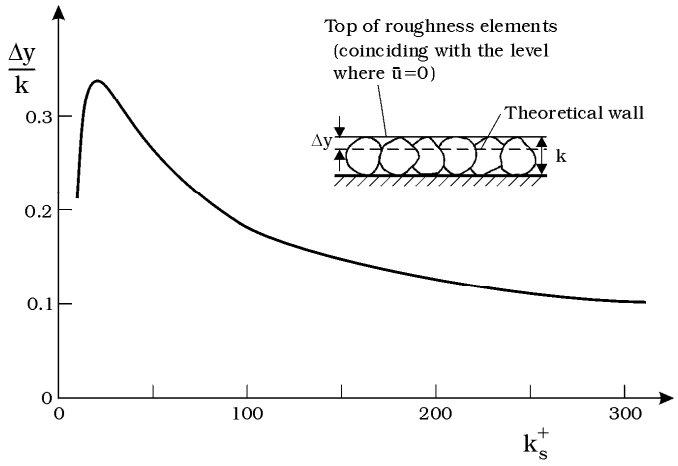

Figure 2.26: Coordinate shift Δy from Rotta (1962) and Cebeci and Chang (1978). (k_s is taken as $2k$).

pipe flows and boundary-layer flows, this derivative has to be zero). To avoid this drawback, Coles' wake function has been corrected. The final form of the velocity expression (including the corrected wake function) is as follows (Coleman and Alanso, 1983):

$$\frac{\overline{u}}{U_f} = \int_0^{y^+} \frac{2\ dy^+}{1+\left\{1+4\varkappa^2(y^+ + \Delta y^+)^2[1-\exp(-\frac{(y^+ + \Delta y^+)}{A_d})]^2\right\}^{\frac{1}{2}}} \quad (2.113)$$
$$+(\frac{y^+}{h^+})^2\ (1-\frac{y^+}{h^+}) + (\frac{2\Pi}{\varkappa})\ (\frac{y^+}{h^+})^2[3-2\frac{y^+}{h^+}]$$

Regarding the Π values, this parameter basically depends on two factors: (1) the driving pressure gradient, and (2) the degree of turbulence in the outer region. A convergent flow (favourable pressure gradient) tends to produce low values of Π, while a divergent flow (adverse pressure gradient) produces high values of Π. Likewise, if the turbulence in the outer region is intense, Π will have low values, while, the turbulence in the outer region is weak, Π will have large values (Coleman and Alanso, 1983). The latter authors report a range of Π from 0 to 0.55.

2.4 Flow resistance

The question here is that, given the mean flow velocity V, how we can calculate the friction velocity U_f, i.e.,

$$U_f = \sqrt{\frac{\tau_0}{\rho}} \tag{2.114}$$

This issue may be best described by reference to a circular pipe flow.

For a *smooth* circular pipe, the flow velocity is given by Eq. 2.42 with coefficients given in Eq. 2.43. Schlichting (1979, p. 603) takes it in the following, slightly different form:

$$\overline{u} = U_f \ (2.5 \ln y^+ \ + \ 5.5) \tag{2.115}$$

Assuming that this velocity distribution is, to a first approximation, valid across the entire section, and therefore putting $y = R$, the pipe radius, will give:

$$U_0 = U_f \ (2.5 \ln(\frac{RU_f}{\nu}) \ + \ 5.5) \tag{2.116}$$

On the other hand, we have obtained in the preceding paragraphs a relationship between the mean flow velocity and the maximum velocity (Eq. 2.84), which reads

$$V = U_0 - (A - B')U_f \tag{2.117}$$

Now, Schlichting (1979, p.609) takes this relation in the following form

$$V = U_0 - 3.75U_f \tag{2.118}$$

Combining Eq. 2.116 with Eq. 2.118, we obtain the following equation (Schlichting, 1979, p. 610)

$$\frac{1}{\sqrt{8}}\frac{V}{U_f} = 2.035 \log(\frac{VD}{\nu}\sqrt{8}\frac{U_f}{V}) - 0.91 \tag{2.119}$$

in which D is the pipe diameter. (Note that log in the above equation should not be confused with the natural logarithm). The coefficients can be adjusted slightly so that the preceding equation agrees with the experimental data. This latter exercise gives the following relation

$$\frac{1}{\sqrt{8}}\frac{V}{U_f} = 2.0 \log(\frac{VD}{\nu}\sqrt{8}\frac{U_f}{V}) - 0.8 \tag{2.120}$$

This is Prandtl's universal law of friction for smooth pipes (Schlichting, 1979, p.611).

In the case of a *rough* circular pipe, we can do the same exercise, but this time with the velocity distribution given by Eq. 2.65

$$\overline{u} = AU_f \ \ln(\frac{30y}{k_s}) \tag{2.121}$$

Putting $y = R$ in the above equation

$$U_0 = AU_f \ \ln(\frac{30R}{k_s}) \tag{2.122}$$

and combining Eqs. 2.122 and 2.118, we get (Schlichting, 1979, p. 621)

$$\frac{U_f}{V} = \frac{1}{\sqrt{8}(2\log\frac{R}{k_s} + 1.68)} \tag{2.123}$$

A comparison with Nikuradse's experimental results shows that closer agreement can be obtained, if the constant 1.68 is replaced by 1.74 (Schlichting, 1979, p.621):

$$\frac{U_f}{V} = \frac{1}{\sqrt{8}(2\log\frac{R}{k_s} + 1.74)} \tag{2.124}$$

In the case of a *transitional-wall-category circular pipe*, Colebrook and White obtains the following resistance relation (Schlichting, 1979, p.621)

$$\frac{1}{\sqrt{8}}\frac{V}{U_f} = 1.74 - 2\log(\frac{k_s}{R} + \frac{18.7}{(\frac{VD}{\nu})(\sqrt{8}\frac{U_f}{V})}) \tag{2.125}$$

Given the mean-flow velocity, the friction velocity can easily be calculated from Eqs. 2.120, 2.124 or 2.125.

In the case of a non-circular pipe flow or an open flow, the preceding resistance relations can be used provided that the pipe diameter D should be replaced by $4r_h$ in which r_h is the hydraulic radius, equal to the cross-sectional area divided by the wetted perimeter (Schlichting, 1979, p. 622). For example, in the case of an open channel with a rough bed, the resistance relation can be found as

$$\frac{V}{U_f} = 5.75\log(\frac{14.8r_h}{k_s}) \tag{2.126}$$

or

$$\frac{V}{U_f} = 2.5 \ln(\frac{14.8 r_h}{k_s}) \tag{2.127}$$

It may be noted that the ratio V/U_f may be traditionally written in terms of the friction coefficient, f, as

$$U_f = \sqrt{\frac{f}{2}} V \tag{2.128}$$

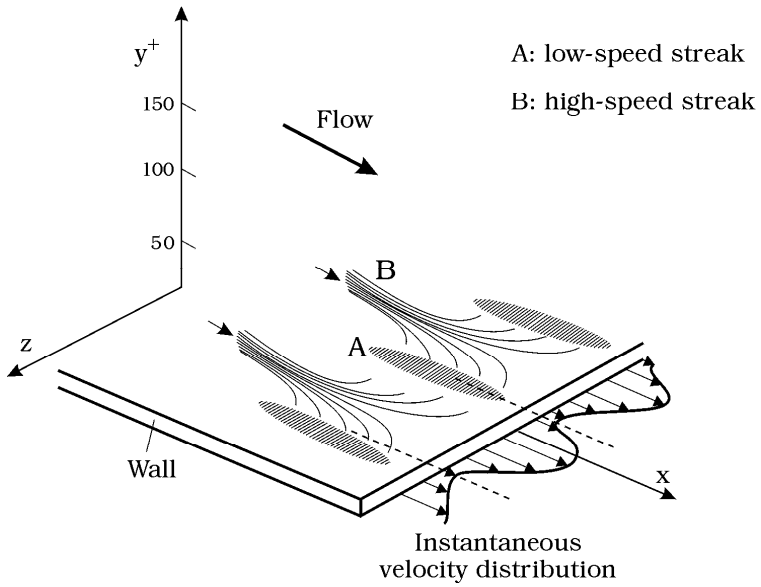

Figure 2.27: Snapshot of flow near the wall.

2.5 Bursting process

Experimental work conducted in 1960s and 70s has shown that the nature of the flow pattern near the wall in a turbulent boundary layer is repetitive; the flow near the wall occurs in the form of a quasi-cyclic process, called the *bursting process*. Reviews of the subject can be found in Laufer (1975), Hinze (1975, pp. 659-668), Cantwell (1981), Grass (1983) and Nezu and Nakagawa (1993).

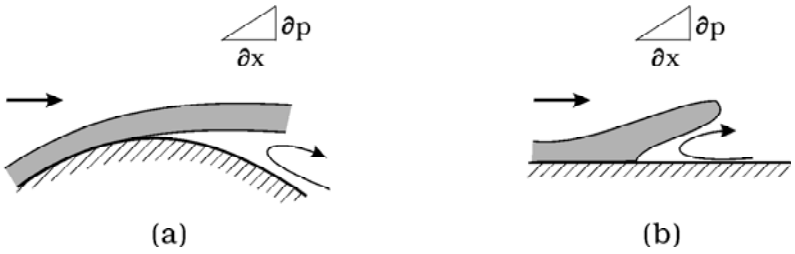

Figure 2.28: Flow separation induced by adverse pressure gradient.

The description of the bursting process in the following paragraphs is mainly based on the work of Offen and Kline (1973, 1975).

Fig. 2.27 gives a snapshot of the flow picture near the wall. As seen, the flow consists of a transverse alternation of low-speed (A) and high-speed (B) regions. These are called low-speed and high-speed streaks. The low-speed and high-speed streaks form locally and temporarily.

Similar to the separation of a boundary layer subject to an adverse pressure gradient (such as, for example, the boundary layer separation over a cylinder, see Fig. 2.28 a), a low-speed wall streak is subject to separation due to a local and temporary adverse pressure gradient $\frac{\partial p}{\partial x}$, Fig. 2.28 b. This causes this coherent, low-speed fluid to entrain into the main body of the flow. This is called the *ejection* event. See Fig. 2.29, Frames 1 and 2.

The fluid ejected into the flow grows in size, as it is convected downstream, while keeping its coherent entity. This continues for some period of time (Fig. 2.29, Frame 3), and finally, at some point ($t = T$), the previously mentioned coherent structure breaks up (Fig. 2.29, Frame 4). At this point, some fluid from the coherent structure returns back to the near-wall region (Fig. 2.29, Frame 5). This fluid impinges the wall (in the form of a high-speed wall streak, called the *in-rush* event), and spreads out sideways (Fig. 2.29, Frame 6). Two-such neighbouring high-speed streaks eventually merge (Fig. 2.29, Frame 6), and retard the flow there, and, as a result, a new low-speed wall streak is formed. The time period spent from the formation of the low-speed streak at time $t = 0$ (Fig. 2.29, Frame 1) to the formation of the next one at time $t = T_1$ (Fig. 2.29, Frame 6) is called the *bursting period*. After the formation of this new low-speed streak, the same chain of events occurs, and the process continues in a repetitive manner.

Fig. 2.30 displays two snapshots (viewed from the side), illustrating the

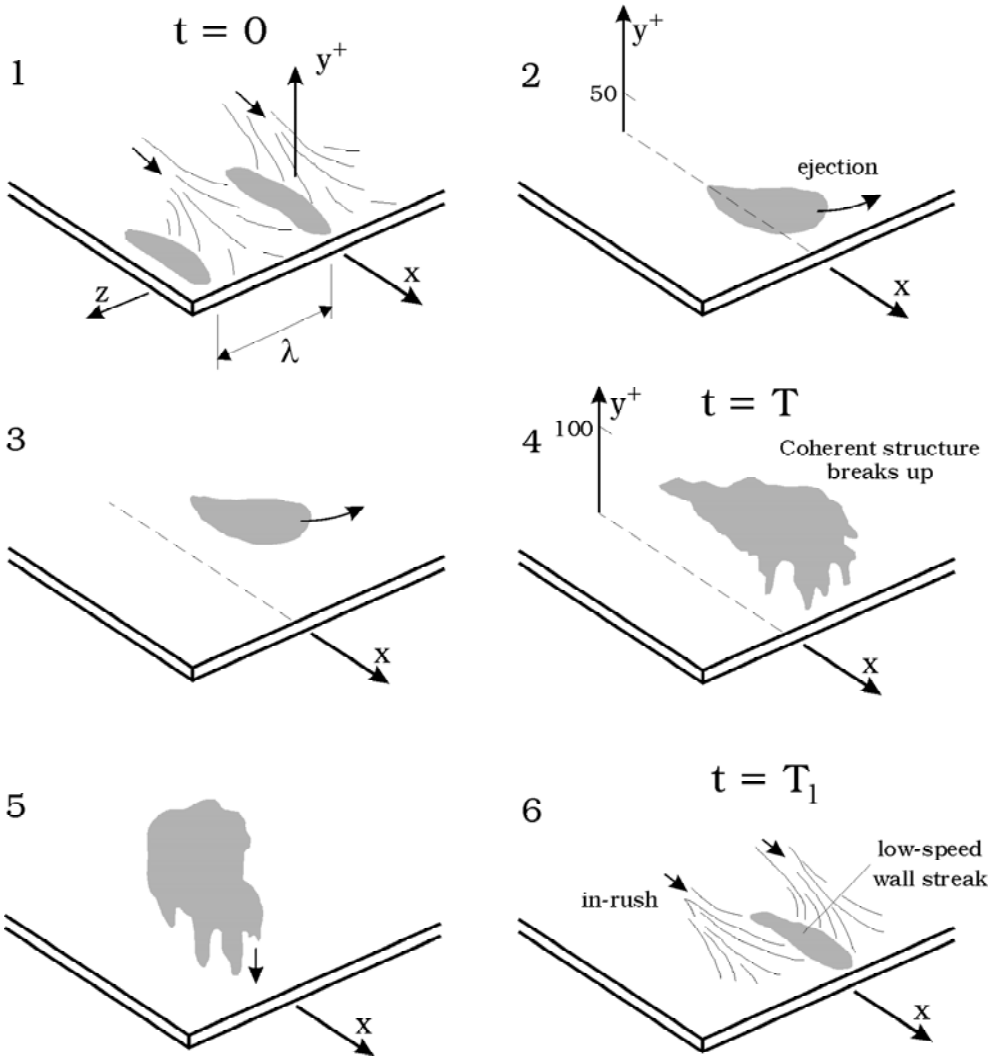

Figure 2.29: Sequence of flow pictures over one bursting period.

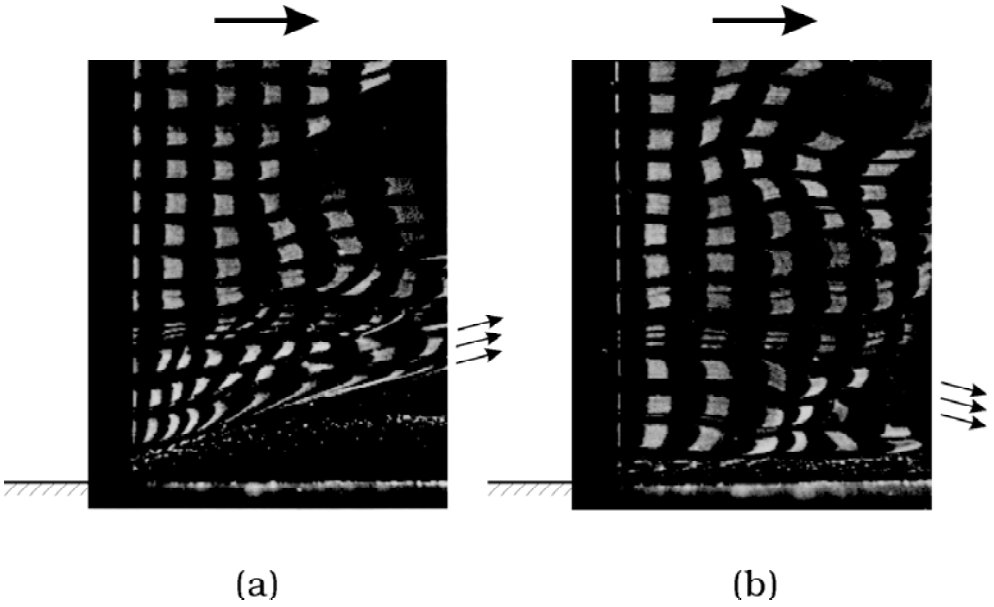

Figure 2.30: (a): ejection; and (b): in-rush events. Grass (1971).

ejection event (Fig. 2.30, a), and the in-rush event (Fig. 2.30 b).

The bursting process has been studied in the case of rough walls, and it was found that practically the same kind of quasi-cyclic process takes place (Grass, 1971, and Grass et al., 1991).

The rest of this section is concerned with quantitative information on the bursting process.

1. The mean spacing of the low-speed wall streaks (Fig. 2.29, Frame 1) is

$$\lambda^+ = \frac{\lambda U_f}{\nu} \simeq 100 \tag{2.129}$$

(see for example, Lee et al., 1974)

2. Fluid ejections originate in

$$5 < y^+ < 50 \tag{2.130}$$

(Nychas et al., 1973). Corino and Brodkey (1969), on the other hand, report that lower half of the viscous sublayer $y^+ < 2.5$ is essentially

passive and the rest ($2.5 < y^+ < 5$) active, being influenced by the quasi-cyclic, bursting events occurring in $5 < y^+ < 70$.

3. The $x-$ and $z-$extents of ejected low-speed fluid structures involve dimensions of the order of

$$20 \text{ to } 40 \text{ of } x^+, \text{and } 15 \text{ to } 20 \text{ of } z^+ \tag{2.131}$$

4. Ejected fluid elements reach y^+s of

$$y^+ = 80 - 100 \tag{2.132}$$

(Nychas et al., 1973). Praturi and Brodkey (1978) report that, in some rare cases, the ejected fluid elements travel up to 300 y^+).

5. The mean streamwise distance from the onset of lift-up of a low-speed wall streak to the break-up of any sign of coherency is about

$$1300 \text{ in } x^+ \tag{2.133}$$

(Offen and Kline, 1973).

6. The mean time between the onset of ejection and break-up (the life time of a burst) is

$$\frac{TU_0}{h} = \begin{array}{l} 2.3 \text{ for the smooth boundary data, and} \\ 1.3 \text{ for the rough boundary data} \end{array} \tag{2.134}$$

of the study by Jackson (1976). As seen, T scales with the outer flow parameters, namely U_0, the free-stream velocity (or the velocity at the free surface in the case of the open channel flow), and h is the boundary-layer thickness/the flow depth.

7. Finally, the mean bursting period

$$\frac{T_1 U_0}{h} = 5 \tag{2.135}$$

(Jackson, 1976). Note that this, too, scales with the outer flow parameters.

There have been several implications of this newly discovered aspect of turbulent boundary-layer flows. One of them is the process of sediment suspension in rivers and in the marine environment. The work conducted in 1970s and 80s indicated that the bursting process is the key mechanism for sediment suspension from/near the bed (see, for example, Sumer and Oguz, 1978, Sumer and Deigaard, 1981, Grass, 1983, and Sumer, 1986).

2.6 Appendix. Dimensional analysis

We may write the unit of any hydrodynamic quantity in the following form

$$[A] = L^{\alpha} T^{\beta} K^{\gamma} \tag{2.136}$$

in which $[A]$ is the unit of A, and L, T, and K are the fundamental units, namely, L is the length, T the time, and K is the force. α, β and γ are positive or negative integers, or they may be zero.

Now, Buckingham's Pi Theorem states the following.

A dimensional function

$$f(A_1,\, A_2,\, ...,\, A_n) = 0 \tag{2.137}$$

can always be converted to the following nondimensional function

$$F(\pi_1, \pi_2, ...\pi_{n-r}) = 0 \tag{2.138}$$

in which A_i $(i = 1, ...n)$ are the dimensional quantities, and r is the number of the fundamental units (normally $r = 3$, i.e., the length, the time and the force). The quantities π_i $(i = 1, ..., n-r)$ are the nondimensional quantities and calculated from

$$\begin{aligned} \pi_1 &= A_1^{x_1} A_2^{y_1} A_3^{z_1} A_4 \\ \pi_1 &= A_1^{x_2} A_2^{y_2} A_3^{z_2} A_4 \\ &\cdots\cdots\cdots \\ \pi_{n-r} &= A_1^{x_{n-r}} A_2^{y_{n-r}} A_3^{z_{n-r}} A_4 \end{aligned} \tag{2.139}$$

Note that the above combinations of A_i (for each π_i) should be selected so that

1. The unit of any one of A_i should not be a combination of the units of the others; and

2. Each and every fundamental unit should be included in at least one of the A_i's.

The advantage of the dimensional analysis is that, first of all, it "translates" the dimensional function into a nondimensional function in a systematic way, secondly and more importantly, in doing so, the number of the quantities included in the dimensional function is reduced by r (normally $r = 3$).

Example 6 *Law of the wall.*

In Section 2.1.1, the flow velocity is written as a function of the following nondimensional quantities (Eq. 2.9)

$$\overline{u} = F(\tau_0,\ y,\ \mu,\ \rho) \tag{2.140}$$

or

$$f(\tau_0,\ \mu,\ \rho,\ \overline{u},\ y) = 0 \tag{2.141}$$

As seen, $n = 5$, and therefore the number of nondimensional quantities will be $n - r = 5 - 3 = 2$. Hence

$$F(\pi_1, \pi_2) = 0 \tag{2.142}$$

in which the nondimensional quantities π_1 and π_2

$$\pi_1 = \tau_0^{x_1} \mu^{y_1}\ \rho^{z_1}\ \overline{u} \tag{2.143}$$

and

$$\pi_2 = \tau_0^{x_2} \mu^{y_2}\ \rho^{z_2} y \tag{2.144}$$

The left and right hand sides of Eq. 2.143 should have the same units. Writing the units of the quantities on both sides of the equation according to Eq. 2.136,

$$L^0 T^0 K^0 = (KL^{-2})^{x_1} (KL^{-2}T)^{y_1} (KL^{-4}T^2)^{z_1} (LT^{-1}) \tag{2.145}$$

or

$$L^0 T^0 K^0 = L^{-2x_1 - 2y_1 - 4z_1 + 1} T^{y_1 + 2z_1 - 1} K^{x_1 + y_1 + z_1} \tag{2.146}$$

which requires

$$\begin{aligned} -2x_1 - 2y_1 - 4z_1 + 1 &= 0, \\ y_1 + 2z_1 - 1 &= 0, \\ x_1 + y_1 + z_1 &= 0 \end{aligned} \tag{2.147}$$

This gives

$$x_1 = -\frac{1}{2}, \quad y_1 = 0, \text{ and } \quad z_1 = \frac{1}{2} \tag{2.148}$$

Hence the first nondimensional quantity

$$\pi_1 = \tau_0^{-1/2} \mu^0 \rho^{1/2} \overline{u} = \frac{\overline{u}}{(\frac{\tau_0}{\rho})^{1/2}} = \frac{\overline{u}}{U_f} \tag{2.149}$$

Regarding the second nondimensional quantity, from Eq. 2.144

$$L^0 T^0 K^0 = (KL^{-2})^{x_2} (KL^{-2}T)^{y_2} (KL^{-4}T^2)^{z_2} L \tag{2.150}$$

and

$$\begin{aligned} -2x_2 - 2y_2 - 4z_2 + 1 &= 0, \\ y_2 + 2z_2 &= 0, \\ x_2 + y_2 + z_2 &= 0 \end{aligned} \tag{2.151}$$

and

$$x_2 = \frac{1}{2}, \quad y_2 = -1, \text{ and } \quad z_2 = \frac{1}{2} \tag{2.152}$$

Then, the second nondimensional quantity

$$\pi_2 = \tau_0^{1/2} \mu^{-1} \rho^{1/2} y = \frac{y(\frac{\tau_0}{\rho})^{1/2}}{\frac{\mu}{\rho}} = \frac{y U_f}{\nu} \tag{2.153}$$

Therefore, the nondimensional function will be

$$F(\frac{\overline{u}}{U_f}, \ \frac{y U_f}{\nu}) = 0 \tag{2.154}$$

or solving the velocity

$$\frac{\overline{u}}{U_f} = f(\frac{y U_f}{\nu}) \tag{2.155}$$

This relation is known as the law of the wall.

2.7 References

1. Bayazit, M. (1976): "Free surface flow in a channel of large relative roughness", J. Hyd. Res., 14, no. 2, 1976, p. 115.

2. Bayazit, M. (1983): "Flow structure and sediment transport mechanics in steep channels. In: Mechanics of Sediment Transport, Proc. of Euromech 156, Istanbul, 12-14. July 1982, A.A. Balkema (Rotterdam), p.197.

3. Cantwell, B.J. (1981): "Organized motion in turbulent flow". Ann. Rev. Fluid Mech., vol 13, p.457.

4. Cebeci, T. and Chang, K.C. (1978): "Calculation of incompressible rough-wall boundary-layer flows". AIAA Journal, vol. 16, No. 7, p.730.

5. Coleman, N.L. and Alanso, C.V. (1983): "Two-Dimensional channel flows over rough surfaces". J. Hydraul. Eng., Proc. ASCE, vol 109, No. 2, p.175.

6. Corino, E.R. and Brodkey, R.S. (1969): "A visual investigation of the wall region in turbulent flow". J. Fluid Mech., vol. 37, p.1.

7. Engelund, F. and Hansen, E. (1967): A Monograph on Sediment Transport in Alluvial Streams, Teknisk Forlag, Copenhagen.

8. Fredsøe, J. Andersen, K.H. and Sumer, B.M. (2000): "Wave plus current over a ripple-covered bed". Coastal Engineering.

9. Grass, A.J. (1971): "Structural features of turbulent flow over smooth and rough boundaries". J. Fluid Mech., vol. 50, p.233.

10. Grass, A.J. (1983): "The influence of boundary layer turbulence on the mechanics of sediment transport". In: Mechanics of Sediment Transport, Proc. of Euromech 156, Istanbul, 12-14. July 1982, A.A. Balkema (Rotterdam).

11. Grass, A.J., Stuart, R.J. and Mansour-Tehrani, M. (1991): "Vortical structures and coherent motion in turbulent flow over smooth and rough boundaries", Phil. Trans. R. Soc. London A, vol. 336, p. 35.

12. Hinze, J.O. (1975): Turbulence. McGraw-Hill.

13. Jackson, R.G. (1976): "Sedimentological and fluid-dynamic implications of the turbulent bursting phenomenon in geopyhsical flows". J. Fluid Mech., vol. 77, p. 531.

14. Kamphuis, J. W. (1974): "Determination of sand roughness for fixed beds". J. Hydraulic Res., Vol. 12, No.2, p.193.

15. Laufer, J. (1954): The Structure of Turbulence in Fully Developed Pipe Flow. NACA, Report No. 1174.

16. Laufer, J. (1975): "New trends in experimental turbulence research". Ann. Review of Fluid Mech., vol. 7, p.307.

17. Lee, M.K., Eckelman, L.D., Hanratty, T.J. (1974): "Identification of turbulent wall eddies through the phase relation of the components of the fluctuating velocity gradient". J. Fluid Mech., vol. 66, p. 17.

18. Monin, A. S. and Yaglom, A. M. (1973): Statistical Fluid Mechanics: Mechanics of Turbulence. MIT Press, Cambridge, Mass.

19. Nezu, I. and Rodi, W. (1986): "Open-Channel flow measurements with a laser Doppler anemometry". ASCE J. Hyd. Eng., vol. 112, No. 5, 335-355.

20. Nezu, I. and Nakagawa, H. (1993): Turbulence in Open-Channel Flow. IAHR Monograph, A.A. Balkema (Roterdam).

21. Nychas, S.G., Hershey, H.C. and Brodkey, R.S. (1973): "A visual study of turbulent shear flow". J. Fluid Mech., vol. 61, p. 513.

22. Offen, G.R. and Kline, S.J. (1973): Experiments on the velocity characteristics of "Bursts" and on the Interactions Between the Inner and Outer Regions of a Turbulent Boundary Layer. Dept. of Mech. Engrg., Stanford University, Report MD-31.

23. Offen, G.R. and Kline, S.J. (1975): "A proposed model of the bursting process in turbulent boundary layers". J. Fluid Mech.., vol. 70, p. 209.

24. Praturi, A.K. and Brodkey, R.S. (1978): "A stereoscopic visual study of coherent structures in turbulent shear flow. J. Fluid Mech., vol. 89, p.251.

25. Rotta, J.C. (1962). "Turbulent boundary layers in incompressible flow". Progress in Aerospace Science, vol. 2, p.1.

26. Schlichting, H. (1979). Boundary-Layer Theory. McGraw-Hill.

27. Sumer, B.M. (1986): "Recent Developments on the Mechanics of sediment suspension", General-Lecture Paper, in the book: Euromech 192: Transport of suspended solids in open channels, A.A. Balkema Publishers, Rotterdam, 1986.

28. Sumer, B.M., Cokgor, S. and Fredsøe, J. (2001): "Suction removal of sediment from between armour blocks". Journal of Hydraulic Engineering, ASCE, vol. 127, No. 4, pp. 293-306, 2001.

29. Sumer, B.M. and Deigaard, R. (1981): "Particle motions near the bottom in turbulent flow in an open channel - Part 2". Journal of Fluid Mechanics, Vol. 109, p. 311.

30. Sumer, B.M. and Oguz, B. (1978): "Particle motions near the bottom in turbulent flow in an open channel". Journal of Fluid Mechanics, Vol. 86, p. 109, 1978.

31. Sumer, B.M., Kozakiewicz, A., Fredsøe, J. and Deigaard, R. (1996): "Velocity and concentration profiles in the sheet flow layer of movable bed". Journal of Hydraulic Engineering, ASCE, vol. 122, No. 10, 549-558.

32. van Driest, E.R. (1956): "On turbulent flow near a wall". J. Aeronautical Sciences, vol. 23, p.1007.

33. Wei, T. and Willmarth, W.W. (1989): "Reynolds-number effects on the structure of a turbulent channel flow". J. Fluid Mech., vol. 204, p. 57.

Chapter 3

Statistical analysis

As has been seen in the previous chapters, hydrodynamic quantities such as the velocity components appear to be random variables. Although recent research has shown that the near-wall turbulent-boundary-layer process is repetitive in nature (Chapter 3, Bursting Process), unless special pattern recognition techniques are used to detect these repetitive, quasi-cyclic events, the turbulence signals even near the wall appear to be largely random. Therefore, it is imperative to use statistical techniques to study the turbulence.

Three topics will be discussed in the present chapter. First we will briefly study the probability density function of the turbulent velocity, then we will concentrate on the correlation and subsequently spectral analysis of turbulence. In the entire analysis, it will be assumed that the turbulence is isotropic unless otherwise stated.

3.1 Probability density function

Consider, for example, the $x-$ component of the velocity, u (Fig. 3.1 a). The velocity u (or its fluctuating component u') is a random variable. Thus, u (or u') must have a *probability density function (p.d.f.)* such that

$$p(u')\ du' = \Pr[u' < U' < u' + du'] \tag{3.1}$$

and

$$\int_{-\infty}^{\infty} p(u')\ du' = 1 \tag{3.2}$$

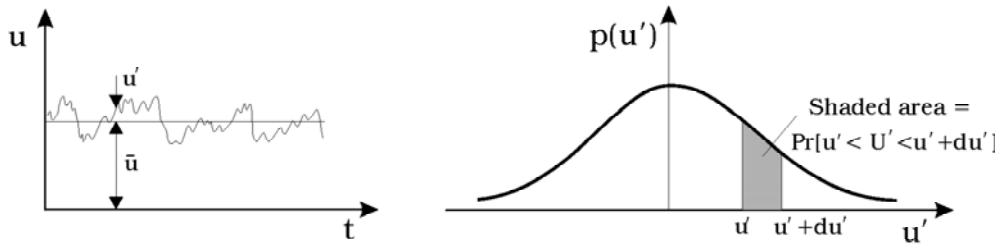

Figure 3.1: Time series and p.d.f. of velocity.

in which $p(u')$ is the p.d.f. of the fluctuating velocity u', and $\Pr[u' < U' < u' + du']$ is the probability of occurrence of the fluctuating velocity between u' and $u' + du'$.

Experiments show that $p(u')$ can be represented by the Gaussian (normal) distribution

$$p(u') = \frac{1}{\sigma_u \sqrt{2\pi}} \exp(-\frac{u'^2}{2\sigma_u^2}) \tag{3.3}$$

in which σ_u is the standard deviation of the velocity of u :

$$\sigma_u = \sqrt{\overline{(u - \overline{u})^2}} = \sqrt{\overline{u'^2}} \tag{3.4}$$

The significance of σ_u is that the probability of occurrence of u' outside the range, for example, $-2\sigma_u < u' < +2\sigma_u$ is only 4.6%, while that outside the range $-3\sigma_u < u' < +3\sigma_u$ is even much smaller, namely 0.3% (if the p.d.f. is represented by the Gaussian distribution).

It may be noted that the p.d.f. of the fluctuating velocity components may be different from the Gaussian distribution, with non-zero skewness, particularly near the wall (see the measurements made very close to the wall, reported in Eckelmann, 1974). This may be linked to the bursting process (Chapter 3).

Fig. 3.2 shows the p.d.f.'s (in the form of frequency histograms) for the two components of the turbulent velocities, u and v, near the wall for three different boundaries, namely the smooth, transitional and rough walls. Note the non-zero skewness in all distributions.

The statistical moments (or central moments) also give some information on the statistical properties of the velocities and other quantities:

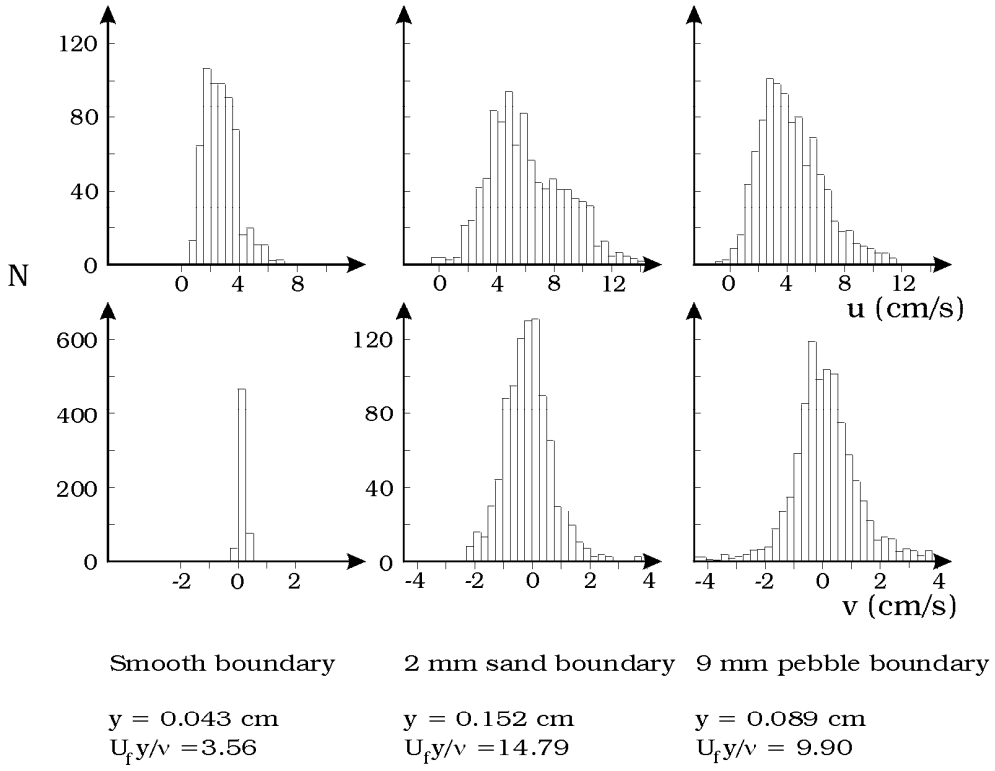

Figure 3.2: Frequency histograms of u and v velocity fluctuations. Grass (1971).

1. The first statistical moment is the mean

$$\overline{u} = \int_{-\infty}^{\infty} u\, p(u)\, du \tag{3.5}$$

2. The second central moment gives the variance

$$\sigma_u^2 = \int_{-\infty}^{\infty} (u - \overline{u})^2\, p(u)\, du = \int_{-\infty}^{\infty} u'^2\, p(u')\, du' \tag{3.6}$$

3. The third central moment,

$$\overline{u'^3} = \int_{-\infty}^{\infty} (u - \overline{u})^3\, p(u)\, du = \int_{-\infty}^{\infty} u'^3\, p(u')\, du' \tag{3.7}$$

gives the skewness factor :

$$S_u = \frac{\overline{u'^3}}{(\sigma_u^2)^{\frac{3}{2}}} \tag{3.8}$$

4. The fourth central moment,

$$\overline{u'^4} = \int_{-\infty}^{\infty} (u - \overline{u})^4 \; p(u) \; du = \int_{-\infty}^{\infty} u'^4 \; p(u') \; du' \tag{3.9}$$

gives the flatness factor:

$$F_u = \frac{\overline{u'^4}}{(\sigma_u^2)^2}$$

3.2 Correlation analysis

There are two kinds of correlations: (1) Space correlations, and (2) time correlations. We will first focus on the space correlations.

3.2.1 Space correlations

Definitions.

Fig. 3.3 gives the definition sketch. Consider the $i-$ component of the fluctuating velocity at Point A, $(u_i')_A$, and $j-$ component of the fluctuating velocity at Point B, $(u_j')_B$. Suppose that these velocities are measured simultaneously.

Two-point double correlation is defined by

$$(O_{ij})_{AB} = \overline{(u_i')_A \; (u_j')_B} \tag{3.10}$$

in which the overbar indicates the time averaging (Eq. 1.1). There are other correlations as well: three-point, four-point,..., and triple, quadruple,...correlations.

Two most important two-point double correlations (Fig. 3.4) are

$$\overline{u'(x) \; u'(x+r)} \tag{3.11}$$

and

$$\overline{v'(x) \; v'(x+r)} \tag{3.12}$$

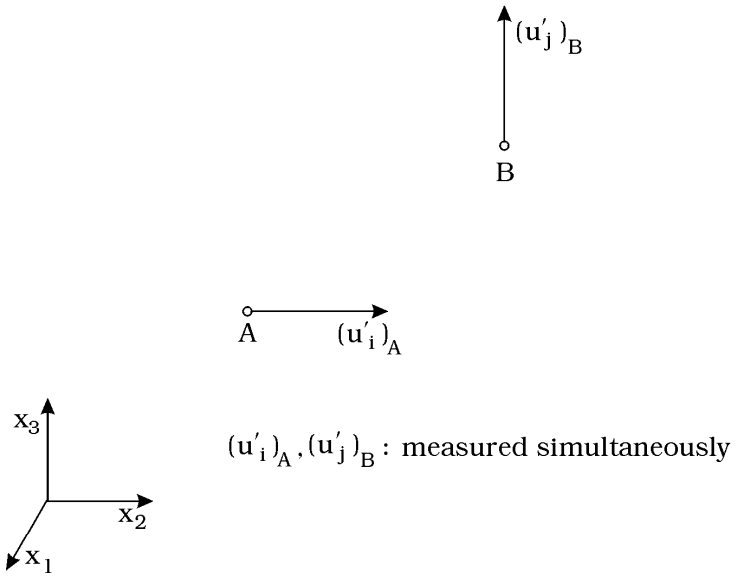

Figure 3.3: Correlation measurement.

in which r is the separation between the two points.

For convenience, these correlations are normalized by $\overline{u'^2}$ and $\overline{v'^2}$, respectively:

$$f(r) = \frac{\overline{u'(x)\ u'(x+r)}}{\overline{u'^2}} \tag{3.13}$$

$$g(r) = \frac{\overline{v'(x)\ v'(x+r)}}{\overline{v'^2}} \tag{3.14}$$

$f(r)$ and $g(r)$ are called the *correlation coefficients.*

The physical interpretation of the correlation functions/coefficients is as follows. The larger the correlation, the better correlated the motions at the two measurement points, and therefore the more likely that these two points belong to the same coherent structure. This would obviously give an idea about the length scale of the coherent structures, as will be detailed later in the section.

Properties of two-point double correlations.

1. The correlation coefficients are unity at $r = 0$:

$$f(0) = g(0) = 1 \tag{3.15}$$

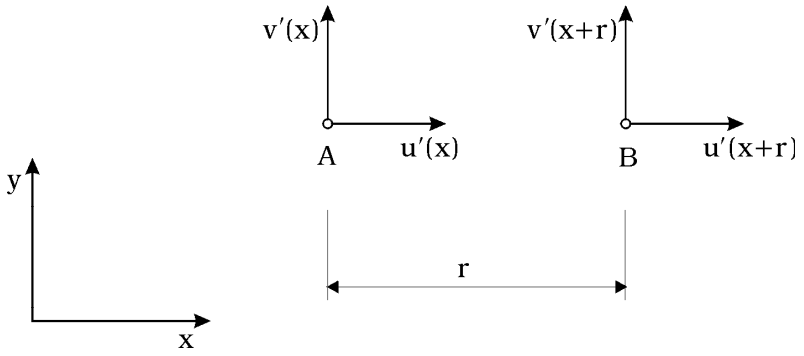

Figure 3.4: Correlation measurement.

(from Eqs. 3.13 and 3.14).

2. There is symmetry between positive and negative separations:

$$f(r) = f(-r), \text{ and } g(r) = g(-r) \tag{3.16}$$

(from the requirement of homogeneity).

3. The correlation coefficients are smaller than or equal to unity:

$$f(r) \leq 1, \text{ and } g(r) \leq 1 \tag{3.17}$$

This can easily be seen from

$$\begin{aligned} \overline{(u'(x) - u'(x+r))^2} &= \overline{u'^2(x)} + \overline{u'^2(x+r)} - 2\overline{u'(x)u'(x+r)} \\ &= 2(\overline{u'^2} - \overline{u'(x)u'(x+r)}) \end{aligned}$$

Since the left hand side of the equation ≥ 0, then $\overline{u'^2} - \overline{u'(x)u'(x+r)} \geq 0$, hence $f(r) \leq 1$.

4. The correlation coefficients tend to zero as the separation distance goes to infinity

$$f(r) \to 0, \text{ and } g(r) \to 0, \text{ as } r \to \infty \tag{3.18}$$

This is because when r is very large, there will be as many $u'(x)u'(x+r)$ products with the negative sign as with the positive sign, therefore, when averaged, $\overline{u'(x)u'(x+r)}$ will be zero. Physically, r is so large that the two points will not lie in the same coherent structure, therefore, their motions will be uncorrelated, meaning that the correlation coefficients should be zero for such large r distances.

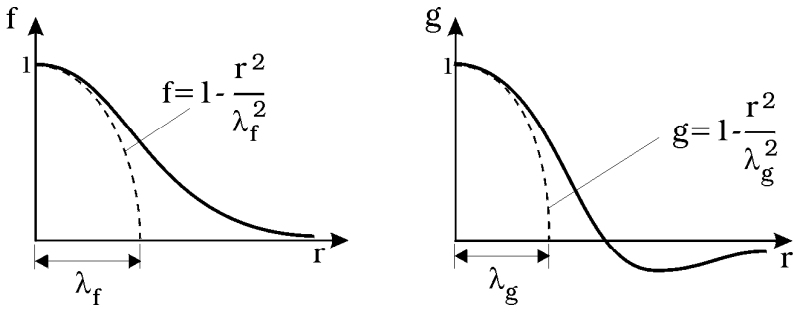

Figure 3.5: Correlation coefficients f and g, and micro scales.

5. While $f(r)$ is always positive, $g(r)$ can take negative values as well. To show this, we employ

$$rg(r) = rf(r) + \frac{1}{2}r^2\frac{\partial f}{\partial r} = \frac{1}{2}\frac{\partial}{\partial r}(r^2 f(r)) \tag{3.19}$$

This is the relationship between $f(r)$ and $g(r)$ in isotropic turbulence, as will be detailed in the following paragraphs. Integrating gives

$$\int_0^\infty rg(r)dr = \frac{1}{2}[r^2 f(r)]_0^\infty = 0 \tag{3.20}$$

provided that $r^2 f(r) = 0$ as $r \to \infty$. (Experiments show that $f(r)$ is like $f(r) \sim e^{-r}$, then it is easy to see that $r^2 f(r) \to 0$ as $r \to \infty$.) For the integral on the left hand side of the equation to be zero, clearly $g(r)$ must have positive and negative values.

The general forms of the functions of $f(r)$ and $g(r)$ are shown in Fig. 3.5.

Finally, we note the following. There is a special class of turbulence, called isotropic turbulence where turbulence characteristics such as $\overline{u'^2}$ are independent of the rotation of the axes. This implies that $\overline{u'^2} = \overline{v'^2} = \overline{w'^2}$. Turbulence in the "core" region in a wind tunnel (where the wall effects are practically nonexistent) may be considered to be isotropic. In such a turbulence field, the correlations coefficients are related with the following equation

$$g(r) = f(r) + \frac{r}{2}\frac{\partial}{\partial r}f(r) \tag{3.21}$$

(see Hinze, 1959, p. 150).

Scales of turbulence.

Micro scales. Expanding $f(r)$ as a Taylor series, and for small values of r, gives

$$f(r) = 1 + \frac{1}{2}(\frac{\partial^2 f}{\partial r^2})_{r=0} \quad r^2 + ... \tag{3.22}$$

Note that the terms with r^n (n being an odd number, $n = 1, 3, 5, ..$) will drop because $f(r) = f(-r)$.

Now, the formal definition of the micro time scale is

$$\frac{1}{\lambda_f^2} = -\frac{1}{2}(\frac{\partial^2 f}{\partial r^2})_{r=0} \tag{3.23}$$

in which λ_f is the micro length scale of turbulence. Inserting the preceding equation in Eq. 3.22, one gets

$$f(r) = 1 - \frac{r^2}{\lambda_f^2} \tag{3.24}$$

As seen from Fig. 3.5, this is a parabola fit to the correlation coefficient for small values of r , and λ_f is the $x-$ intercept of the fitted parabola.

Likewise,

$$g(r) = 1 - \frac{r^2}{\lambda_g^2} \tag{3.25}$$

in which λ_g is another micro length scale.

These length scales can also be expressed in terms of the fluctuating-velocity gradients:

$$\frac{1}{\lambda_f^2} = \frac{1}{2\overline{u'^2}}\overline{(\frac{\partial u'}{\partial r})^2} \tag{3.26}$$

and

$$\frac{1}{\lambda_g^2} = \frac{1}{2\overline{v'^2}}\overline{(\frac{\partial v'}{\partial r})^2} \tag{3.27}$$

(see Raudkivi and Callander, 1975, p. 167).

λ_f and λ_g are not independent of each other. In *isotropic turbulence*, from Eq. 3.21,

$$(\frac{\partial^2}{\partial r^2} g(r))_{r=0} = 2(\frac{\partial^2}{\partial r^2} f(r))_{r=0} \tag{3.28}$$

and inserting Eqs. 3.24 and 3.25,

$$\lambda_f = \sqrt{2}\lambda_g \tag{3.29}$$

Macro scales. The macro scales of turbulence are defined by

$$\Lambda_f = \int_0^\infty f(r)dr \tag{3.30}$$

and

$$\Lambda_g = \int_0^\infty g(r)dr \tag{3.31}$$

This length scale is indicated in Fig. 3.6 where the area of the rectangle $\Lambda_f \times 1$ is equal to the area under the correlation curve.

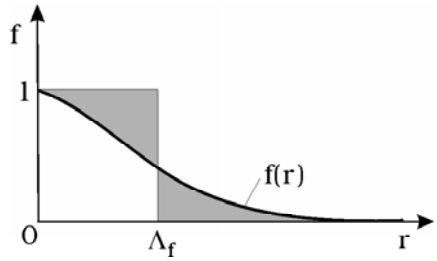

Figure 3.6: Definition of macro scale.

Λ_f or Λ_g can be interpreted as the length scales of coherent structures (or the so-called *eddies*, the rotating entities) of turbulence.

Similar to the micro scales, the macro scales are also related to each other. In *isotropic turbulence*, integrating Eq. 3.21 gives

$$\int_0^\infty g(r)dr = \int_0^\infty f(r)dr + \frac{1}{2}[rf(r)\mid_0^\infty - \frac{1}{2}\int_0^\infty f(r)dr \tag{3.32}$$

which gives

$$\Lambda_f = 2\Lambda_g \tag{3.33}$$

3.2.2 Time correlations

There are two kinds of time correlations: Eulerian time correlations, and Lagrangian time correlations.

The *Eulerian time correlation* is defined by

$$R_E(t) = \frac{\overline{u'(\tau)u'(\tau+t)}}{\overline{u'^2}} \tag{3.34}$$

This is for the $x-$ component of the velocity. Likewise, other Eulerian correlation coefficient can also be defined for the $y-$ and $z-$ components of the velocity.

Similar to space correlations, one has

$$R_E(0) = 1 \tag{3.35}$$

$$R_E(t) \leq 1 \tag{3.36}$$

and

$$R_E(t) \to 0, \text{ as } t \to \infty \tag{3.37}$$

(Similar relations for the other components of the velocity).

The micro and macro time scales can also be defined, similar to the space correlations.

The micro time scale is defined by

$$\frac{1}{\tau_E^2} = -\frac{1}{2}\left(\frac{\partial^2 R_E(t)}{\partial t^2}\right)_{t=0} \tag{3.38}$$

(cf. Eq.3.23), or

$$R_E(t) = 1 - \frac{t^2}{\tau_E^2} \tag{3.39}$$

(cf. Eq. 3.24).

The macro time scale, on the other hand, is defined by

$$T_E = \int_0^\infty R_E(t)dt \tag{3.40}$$

The macro time scale can be interpreted as the time during which a coherent structure (or an eddy) passes the measurement point.

We expect that the macro time scale and the macro length scale are related. To find this relation, G.I. Taylor made the so-called *frozen-turbulence approximation*. Consider the coherent structure at time t in Fig. 3.7. The size of this coherent structure is Λ_f, the macro length scale of turbulence.

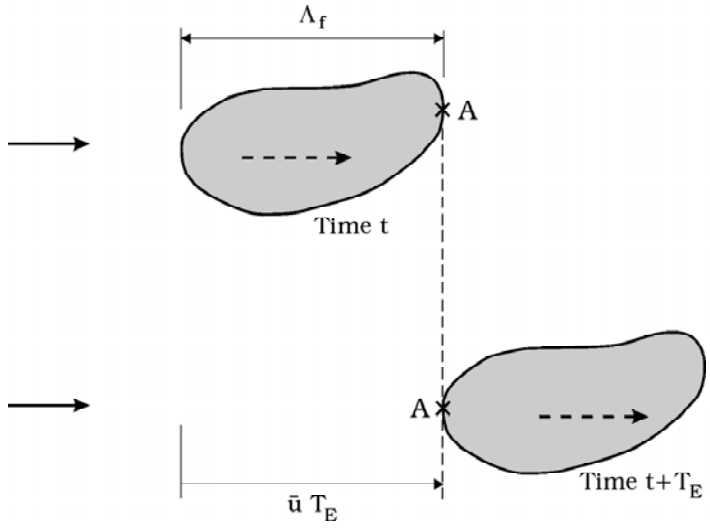

Figure 3.7: Taylor's frozen turbulence approximation.

Consider the measurement point A. Now, with the frozen-turbulence approximation, the size of the coherent structure will remain unchanged, as it is convected downstream. The time for the coherent structure to pass Point A is T_E (by virtue of the physical interpretation in the previous paragraph). Therefore, the distance that the coherent structure travels can, to a first approximation, be written as $\overline{u}T_E$ in which $\overline{u}$ is the mean velocity at the measurement point. From the figure, this distance is equal to the size of the coherent structure, hence

$$\Lambda_f = \overline{u}T_E \tag{3.41}$$

This relationship enables the length scale to be calculated from the knowledge of the time scale. (The latter is easier to measure than the former).

The *Lagrangian time correlation* is defined in the same way as in the case of the Eulerian time correlation. However, the velocity is now measured by tracking the fluid particle, as the particle travels. Therefore, the Eulerian time series (which is the basis for the Eulerian time correlation) is to be replaced by the time series from the Lagrangian particle tracking. Then, all the equations given for the Eulerian correlation (Eqs. 3.34 - 3.41) are equally valid for the Lagrangian correlation.

So, the Lagrangian correlation coefficient (cf. Eq. 3.34)

$$R_L(t) = \frac{\overline{V'(\tau)V'(\tau+t)}}{\overline{V'^2}} \tag{3.42}$$

in which V' is the Lagrangian fluctuating velocity, and, for later use, the Lagrangian macro time scale

$$T_L = \int_0^\infty R_L(t)\ dt \tag{3.43}$$

cf., Eq. 3.40).

It may be noted that, in the laboratory, tracking of particles can be achieved by means of an ordinary camera (or, two special cameras used in the field of photogrammetry for 3-D tracking), combined with a stroboscope (Sumer and Oguz, 1978, and Sumer and Deigaard, 1981), or using video techniques.

Of particular interest is the physical interpretation for the Lagrangian macro time scale. The Lagrangian macro time scale may be interpreted as the time during which a coherent structure keeps its "identity". Also, the length scale to be obtained by application of Eq. 3.41 may be interpreted as the distance traveled by the coherent structure.

3.3 Spectrum analysis

In turbulent flows, there is a continuous, broad range of length/time scales. For example, smoke coming out of a smoke stack has flow structures with varying sizes; Larger eddies (coherent structures) contain smaller eddies; these smaller eddies contain even smaller eddies, and so on.

The correlation analysis cannot address the issue of the previously mentioned continuous, broad range of length/time scales. (It gives only two discrete length/time scales (the micro and the macro scales), and no more than that).

This continuous, broad range of scales can be studied only by use of the spectrum analysis. We will study this in this section.

The analysis will be developed for isotropic turbulence for convenience.

There are two kinds of spectrum analyses. One involves the space correlations, and the other involves time correlations. The spectrum function in the first case is resolved in the wave number space, while that in the second

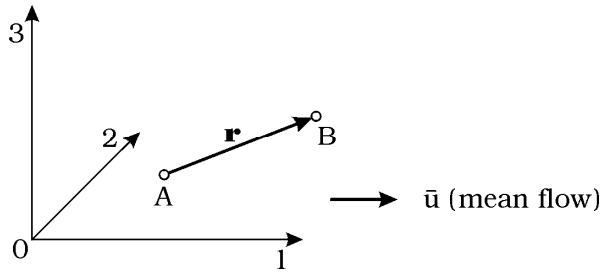

Figure 3.8: Definition sketch.

case is resolved in the frequency space. We will consider in this section the former spectrum analysis. However, the analysis in the latter is basically the same, provided that the wave number is to be replaced by the frequency.

3.3.1 General considerations

The Fourier transform of two-point double correlation Q_{ij} (see Eq. 3.10 for the definition of Q_{ij}) is

$$\Phi_{ij}(\mathbf{k}) = \frac{1}{(2\pi)^3} \int_{-\infty}^{\infty} Q_{ij}\,(\mathbf{r})\; e^{-i\mathbf{k}\cdot\mathbf{r}} d\mathbf{r} \tag{3.44}$$

in which $\mathbf{r}$ is the separation vector (Fig. 3.8), $d\mathbf{r} = dr_1 dr_2 dr_3$, $\mathbf{k}$ is the wave number vector and i is the imaginary unit, $i = \sqrt{-1}$. The inverse transform, on the other hand, is

$$Q_{ij}\,(\mathbf{r}) = \int_{-\infty}^{\infty} \Phi_{ij}(\mathbf{k})\; e^{i\mathbf{k}\cdot\mathbf{r}} d\mathbf{k} \tag{3.45}$$

in which $d\mathbf{k} = dk_1 dk_2 dk_3$ is an element of volume in wave number space.

Now, for $r = 0$, the preceding equation becomes

$$Q_{ij}\,(0) = \int_{-\infty}^{\infty} \Phi_{ij}(\mathbf{k})\; d\mathbf{k}$$

and setting $i = j$,

$$Q_{ii}\,(0) = \int_{-\infty}^{\infty} \Phi_{ii}(\mathbf{k})\; d\mathbf{k} \tag{3.46}$$

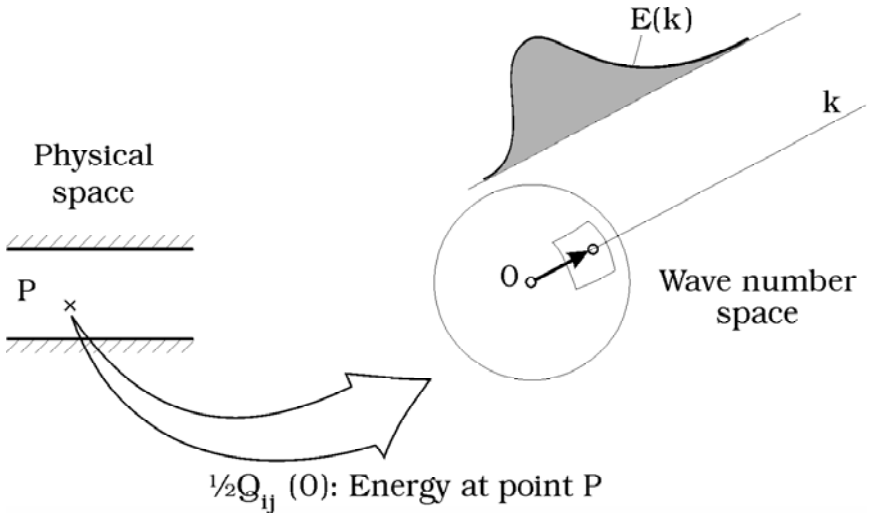

Figure 3.9: Energy spectrum. Isotropic turbulence.

Here, $Q_{ii}\,(0)$ is two times the mean kinetic energy of turbulence per unit mass in the i-th direction:

$$Q_{ii}\,(0) = \overline{u_i' u_i'} = 2\,[\frac{1}{2}(\overline{u'^2} + \overline{v'^2} + \overline{w'^2})] \tag{3.47}$$

We write Eq. 3.46 in the following form

$$Q_{ii}\,(0) = \int_{-\infty}^{\infty}\int_{-\infty}^{\infty}\int_{-\infty}^{\infty} \Phi_{ii}(k_1,k_2,k_3)\; dk_1 dk_2 dk_3 \tag{3.48}$$

Since the left hand side of the above equation is proportional to the turbulent energy, then $\Phi_{ii}(k_1,k_2,k_3)$ will be like the energy density in the wave number space. We shall return to this in the following paragraphs.

In the case of *isotropic turbulence*, there will be spherical symmetry. Therefore, the spherical coordinates can be used in the wave number space. Eq. 3.48 in this case will read

$$\begin{aligned} Q_{ii}\,(0) &= \int_{k=0}^{\infty}\int_{A(k)} \Phi_{ii}(k)\; dk\; dA(k) \\ &= \int_{k=0}^{\infty} \Phi_{ii}(k)\; dk \int_{A(k)} dA(k) = \int_{k=0}^{\infty} (4\pi k^2)\Phi_{ii}(k)\; dk \end{aligned}$$

or

$$\frac{1}{2}Q_{ii}\,(0) = \int_{k=0}^{\infty} E(k)\; dk \tag{3.49}$$

in which

$$E(k) = 2\pi k^2 \Phi_{ii}(k) \tag{3.50}$$

1. Eq. 3.49 is an important equation. As pointed out in the preceding paragraphs, the left hand side of the equation is the turbulent energy (per unit mass), therefore, $E(k)$ will be the energy density in the wave number space k. The function $E(k)$ is called the *energy spectrum function.*

2. It may be noted that the spherical symmetry enables us to replace the three-dimensional spectrum function $\Phi_{ii}(k_1, k_2, k_3)$ (Eq. 3.48) with a one-dimensional spectrum function, $E(k)$.

3. The relation given in Eq. 3.49 can be envisaged as follows (see the sketch in Fig. 3.9): The velocity time series of the three components of the velocity are recorded at the measurement point P. From these time series, the turbulent energy per unit mass, $\frac{1}{2}Q_{ii}\,(0)$, is calculated, using Eq. 3.47. Then, according to Eq. 3.49, this energy is decomposed into infinite number of small energies, i.e., $E(k)\; dk$, in the wave number space. Each of these small energies corresponds to a wave number, k, which itself corresponds to a wave length (or to a turbulence "length scale")

$$\lambda = \frac{2\pi}{k} \tag{3.51}$$

   As seen, the objective set at the beginning of this section, namely the study of the continuous, broad range of length scales of turbulence, apparently can be achieved by the application of the energy spectrum function $E(k)$. In the following section, we will have a closer look at this function.

3.3.2 Energy balance in wave number space

In *isotropic turbulence*, the previously mentioned correlation function $Q_{ij}(\mathbf{r})$ satisfies the following equation (Hinze, 1959, p. 159, and Raudkivi and

Callander, 1975, p. 163)

$$\frac{\partial}{\partial t}Q_{ij}(\mathbf{r}) = S_{ij}(\mathbf{r}) + 2\nu\frac{\partial^2}{\partial r_k \partial r_k}Q_{ij}(\mathbf{r}) \tag{3.52}$$

in which

$$S_{ij}(\mathbf{r}) = \frac{\partial}{\partial r_k}(S_{ik,j} + S_{kj,i}) \tag{3.53}$$

in which

$$(S_{ik,j})_{AB} = \overline{(u_i')_A (u_k')_A (u_j')_B} \tag{3.54}$$

and

$$(S_{i,kj})_{AB} = \overline{(u_i')_A (u_k')_B (u_j')_B} \tag{3.55}$$

It should be noted that Eq. 3.52 stems from the N.-S. equation.

The Fourier transform of Eq. 3.52

$$\frac{\partial}{\partial t}\Phi_{ij}(\mathbf{k}) = \Omega_{ij}(\mathbf{k}) - 2\nu k^2 \Phi_{ij}(\mathbf{k}) \tag{3.56}$$

in which

$$\Omega_{ij}(\mathbf{k}) = \frac{1}{(2\pi)^3}\int_{-\infty}^{\infty} S_{ij}(\mathbf{r})\ e^{-i\mathbf{k}\cdot\mathbf{r}} d\mathbf{r} \tag{3.57}$$

and the inverse transform reads

$$S_{ij}(\mathbf{r}) = \int_{-\infty}^{\infty} \Omega_{ij}(\mathbf{k})\ e^{-i\mathbf{k}\cdot\mathbf{r}} d\mathbf{k} \tag{3.58}$$

Now, putting $i = j$ in Eq. 3.56 gives

$$\frac{\partial}{\partial t}\Phi_{ii}(\mathbf{k}) = \Omega_{ii}(\mathbf{k}) - 2\nu k^2 \Phi_{ii}(\mathbf{k}) \tag{3.59}$$

and multiplying both sides of the latter equation by $2\pi k^2$, and recalling $E(k) = 2\pi k^2 \Phi_{ii}(k)$ (Eq. 3.50), one gets

$$\frac{\partial}{\partial t}E(k) = T(k) - 2\nu k^2 E(k) \tag{3.60}$$

in which

$$T(k) = 2\pi k^2 \Omega_{ii}(k) \tag{3.61}$$

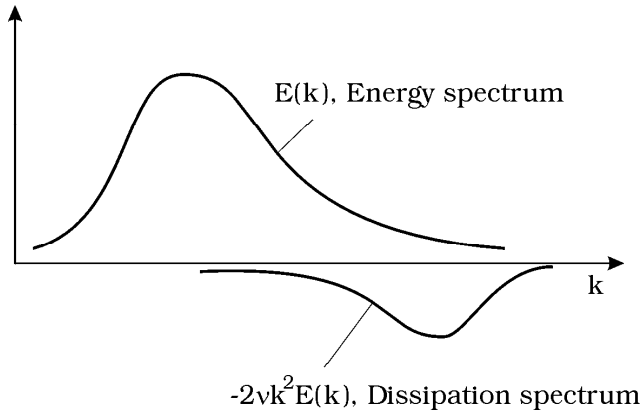

Figure 3.10: Energy spectrum and dissipation spectrum. (Note that peaks are well apart).

This equation (Eq. 3.60) represents the "turbulent energy balance" in the wave number space. To study the physical meaning of each term in the equation, we integrate Eq. 3.60 from $k = 0$ to ∞:

$$\frac{\partial}{\partial t}\int_0^\infty E(k)dk = \int_0^\infty T(k)dk - 2\nu\int_0^\infty k^2 E(k)dk \tag{3.62}$$

It can be shown that the first term on the right hand side of the preceding equation is zero (Hinze, 1959, p. 178). Hence Eq. 3.62 will be

$$\frac{\partial}{\partial t}\int_0^\infty E(k)dk = -2\nu\int_0^\infty k^2 E(k)dk \tag{3.63}$$

Recall that $\int_0^\infty E(k)dk$ is the turbulent energy per unit mass (Eq. 3.49); hence, the left hand side of the above equation will represent the rate of change of the turbulent energy. Now, the integral on the right hand side of the equation, $\int_0^\infty k^2 E(k)dk$, is always positive. This means that

$$\frac{\partial}{\partial t}\int_0^\infty E(k)dk < 0 \tag{3.64}$$

From the above analysis, the following deductions can be made:

1. Turbulent energy in isotropic turbulence decreases with time (Eq. 3.64). This is due to viscous dissipation, governed by the term on the right hand side of Eq. 3.63.

2. As seen from Eq. 3.63, the latter term is weighted by the factor k^2, and clearly is more effective at large wave numbers (i.e., at small size eddies) than at small wave numbers (i.e., at large size eddies), Fig. 3.10.

3. The fact that the first term on the right hand side in Eq. 3.62 is zero implies that it is neither a source term nor a sink term. It can be shown that this term, namely $T(k)$, is responsible for the transfer of turbulent energy from small wave numbers to large wave numbers (see Example 7 below).

Summarizing at this point,

1. Most of the turbulent energy is contained in small wave numbers (large eddies, or large scale motion) (Fig. 3.10);

2. Most of the dissipation occurs at large wave numbers (small eddies, or small scale motion) (Fig. 3.10); and

3. Between the small wave numbers and large wave numbers, there is a range of wave numbers responsible for transferring turbulent energy from small to large wave numbers.

Example 7 *Transfer of turbulent energy in the wave number space.*

Integrate Eq.3.60 from $k = 0$ to k:

$$\frac{\partial}{\partial t}\int_0^k E(k)dk = \int_0^k T(k)dk - 2\nu\int_0^k k^2 E(k)dk \tag{3.65}$$

Consider the interval in the wave number space from $k = 0$ to k (Fig. 3.10). The first term on the left hand side of the above equation represents the change in the turbulent energy in this interval per unit time. The third term represents the viscous dissipation in this interval per unit time (Fig. 3.11).

Experiments show that the sign of the term $\int_0^k T(k)dk$ is the same as that of the viscous dissipation. Therefore, $\int_0^k T(k)dk$ should be an efflux, rather than an influx. This efflux cannot take place at the $k = 0$ end of the considered interval, because $k = 0$ forms a closed end (there is no negative

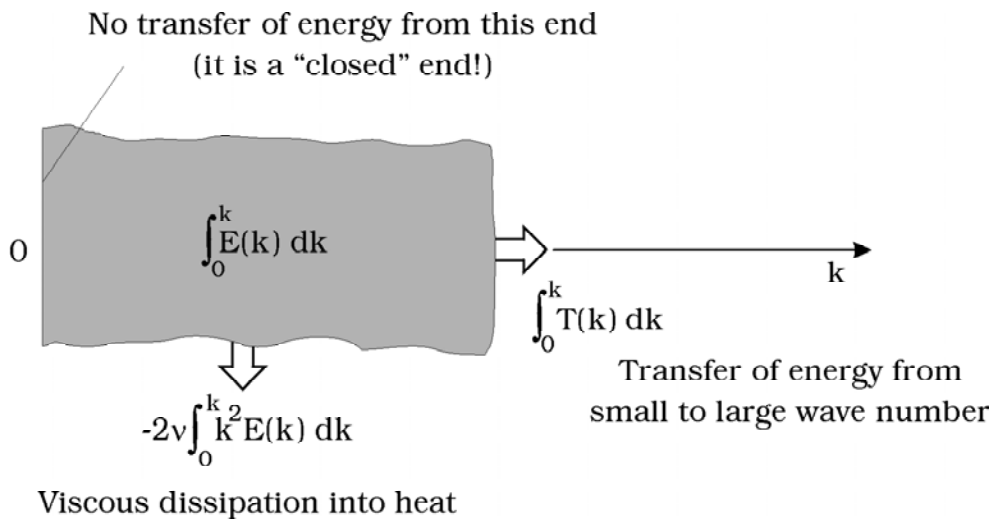

Figure 3.11: Transfer of energy in wave-number space.

wave numbers!). Therefore, this efflux must take place at the other end of the interval, namely at $k = k$ (Fig. 3.11).

So, the picture is as follows. In the interval $(0, k)$ in the wave-number space, some part of the turbulent energy is dissipated into heat (viscous dissipation), and some part of it is transferred to wave numbers larger than k. The latter means that *there is, on average, a continuous flow of turbulent energy from small wave numbers to large wave numbers.* The term responsible for this is $T(k)$. This term originates from the inertia terms in the N.-S. equations. Therefore, the previously mentioned transfer of energy is called the *inertial transfer.*

3.3.3 Kolmogoroff's theory. Universal equilibrium range and inertial subrange

In the process of turbulent energy transfer from small wave numbers (large scale motion) to large wave numbers (small-scale motion), a point is reached beyond which the turbulence will "forget" the influence of the initial large-scale motion. From this point to the wave numbers where the viscous dissipation occurs, there is a range of wave numbers in which the character of turbulence will be the same in all flows (in streams, in atmospheric boundary-

layer turbulence, etc.). This range is called *the universal equilibrium range.* It is called universal because the character of turbulence in this range is independent of the flow environment; and it is called equilibrium because the energy input is in balance with the energy dissipation, as will be detailed later in the section. Kolmogoroff's theory is concerned with this range.

Kolmogoroff's first hypothesis states that, irrespective of the large-scale motion, the turbulence in the universal equilibrium range is isotropic. Now, the energy spectrum function in this range is a function of the following quantities

$$E = f(\varepsilon,\ \nu,\ k) \tag{3.66}$$

in which ε is the dissipation of turbulent energy per unit mass and per unit time:

$$\varepsilon = \nu\overline{(\frac{\partial u_i'}{\partial x_\alpha} + \frac{\partial u_\alpha'}{\partial x_i})\frac{\partial u_i'}{\partial x_\alpha}} \tag{3.67}$$

(Eq. 1.32).

ε is involved because it represents the dissipation of turbulent energy. ν should be involved because the energy is dissipated into heat through viscosity. The wave number, k, is involved because the turbulent energy process is primarily dependent on the wave number (Eq. 3.60). (k is taken instead of k_1, k_2 and k_3 because of the spherical symmetry; isotropic turbulence!). Note that E (rather than Φ_{ii}) is adopted here to represent the energy spectrum because we assume that turbulence is isotropic.

From dimensional analysis, one gets

$$E(k) = v^2\ \eta\ \theta(\eta k) \tag{3.68}$$

in which θ is a nondimensional function of ηk, the quantity v is

$$v = (\nu\varepsilon)^{\frac{1}{4}} \tag{3.69}$$

and η is

$$\eta = (\frac{\nu^3}{\varepsilon})^{\frac{1}{4}} \tag{3.70}$$

Here the unit of v is $[v] = (\frac{cm^2}{s}\frac{cm^2}{s}(\frac{cm}{s.cm})^2)^{\frac{1}{4}} = \frac{cm}{s}$, and that of η is $[\eta] = ((\frac{cm^2}{s})^3\frac{1}{\frac{cm^2}{s}(\frac{cm}{s.cm})^2})^{\frac{1}{4}} = cm$. The quantity v is called the characteristic velocity, while η is called the characteristic length. Based on the quantities v and η, the following characteristic time may be defined

$$\tau = \frac{\eta}{v} = (\frac{\nu}{\varepsilon})^{\frac{1}{2}} \tag{3.71}$$

The above characteristic length, η, and the characteristic time, τ, are involved in the large wave number range (small scale motion); they represent the smallest scales of turbulence, namely η *the smallest length scale (*known as *the Kolmogoroff scale)*, and τ *the smallest time scale.* These are the smallest scales of turbulence because scales smaller than these involve molecular motion.

The nondimensional equation obtained for the spectrum function (Eq. 3.68) can be developed further, following Kolmogoroff's second hypothesis. The latter states that the peaks of the energy spectrum and that of the dissipation spectrum are sufficiently apart. This is illustrated in Fig. 3.10. The latter implies that there is a dominating wave number range in the energy spectrum (small wave numbers, or alternatively, large eddies) which contain most of the turbulent energy, while there is another dominating wave number range (large wave number, or alternatively small eddies) which are associated with the viscous dissipation. According to Kolmogoroff's second hypothesis, these wave number ranges are sufficiently apart, meaning that there must be a wave number range between these two ranges where there is no significant energy, and there is no significant dissipation.

First of all, this range should be a part of the universal equilibrium range, because it contains no significant energy. (Recall the definition of the universal equilibrium range at the beginning of this subsection: In the universal equilibrium range, the energy input is in balance with the energy dissipation; no significant energy presence).

Secondly, in this range, the only significant activity is that the turbulent energy is transferred from small wave numbers to large wave numbers. This process is governed by the inertia terms in the N.-S. equation, as described in Example 7 above. Therefore, this particular range of wave numbers is called the inertial subrange. ("inertial" because of the previously mentioned inertia terms; and "subrange" because this range is a part of the universal equilibrium range, as pointed out in the preceding paragraphs).

Now, in the inertial subrange, the energy spectrum should be independent of the viscosity because no significant dissipation takes place in this range, as mentioned previously. This is an important statement. Because, for the viscosity to drop out in Eq. 3.68, the function $\theta(\eta k)$ has to be given in the following form

$$\theta(\eta k) = \text{Constant} \times (k\eta)^{-\frac{5}{3}} \tag{3.72}$$

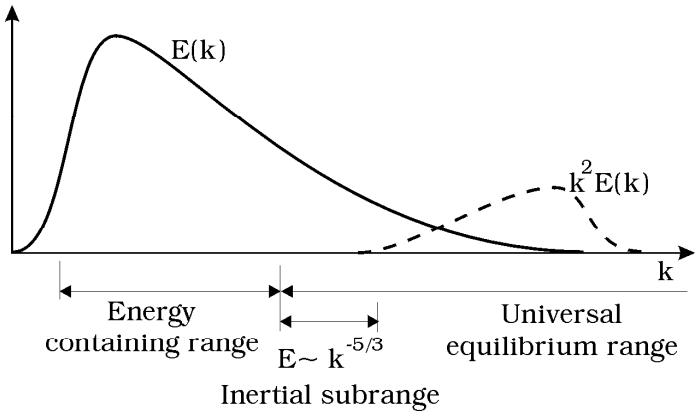

Figure 3.12: General picture of energy spectrum.

Thus, inserting Eq. 3.72 in Eq. 3.68, the spectrum function is found to be

$$E(k) = \text{Constant } \times \varepsilon^{\frac{2}{3}}\ k^{-\frac{5}{3}} \tag{3.73}$$

This is known as -5/3-law. Experiments confirm the presence of this subrange where the spectrum is given by the -5/3 law.

Finally, Fig. 3.12 gives a schematic picture of the spectral representation of the process.

3.3.4 One-dimensional spectrum

$E(k)$ is not an easily measurable quantity. To get around the problem, we define the following one-dimensional spectrum

$$\begin{aligned} F(k) &= \frac{1}{2\pi}\int_{-\infty}^{\infty} Q_{11}(r)\ e^{-ikr}dr \\ &= \frac{1}{2\pi}\int_{-\infty}^{\infty} \overline{u'^2}\ f(r)\ e^{-ikr}dr \end{aligned} \tag{3.74}$$

Since $f(r)$ is an even function of r,

$$F(k) = \frac{\overline{u'^2}}{\pi}\int_0^{\infty} f(r)\ \cos(kr)\ dr \tag{3.75}$$

The inverse transform is

$$\overline{u'^2} f(r) = 2 \int_0^\infty F(k)\ \cos(kr)\ dk \tag{3.76}$$

It can be shown that, in *isotropic turbulence*, the one-dimensional spectrum $F(k)$ is related to the energy spectrum function $E(k)$

$$E(k) = k^2 F''(k) - kF'(k) \tag{3.77}$$

(see for example Raudkivi and Callander, 1975, p.174).

Incidentally, inserting Eq. 3.73 into Eq. 3.77 gives

$$\frac{\varepsilon^{\frac{2}{3}}}{k^{\frac{5}{3}}} = k^2 F''(k) - kF'(k) \tag{3.78}$$

This has a solution:

$$F(k) = \frac{9}{55}\varepsilon^{\frac{2}{3}} k^{-\frac{5}{3}} + \frac{k^2}{2} C_1 + C_2 \tag{3.79}$$

The second and third terms on the right-hand-side of the preceding equation should drop because $F(k)$ should go to zero for large values of k, and therefore

$$F(k) = \text{ Constant} \times \varepsilon^{\frac{2}{3}} k^{-\frac{5}{3}} \tag{3.80}$$

Example 8 *The correlation function $f(r)$ is approximated by*

$$f(r) = \exp(-\frac{r}{\Lambda_f})$$

Find the one-dimensional and three-dimensional spectrum functions.

The one-dimensional spectrum function from Eq. 3.75

$$F(k) = \frac{\overline{u'^2}}{\pi} \int_0^\infty f(r)\ \cos(kr)\ dr = \frac{\Lambda_f\ \overline{u'^2}}{\pi(1 + (k\Lambda_f)^2)}$$

For $k = 0$:

$$k = 0 :\ F(0) = \frac{\Lambda_f\ \overline{u'^2}}{\pi}$$

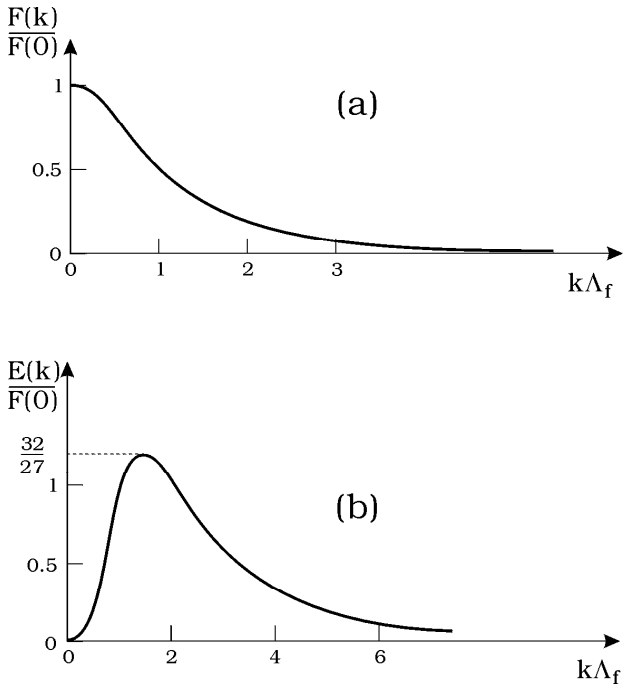

Figure 3.13: 1-D and 3-D energy spectra for the numerical example.

Hence,

$$F(k) = \frac{F(0)}{1 + (k\Lambda_f)^2}$$

(see Fig. 3.13 a).

Regarding the three-dimensional energy spectrum function $E(k)$, considering that the turbulence is isotropic, therefore using Eq. 3.77

$$E(k) = 8F(0)\frac{(k\Lambda_f)^4}{(1 + (k\Lambda_f)^2)^3}$$

(see Fig. 3.13 b for $E(k)$).

Example 9 *One-dimensional spectrum function for a boundary layer in an open channel.*

Fig. 3.14 a shows the one-dimensional spectrum function obtained for an open channel flow by Raichlen (1967). (The results are normalized as

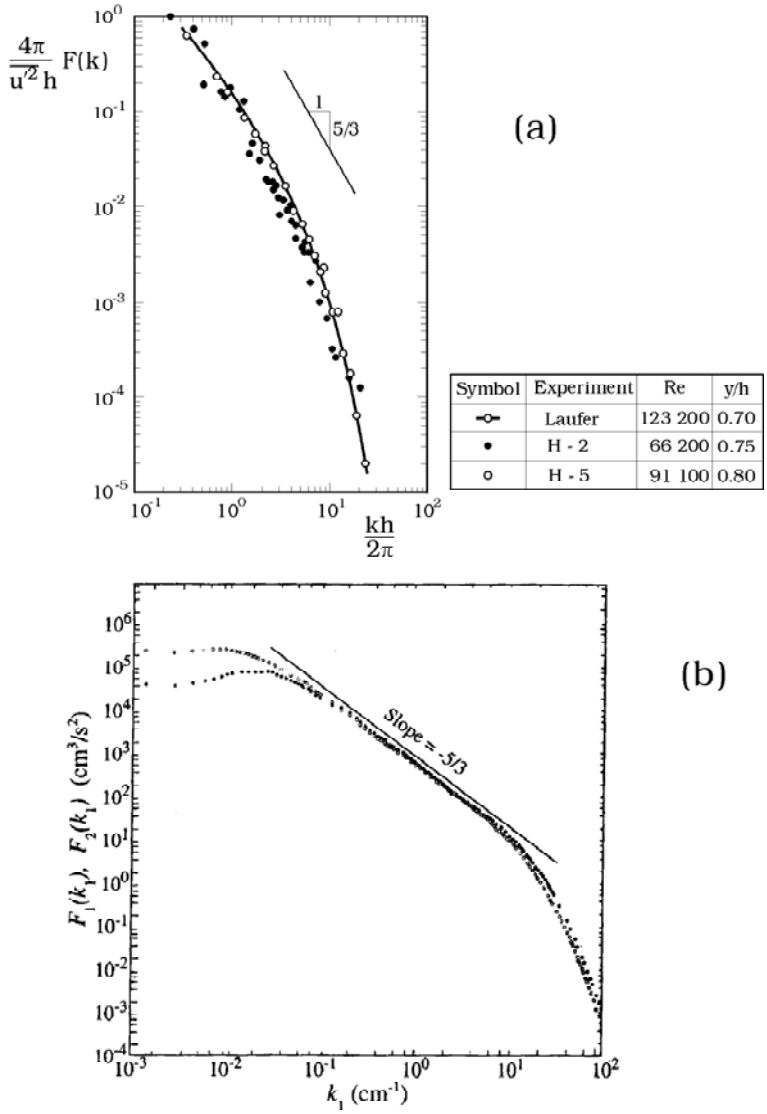

Figure 3.14: 1-D energy spectra. (a): measured in an open channel. Raichlen (1967). (b): measured in a jet. Champagne (1978).

indicated in the figure. The Reynolds number is defined as $Re = \frac{4RV}{\nu}$ in which R is the hydraulic radius). Fig. 3.14 b, on the other hand, shows the one-dimensional spectrum measured in a jet.

It may be noticed that, over a wave number interval, namely $1 < \frac{kh}{2\pi} < 6$, in Fig. 3.14 a, $E(k)$ is apparently

$$E(k) \sim k^{-\frac{5}{3}}$$

revealing the previously mentioned Kolmogoroff's -5/3 law. The same holds true for the second example (Fig. 3.14 b) for the range 4×10^{-2} cm$^{-1} < k_1 <$ 10 cm^{-1}.

3.4 References

1. Champagne, F.H. (1978): "The fine-scale structure of the turbulent velocity field". Journal of Fluid Mechanics, Vol. 86, pp. 67-108.

2. Eckelman, H. (1974): "The structure of the viscous sublayer and the adjacent wall region in a turbulent channel flow". J. Fluid Mech., vol. 65, p.439.

3. Hinze, J.O. (1959): Turbulence. McGraw-Hill.

4. Raichlen, F. (1967): "Some turbulence measurements in water". J. Eng. Mech. Proc. ASCE, p.73.

5. Raudkivi, A.J. and Callander, R.A. (1975). Advanced Fluid Mechanics. Edward Arnold.

6. Sumer, B.M. and Deigaard, R. (1981): "Particle motions near the bottom in turbulent flow in an open channel - Part 2". Journal of Fluid Mechanics, Vol. 109, pp. 311-337.

7. Sumer, B.M. and Oguz, B. (1978): "Particle motions near the bottom in turbulent flow in an open channel". Journal of Fluid Mechanics, Vol. 86, pp. 109-127.

Chapter 4

Diffusion and dispersion

Diffusion/dispersion is another important property of turbulent flows. Some examples are: (1) Waste products released into a recipient environment such as a stream or the ocean undergo rapid diffusion; (2) Smoke (or exhaust gases) released into the atmosphere diffuses rapidly when there is strong wind; (3) Likewise, dredged material (sand, silt, etc.), when dumped into the sea, is subjected to large diffusion.

The objective of this chapter is to describe the diffusion and dispersion processes in turbulent flows. First, we will study the diffusion process in a turbulent flow field (a general analysis), and then, we will turn our attention to the so-called longitudinal dispersion process, a process caused by the combined action of the turbulent diffusion and the velocity variation in the flow.

4.1 One-Particle analysis

Release a lump of dispersant into the flow in the form of an *instantaneous point source.* The point of release is $\mathbf{x} = 0$, and time $t = 0$ (Fig. 4.1). This dispersant will undergo diffusion as it is convected downstream, as sketched in Fig. 4.1.

(Note that we will use the term *dispersant* to refer to any kind of passive quantity such as waste products, suspended sediment, heat, etc. Also note that we assume that there is no interaction between the dispersant and the flow; the dispersant acts as a "passive" quantity).

The diffusion of the dispersant is caused by the following mechanism.

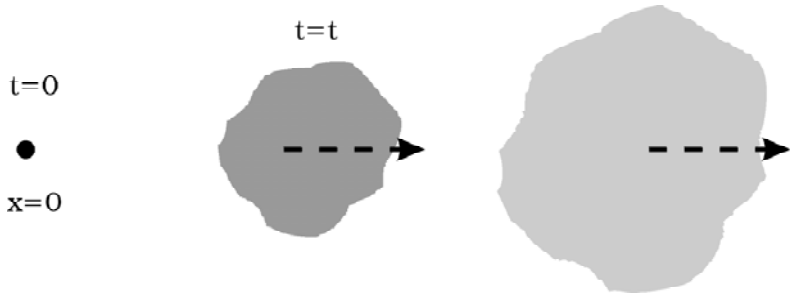

Figure 4.1: Definition sketch.

The instantaneous point source is actually formed by many dispersant particles. Since the flow is turbulent, each particle will follow a random path. This will cause the particles to get farther and farther apart as they travel (Fig. 4.2). The end result will be the continuous spreading (diffusion) of the dispersant, as sketched in Fig. 4.1.

The diffusion of a passive quantity can be studied by adopting one of the following two approaches.

1. Release the dispersant in the form of a lump at $\mathbf{x} = 0$ and at time $t = 0$; and follow the cloud of the dispersant as it "grows" and is convected downstream; or

2. Release one particle at $\mathbf{x} = 0$ and at time $t = 0$, and follow its path $\mathbf{x} = \mathbf{x}(t)$; Repeat this exercise many times, and determine the statistical properties of $\mathbf{x}(t)$. This approach is called the *one-particle analysis*.

In the following paragraphs, the latter approach will be adopted.

For simplicity, we shall study the process in *one dimension*.

The particles are released at $x = 0$, at time $t = 0$. They follow random paths $x(t)$. The objective of the analysis is to determine the statistical properties of $x(t)$. These statistical properties are (Fig. 4.3)

1. The mean value of x, namely $\overline{x}$; this will give the mean position of the dispersing cloud as it is convected downstream.

2. The variance of x, namely $\overline{(x - \overline{x})^2}$; this will give a measure of the degree of dispersion of the cloud.

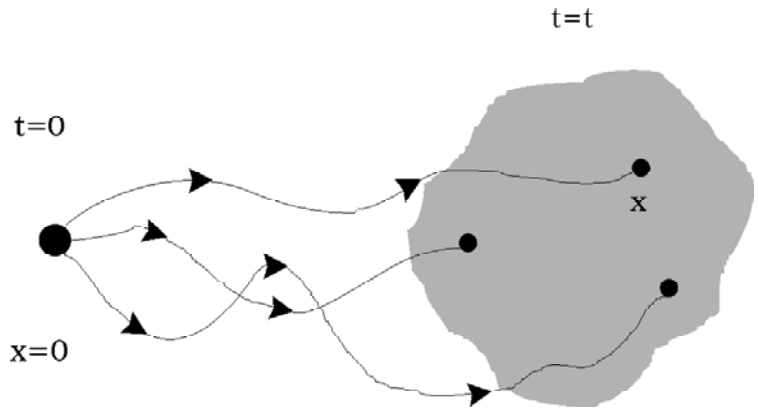

Figure 4.2: Random paths of particles.

3. Other statistical moments; and

4. The probability density function (p.d.f.) of the particle position, namely $p(x)$. This quantity is proportional to the concentration, as will be demonstrated later in the chapter.

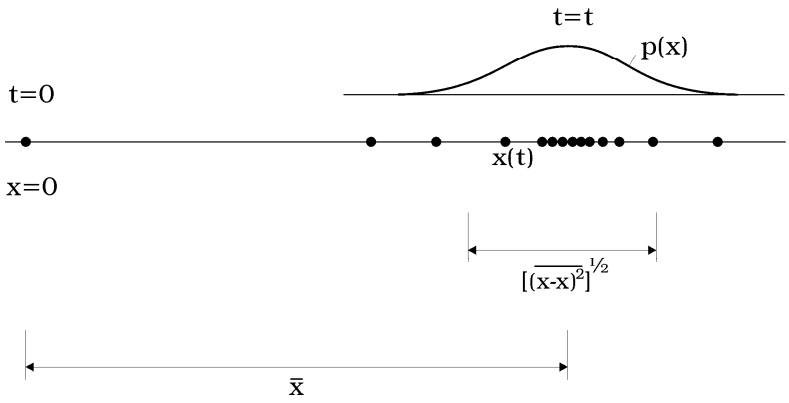

Figure 4.3: One-dimensional diffusion.

The particle velocity (the Lagrangian velocity):

$$V = \frac{dx}{dt} \tag{4.1}$$

Integrating gives

$$x(t) = \int_0^t V(t')\ dt' \tag{4.2}$$

Now, ensemble averaging gives the *mean* particle position (the position of the centroid of the particle cloud):

$$\overline{x(t)} = \overline{\int_0^t V(t')\ dt'} = \int_0^t \overline{V(t')}\ dt' \tag{4.3}$$

Here, the ensemble averaging is

$$\overline{\phi} = \frac{\sum_{n=1}^{N} \phi_n}{N} \tag{4.4}$$

in which ϕ is any hydrodynamic quantity, ϕ_n the value of ϕ in one realization, and N the total number of realizations. (In the present context, one realization is one release of particle).

The *variance*, on the other hand, can be calculated in the following way. Let

$$y(t) = x(t) - \overline{x(t)} \tag{4.5}$$

Then, from Eq. 4.2

$$\begin{aligned} y(t) &= x(t) - \overline{x(t)} = \int_0^t V(t')\ dt' - \int_0^t \overline{V(t')}\ dt' \\ &= \int_0^t [V(t') - \overline{V(t')}]\ dt' \end{aligned} \tag{4.6}$$

The integrand here is the fluctuating part of the particle velocity

$$V' = V - \overline{V} \tag{4.7}$$

Hence,

$$y(t) = \int_0^t V'(t')\ dt' \tag{4.8}$$

Differentiating $\overline{y^2(t)}$ with respect to t

$$\frac{d}{dt}\overline{y^2(t)} = 2\ \overline{y\frac{dy}{dt}} \tag{4.9}$$

and from Eq. 4.8

$$\begin{aligned} \frac{d}{dt}\overline{y^2(t)} &= 2\,\overline{[\int_0^t V'(t')\,dt']\,V'(t)} \\ &= 2\int_0^t \overline{V'(t')\,V'(t)}\,dt' \end{aligned} \tag{4.10}$$

The integrand in the preceding equation, $\overline{V'(t')\,V'(t)}$, recalling the Lagrangian correlation coefficient (Eq. 3.42):

$$\overline{V'(t')\,V'(t)} = \overline{V'^2}\frac{\overline{V'(t')V'(t)}}{\overline{V'^2}} = R_L(t-t')\,\overline{V'^2} \tag{4.11}$$

Then,

$$\frac{d}{dt}\overline{y^2(t)} = 2\,\overline{V'^2}\int_0^t R_L(t-t')\,dt' \tag{4.12}$$

To summarize at this point,

1. The mean particle position is given by Eq. 4.3; and
2. The variance of the particle position is given by Eq. 4.12.

Now, we will continue with the analysis for the following two extreme cases: (1) For small times ($t \ll T_L$); and (2) For large times ($t \gg T_L$) in which T_L is the Lagrangian macro time scale defined by

$$T_L = \int_0^\infty R_L(t)\,dt \tag{4.13}$$

(Eqs. 3.42 and 3.43). Recall that Lagrangian macro time scale, T_L, may be interpreted as the time during which a coherent structure keeps its "identity" / coherence (Section 3.2.2).

4.1.1 Diffusion for small times

For small times ($t \ll T_L$), the fluid particle keeps its identity/coherence, meaning that the particle velocity will be pretty much the same as that at the point where the particle starts its travel, namely at $x = 0$ at time $t = 0$. This velocity is the Eulerian velocity at $x = 0$:

$$V(t) \simeq V(t=0) \equiv u(x=0) \tag{4.14}$$

Now, the mean particle position, from Eq. 4.3:

$$\overline{x(t)} = \int_0^t \overline{V(t')}\, dt' = \int_0^t \overline{u(x=0)}\, dt' = \overline{u(x=0)} \int_0^t dt' = \overline{u(x=0)}\, t \tag{4.15}$$

Regarding the variance, for small times ($t \ll T_L$), first of all, $\overline{V'^2} \simeq \overline{u'^2(x=0)}$, and secondly, $R_L(t-t') \simeq 1$. Therefore, Eq. 4.12

$$\frac{d}{dt}\overline{y^2(t)} = 2\ \overline{u'^2(x=0)}\ t$$

and integrating gives

$$\overline{y^2(t)} = \overline{u'^2(x=0)}\ t^2 \tag{4.16}$$

Now, assume that the flow/turbulence is *homogenous*. Then the statistical properties of velocity should be invariant with respect to the position:

$$\overline{u(x=0)} \equiv \overline{u(x)} = \overline{u} = \text{ constant} \tag{4.17}$$

and

$$\overline{u'^2(x=0)} \equiv \overline{u'^2(x)} = \overline{u'^2} = \text{ constant} \tag{4.18}$$

Thus, the mean particle position and the variance will be (from Eqs. 4.15, 4.16, 4.17, 4.18)

$$\overline{x(t)} = \overline{u}\ t \tag{4.19}$$

and

$$\overline{y^2(t)} = \overline{u'^2}\ t^2 \tag{4.20}$$

The p.d.f. of the particle position, on the other hand, will be the same as that of the Eulerian velocity provided that u should be replaced with $\frac{x}{t}$.

4.1.2 Diffusion for large times

Mean and variance of particle position.

For large times ($t \gg T_L$), the analysis will be developed further for the following special case. Namely, the particle velocity is a stationary random function (s.r.f.) of time.

(The particle velocity is a s.r.f. of time if the probability density function of particle velocity is invariant with respect to time, i.e.,

$$p[V(t)] \equiv p[V(t+\tau)] \tag{4.21}$$

meaning that the statistical properties of the particle velocity such as the mean $\overline{V}$ and the variance $\overline{(V-\overline{V})^2} = \overline{V'^2}$ are time invariant. Homogeneity in space is equivalent to being stationary in time).

First, consider the mean particle position. From Eq. 4.3 (taking $\overline{V(t')}$ outside the integral because it is constant),

$$\overline{x(t)} = \int_0^t \overline{V(t')}\, dt' = \overline{V}\, t \tag{4.22}$$

The mean particle velocity should be equal to the Eulerian mean velocity, $\overline{u}$. (The fact that the Lagrangian velocity is a stationary random function of time requires the homogeneity in the Eulerian sense; therefore, $\overline{V} \equiv \overline{u}$). Hence,

$$\overline{x(t)} = \overline{u}\, t \tag{4.23}$$

Next, consider the variance of the particle position. Eq. 4.12:

$$\frac{d}{dt}\overline{y^2(t)} = 2\, \overline{V'^2} \int_0^t R_L(t-t')\, dt' \tag{4.24}$$

Change the notation

$$\xi = t - t' \tag{4.25}$$

then Eq. 4.24 will be

$$\frac{d}{dt}\overline{y^2(t)} = 2\, \overline{V'^2} \int_{\xi=0}^t R_L(\xi)\, d\xi \tag{4.26}$$

Integrating by parts gives

$$\overline{y^2(t)} = 2\, \overline{V'^2}\left(\int_{\xi=0}^t R_L(\xi)\, d\xi\right) t - 2\overline{V'^2} \int_{\xi=0}^t \xi R_L(\xi)\, d\xi \tag{4.27}$$

For large times ($t \gg T_L$), t is so large that the integrals in the preceding equation converge (provided, of course, that the form of $R_L(\xi)$ is such that the integrals do converge). Furthermore, the second term on the right hand side is small compared with the first term. Hence, for large times,

$$\overline{y^2(t)} = 2\, \overline{V'^2}\left(\int_{\xi=0}^t R_L(\xi)\, d\xi\right) t \tag{4.28}$$

The integral for large times can be approximated to

$$\int_{\xi=0}^{t} R_L(\xi)\ d\xi \simeq \int_{\xi=0}^{\infty} R_L(\xi)\ d\xi = T_L \tag{4.29}$$

(from Eq.4.13). Inserting the latter equation in Eq. 4.28, and also considering that $\overline{V'^2}$ is identically equal to $\overline{u'^2}$ (due to the fact that $V(t)$ is a stationary random function of time), the variance is obtained as

$$\overline{y^2(t)} = 2\ \overline{u'^2} T_L\ t \tag{4.30}$$

(As will be detailed in the following paragraphs, this is diffusion because $\overline{y^2(t)} \sim t$).

To summarize, the mean particle position and the variance are given by Eqs. 4.23 and 4.30, respectively.

As seen from Eqs. 4.20 and 4.30, the variance is

$$\overline{y^2(t)} \sim t^2 \text{ for small times } (t \ll T_L) \tag{4.31}$$

and

$$\overline{y^2(t)} \sim t \text{ for large times } (t \gg T_L) \tag{4.32}$$

This implies that the spreading occurs very fast in the beginning of the process ($\overline{y^2(t)} \sim t^2$), and then the rate at which the spreading occurs reaches an equilibrium stage where $\overline{y^2(t)} \sim t$, as sketched in Fig. 4.4.

P.d.f. of particle position.

The particle displacement (Eq. 4.2)

$$x(t) = \int_0^t V(t')\ dt'$$

can be considered as the sum of a series integral over a fixed interval, say τ,

$$x(t) = \int_0^t V(t')\ dt' = \sum_n \int_{n\tau}^{(n+1)\tau} V(t')\ dt' \tag{4.33}$$

such that each integral has only a partial statistical connection with each other. For times $t \gg T_L$, the number of such integrals becomes sufficiently large so that we have a situation like that covered by the central limit theorem.

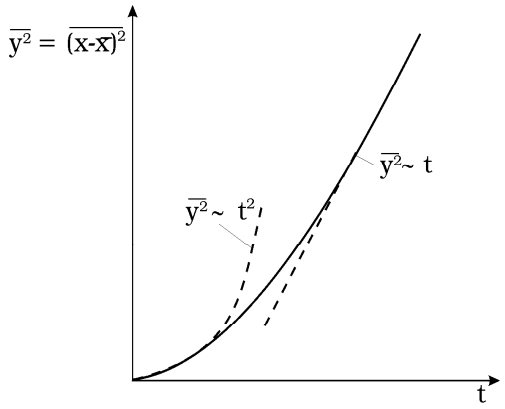

Figure 4.4: Variance of particle position.

The central limit theorem states that *for a series of statistically independent terms, the p.d.f. of the sum tends to the Gaussian distribution (normal distribution), as the number of terms approaches infinity, irrespective of the probability distributions of each term, which form the sum.*

Therefore, for large times $t \gg T_L$, the p.d.f. of $x(t)$ will be

$$p(x) = \frac{1}{\sqrt{2\pi}\ \sqrt{\overline{(x-\overline{x})^2}}} \exp(-\frac{(x-\overline{x})^2}{2\overline{(x-\overline{x})^2}}) \tag{4.34}$$

or, for convenience, changing the notation to $y = x - \overline{x}$,

$$p(y) = \frac{1}{\sqrt{2\pi}\ \sqrt{\overline{y^2}}} \exp(-\frac{y^2}{2\ \overline{y^2}}) \tag{4.35}$$

Inserting Eq. 4.30 in the preceding equation,

$$p(y) = \frac{1}{\sqrt{2\pi}\ \sqrt{2\ \overline{u'^2} T_L\ t}} \exp(-\frac{y^2}{2\ (2\ \overline{u'^2} T_L\ t)}) \tag{4.36}$$

We shall return to this equation later in the section.

Now, consider the diffusion equation

$$\frac{\partial c}{\partial t} = D \frac{\partial^2 c}{\partial y^2} \tag{4.37}$$

in which D is the diffusion coefficient, y the space coordinate, and t the time. Consider the initial condition

$$t = 0 : \qquad c = \delta(y) \tag{4.38}$$

in which $\delta(y)$ is the Dirac delta function, which is defined by

$$\begin{aligned} \delta(y) &= 0 \text{ for } y \neq 0 \\ \delta(y) &= \infty \text{ for } y = 0 \end{aligned}$$

and

$$\int_{-\infty}^{\infty} \delta(y) dy = 1$$

The solution to the diffusion equation with the above initial condition is

$$c(y) = \frac{1}{\sqrt{2\pi}\ \sqrt{2Dt}} \exp(-\frac{y^2}{2\ (2\ D\ t)}) \tag{4.39}$$

Now, compare the above equation with Eq. 4.36. From this comparison, the following deductions can be made:

1. The p.d.f. of the particle position for large times ($t \gg T_L$) satisfies the diffusion equation (cf., 4.37)

$$\frac{\partial p}{\partial t} = D \frac{\partial^2 p}{\partial y^2} \tag{4.40}$$

2. The diffusion coefficient of the diffusion process is

$$D = \overline{u'^2} T_L \tag{4.41}$$

which can, from Eq. 4.30, also be written as

$$D = \overline{u'^2} T_L = \frac{1}{2} \frac{d\overline{y^2(t)}}{dt} \tag{4.42}$$

D is called the turbulent diffusion coefficient.

The theory summarized in the preceding paragraphs was developed by G.I. Taylor (1921). It was later extended to the three-dimensional case

by Batchelor (1949). For further reading, consult Batchelor and Townsend (1956) and Monin and Yaglom (1973).

Flux due to turbulent diffusion.

The probability that a particle is present in the interval $(y, y + dy)$

$$\Pr[y < Y < y + dy] = \frac{m}{M} \tag{4.43}$$

where M is the total number of released particles, and m is the number of particles occupying the interval $(y, y + dy)$.

This probability can also be written as

$$\Pr[y < Y < y + dy] = p(y)\ dy \tag{4.44}$$

From the preceding two equations, one gets

$$p(y) = \frac{1}{M}\frac{m}{dy} \tag{4.45}$$

Here, $\frac{m}{dy}$, the number of particles per unit length, is the concentration $\overline{c}$ in the one-dimensional case. So,

$$p(y) = \frac{\overline{c}(y)}{M} \tag{4.46}$$

Now, the probability that a particle is present in the half space $(-\infty, y)$ is

$$\Pr[-\infty < Y < y] = \frac{m_1}{M} \tag{4.47}$$

in which m_1 is the number of particles occupying the interval $(-\infty, y)$. Likewise, this probability can be written as

$$\Pr[-\infty < Y < y] = \int_{-\infty}^{y} p(y)\ dy \tag{4.48}$$

Then from Eqs. 4.47 and 4.48

$$m_1 = M \int_{-\infty}^{y} p(y)\ dy \tag{4.49}$$

Differentiate the above equation with respect to time

$$-\frac{\partial m_1}{\partial t} = -M\frac{\partial}{\partial t}\int_{-\infty}^{y} p(y)\ dy \tag{4.50}$$

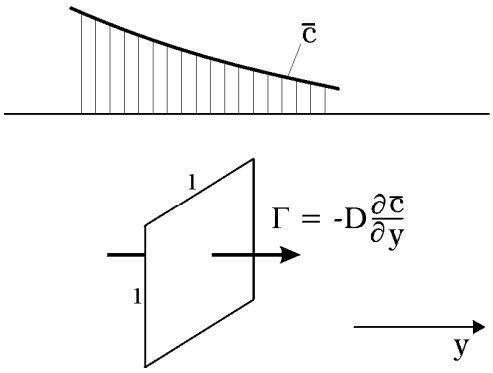

Figure 4.5: Flux due to turbulent diffusion.

Here $-\frac{\partial m_1}{\partial t}$ is the rate of change in the number of the particles which occupy the region $(-\infty, y)$, i.e., the decrease in the number of particles in the region $(-\infty, y)$ per unit time. This means that there is a continuous supply of particles from the region $(-\infty, y)$ to the region $(y, +\infty)$ at a rate $-\frac{\partial m_1}{\partial t}$, i.e., the number of particles passing through the section y per unit time is $-\frac{\partial m_1}{\partial t}$.

The expression for $p(y)$ is given in Eq. 4.35. Substituting this equation in Eq. 4.50, and integrating and then differentiating with respect to time gives

$$-\frac{\partial m_1}{\partial t} = M \, \frac{y}{2t} \, p(y) \tag{4.51}$$

Differentiating Eq. 4.35 with respect to y, on the other hand, gives

$$\frac{\partial p}{\partial y} = -\frac{y}{2Dt} \, p(y) \tag{4.52}$$

From the preceding two equations,

$$-\frac{\partial m_1}{\partial t} = -MD\frac{\partial p}{\partial y}$$

or

$$-\frac{\partial m_1}{\partial t} = -D\frac{\partial (Mp)}{\partial y} \tag{4.53}$$

From Eq. 4.46, $\overline{c} = Mp$. Inserting this in the above equation gives

$$-\frac{\partial m_1}{\partial t} = -D\frac{\partial \overline{c}}{\partial y} \tag{4.54}$$

Changing notation

$$\Gamma = -\frac{\partial m_1}{\partial t}$$

then Eq. 4.54

$$\Gamma = -D\frac{\partial \overline{c}}{\partial y} \tag{4.55}$$

The quantity Γ, the number of particles passing through the section y per unit time (Fig. 4.5), is called the *flux (*the *flux due to turbulent diffusion).* Notice the similarity between the flux due to turbulent diffusion and that due to molecular diffusion, namely $\Gamma_{mol} = -D_{mol}\frac{\partial c}{\partial y}$ (Fick's law) in which D_{mol} is the molecular diffusion coefficient.

Example 10 *Conservation of mass in turbulent flows*

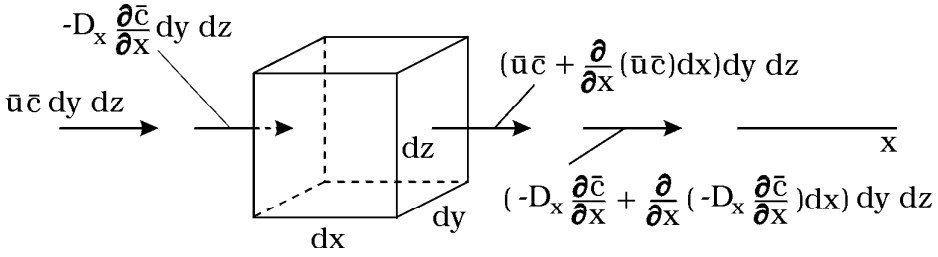

Figure 4.6: Definition sketch.

Consider the fluid element $dx\ dy\ dz$ in Fig. 4.6. The influx of mass in the $x-$ direction is

$$\overline{u}\ \overline{c}\ dy\ dz \qquad \text{(due to convection)} \tag{4.56}$$

and

$$-D_x\ \frac{\partial \overline{c}}{\partial x}\ dy\ dz \qquad \text{(due to turbulent diffusion)} \tag{4.57}$$

(from Eq. 4.55).

The efflux, on the other hand,

$$[\overline{u}\ \overline{c}\ + \frac{\partial}{\partial x}(\overline{u}\ \overline{c})\ dx]\ dy\ dz \qquad \text{(due to convection)} \tag{4.58}$$

and

$$[-D_x \frac{\partial \overline{c}}{\partial x} + \frac{\partial}{\partial x}(-D_x \frac{\partial \overline{c}}{\partial x})\, dx]\, dy\, dz \qquad \text{(due to turbulent diffusion)} \quad (4.59)$$

Thus the net influx in the $x-$ direction is

$$-\frac{\partial}{\partial x}(\overline{u}\,\overline{c})\, dx\, dy\, dz - \frac{\partial}{\partial x}(-D_x \frac{\partial \overline{c}}{\partial x})\, dx\, dy\, dz \quad (4.60)$$

Similar expressions for the $y-$ and $z-$ directions:

$$-\frac{\partial}{\partial y}(\overline{v}\,\overline{c})\, dx\, dy\, dz - \frac{\partial}{\partial y}(-D_y \frac{\partial \overline{c}}{\partial y})\, dx\, dy\, dz \quad (4.61)$$

$$-\frac{\partial}{\partial z}(\overline{w}\,\overline{c})\, dx\, dy\, dz - \frac{\partial}{\partial z}(-D_z \frac{\partial \overline{c}}{\partial z})\, dx\, dy\, dz \quad (4.62)$$

On the other hand, the rate of change of mass in the volume $dx\ dy\ dz$

$$\frac{\partial}{\partial t}(\overline{c}\, dx\, dy\, dz) \quad (4.63)$$

The conservation of mass requires that the rate of change of mass should be equal to the net influx. Hence, from Eqs. 4.60-4.63, and using the continuity equation (Eq. 1.6), namely

$$\frac{\partial \overline{u}}{\partial x} + \frac{\partial \overline{v}}{\partial y} + \frac{\partial \overline{w}}{\partial z} = 0 \quad (4.64)$$

one gets

$$\frac{\partial \overline{c}}{\partial t} + \overline{u}\frac{\partial \overline{c}}{\partial x} + \overline{v}\frac{\partial \overline{c}}{\partial y} + \overline{w}\frac{\partial \overline{c}}{\partial z} = \frac{\partial}{\partial x}(D_x \frac{\partial \overline{c}}{\partial x}) + \frac{\partial}{\partial y}(D_y \frac{\partial \overline{c}}{\partial y}) + \frac{\partial}{\partial z}(D_z \frac{\partial \overline{c}}{\partial z}) \quad (4.65)$$

or, in index notation

$$\frac{\partial \overline{c}}{\partial t} + \overline{u_i}\frac{\partial \overline{c}}{\partial x_i} = \frac{\partial}{\partial x_i}(D_{\underline{i}} \frac{\partial \overline{c}}{\partial x_i}) \quad (4.66)$$

and including the molecular diffusion effect as well

$$\frac{\partial \overline{c}}{\partial t} + \overline{u_i}\frac{\partial \overline{c}}{\partial x_i} = \frac{\partial}{\partial x_i}(D_{\underline{i}} + D_{mol}) \frac{\partial \overline{c}}{\partial x_i}) \quad (4.67)$$

However, note that, normally, $D_{mol} \ll D_{\underline{i}}$.

4.2 Longitudinal dispersion

4.2.1 Mechanism of longitudinal dispersion

The mechanism of longitudinal dispersion may be best described by reference to an open-channel flow, Fig. 4.7. Release a lump of dispersant in the form of a point source at section $x = 0$ and $t = 0$. Consider that the released dispersant is formed by many particles. Now, these particles are subject to two effects:

1. The turbulent motion in the $y-$ direction; Under this effect, the particles travel up and down in a random fashion.

2. The streamwise motion in the $x-$ direction. The particles take the velocity $\overline{u}(y)$, plus a small fluctuating velocity u'. (However, the latter is negligible with respect to the former).

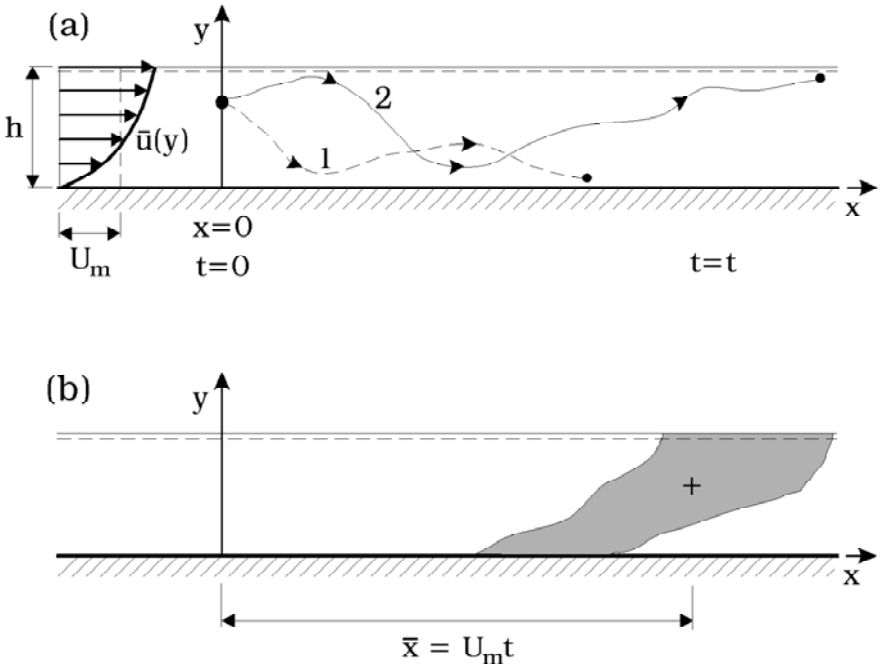

Figure 4.7: Longitudinal dispersion.

Particles near the bottom will experience relatively smaller velocities $\overline{u}(y)$, and therefore will be retarded (Path 1 in Fig. 4.7 a) while particles near the free surface will experience relatively larger velocities $\overline{u}(y)$, and therefore will be moved large distances (Path 2 in Fig. 4.7 a). This implies that the particles are prone to disperse farther and farther apart in the streamwise direction. Thus, the end result will be the progressive dispersion of the dispersant in the streamwise direction, as sketched in Fig. 4.7 b. This process is called the *longitudinal dispersion.*

When compared with the ordinary diffusion process studied in the previous section (cf., Fig. 4.1 and 4.2), the key effect here is that the dispersion is caused mainly by the velocity variation $\overline{u}(y)$ across the depth, whereas the dispersion in the ordinary diffusion process is caused by the random paths of particles; no spatial variation in the mean velocity exists in the latter process.

For the above reason, the present diffusion process is sometimes called the mechanical dispersion.

From the preceding considerations, it can easily be seen that

1. there will be no longitudinal dispersion, when the velocity distribution across the depth is uniform; and

2. likewise, there will be no longitudinal dispersion when there is no turbulent motion across the depth (i.e., when there is no turbulent diffusion across the depth). (Note, however, that the existing molecular diffusion will cause longitudinal dispersion although the degree of dispersion in this case is several orders of magnitude smaller than the turbulent longitudinal dispersion, Taylor, 1953, 1954, Elder, 1959).

4.2.2 Application of one-particle analysis

Fig. 4.8 shows the path of a particle. Here, $V(t)$ is the streamwise velocity of the particle. $V(t)$ is actually the sum of two velocities:

1. the velocity $\overline{u}(y)$ at the position where the particle is at that particular time t, and

2. the $x-$ component of the fluctuating velocity u', which occurs at that position, and at that particular time, t.

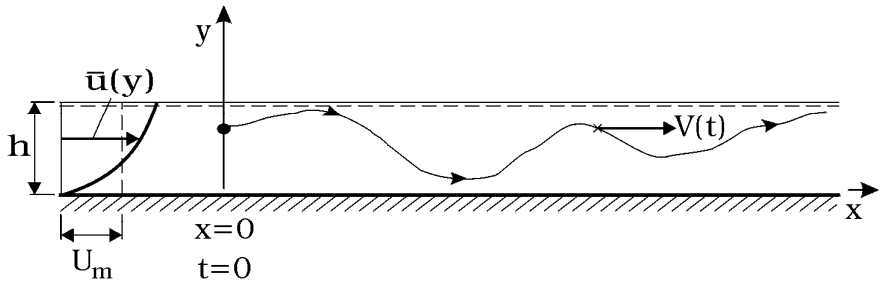

Figure 4.8: Particle velocity V samples from the velocity profile $\overline{u}(y)$.

The fluctuating velocity is small compared with $\overline{u}(y)$, and therefore can be neglected, as already stated in the preceding paragraphs. Hence, the particle velocity can be taken as $V(t) = \overline{u}(y(t))$.

Now, release many particles at time $t = 0$, and determine their velocities, $V(t)$, at time t. Let the probability density function (p.d.f.) of these velocities be $p(V(t))$. Next, do the same exercise, but this time determine their velocities at time $t + \tau$. Let the p.d.f. of the latter velocities be $p(V(t + \tau))$. Now, if t is sufficiently large, then the two p.d.f.s will be identical

$$p(V(t)) \equiv p(V(t + \tau)) \tag{4.68}$$

This implies that the velocity $V(t)$ is a stationary random function of time (Section 4.1.2).

The immediate implication of this is that the theory given in the previous section in conjunction with the ordinary diffusion process for large times (Section 4.1.2) can be applied to the present process because, as in the previous case, the particle velocity is a stationary random function of time. By application of the one-particle analysis, we reach the following conclusions.

1. The mean particle position (or the position of the centroid of the dispersant) will be at (Fig. 4.7 b)

$$\overline{x}(t) = U_m t \tag{4.69}$$

(from Eq. 4.23). Here, U_m is the mean Eulerian velocity, and equal to the cross-sectional average velocity (Fig. 4.8)

$$U_m = \frac{1}{h} \int_0^h \overline{u}(y)\ dy \tag{4.70}$$

2. The variance will be

$$\overline{(x-\overline{x})^2} = 2\,\overline{V'^2} T_{L1}\; t \tag{4.71}$$

(from Eq. 4.30). Here T_{L1} is the Lagrangian time scale defined by

$$T_{L1} = \int_0^\infty R_{L1}(t)\; dt \tag{4.72}$$

in which $R_{L1}(t)$ is the Lagrangian correlation coefficient

$$R_{L1}(t) = \frac{\overline{V'(\tau)V'(\tau+t)}}{\overline{V'^2}} \tag{4.73}$$

in which

$$V' = V - U_m \tag{4.74}$$

Here, the subindex 1 is used to distinguish the present application from the ordinary diffusion.

3. The p.d.f. of the particle position tends to the Gaussian (normal) distribution for large times ($t \gg T_{L1}$):

$$p(x) = \frac{1}{\sqrt{2\pi}\;\sqrt{\overline{(x-\overline{x})^2}}} \exp(-\frac{(x-\overline{x})^2}{2\overline{(x-\overline{x})^2}}) \tag{4.75}$$

(from Eq. 4.34).

4. The diffusion coefficient of the process is

$$D_1 = \overline{V'^2} T_{L1} = \frac{1}{2}\frac{d\overline{(x-\overline{x})^2}}{dt} \tag{4.76}$$

(from Eq. 4.42). Here, D_1 is called the *longitudinal dispersion coefficient.*

5. The p.d.f. of particle position satisfies the diffusion equation

$$\frac{\partial p}{\partial t} = D_1 \frac{\partial^2 p}{\partial (x-\overline{x})^2} \tag{4.77}$$

(from Eq. 4.40). Here, $\frac{\partial}{\partial t}$ is the time derivative when considering the moving coordinate $x - \overline{x}(t)$. Changing to the fixed coordinate x,

$$\frac{\partial}{\partial t} = \frac{\partial}{\partial t} + \frac{\partial}{\partial x}\frac{\partial x}{\partial t} = \frac{\partial}{\partial t} + \frac{\partial \overline{x}(t)}{\partial t}\frac{\partial}{\partial x} = \frac{\partial}{\partial t} + U_m\frac{\partial}{\partial x} \tag{4.78}$$

Then, Eq. 4.77 becomes

$$\frac{\partial p}{\partial t} + U_m\frac{\partial p}{\partial x} = D_1\frac{\partial^2 p}{\partial x^2} \tag{4.79}$$

6. From Eqs. 4.79 and 4.46

$$\frac{\partial < c >}{\partial t} + U_m\frac{\partial < c >}{\partial x} = D_1\frac{\partial^2 < c >}{\partial x^2} \tag{4.80}$$

in which $< c >$ is the cross-sectional average concentration:

$$< c >= \frac{1}{h}\int_0^h \overline{c}\ dy \tag{4.81}$$

Eq. 4.80 is called the *dispersion equation.*

The above analysis shows that the longitudinal dispersion process is represented by a one-dimensional diffusion equation with constant coefficients U_m and D_1 (Eq. 4.80). The process is also governed by the general diffusion equation (Eq. 4.65):

$$\frac{\partial \overline{c}}{\partial t} + \overline{u}\frac{\partial \overline{c}}{\partial x} + \overline{v}\frac{\partial \overline{c}}{\partial y} = \frac{\partial}{\partial x}(D_x\ \frac{\partial \overline{c}}{\partial x}) + \frac{\partial}{\partial y}(D_y\ \frac{\partial \overline{c}}{\partial y}) \tag{4.82}$$

Clearly, the one-dimensional equation (Eq. 4.80) is much simpler than the two-dimensional representation (Eq. 4.82). (This is the advantage of the longitudinal-dispersion concept). Obviously, this is at the expense of the calculated concentration. In the one-dimensional representation, the cross-sectional average concentration is calculated, whereas, in the two-dimensional representation, the point-concentration is calculated. However, this is not a problem, because, in longitudinal-dispersion problems, the calculation with the cross-sectional average concentration is normally good enough (the concentration variations in the longitudinal direction are important, not the variations over the cross section).

For the application of the previously mentioned one-dimensional dispersion equation, two quantities need to be known: the cross-sectional average velocity, U_m, and the longitudinal dispersion coefficient, D_1.

U_m is obtained simply by integrating the velocity distribution over the cross-section, and dividing it by the cross-sectional area. This is done if the velocity distribution is known theoretically (for ex., in the form of the logarithmic law). Otherwise, the velocity distribution over the cross-section is measured, for example, as in the case of a natural stream, and the mean velocity calculation is based on the measured velocity.

The longitudinal dispersion coefficient, on the other hand, can be calculated theoretically (see the next section), or it can be calculated numerically, based on the measured velocity distribution over the cross section, as will be detailed in Section 4.4.

G.I. Taylor (1953, 1954) introduced the concept of the longitudinal dispersion. In his study, the flow environment was a circular pipe. His theoretical work and his experiments showed that the longitudinal dispersion coefficient in a turbulent pipe flow (Taylor, 1954) is $\frac{D_1}{aU_f} = 10$ in which a is the radius of the pipe, and U_f is the friction velocity. Taylor's work laid the groundwork for the later research in 1960s and 70s in the area of dispersion in natural streams, estuaries, etc. and also in industrial flows (such as pipe flows).

4.3 Calculation of dispersion coefficient

In this section, we shall calculate the longitudinal dispersion coefficient for an open channel flow (Fig. 4.7). We shall do this exercise for heavy particles (for example, sand, or silt in water). This feature will be represented by the fall velocity of the particles, w. However, the case of the neutrally-buoyant particles/dispersant will be captured by setting w equal to zero in the end solutions.

The analysis presented in the following paragraphs is mainly based on the work of Sumer (1974). It may be noted that the method used in the analysis was first introduced by Aris (1956) and also employed by Sayre (1968).

4.3.1 Formulation

The conservation of mass (Fig. 4.7) from Eq. 4.65:

$$\frac{\partial \overline{c}}{\partial t} + \overline{u}(y)\frac{\partial \overline{c}}{\partial x} - w\frac{\partial \overline{c}}{\partial y} = \frac{\partial}{\partial x}(\epsilon(y)\frac{\partial \overline{c}}{\partial x}) + \frac{\partial}{\partial y}(\epsilon(y)\frac{\partial \overline{c}}{\partial y}) \tag{4.83}$$

in which w is the fall velocity of the particles, and $\epsilon(y)$ is the turbulent diffusion coefficient. It is assumed that $\epsilon(y)$ is the same for both $x-$ and $y-$ directions.

The boundary conditions:

$$y = 0 \text{ and } h: \qquad \epsilon(y)\frac{\partial \overline{c}}{\partial y} + w\overline{c} = 0 \tag{4.84}$$

implying that there is no net transport across the boundaries.

The initial condition is (for a uniformly distributed plane source)

$$t = 0: \qquad \overline{c}(x, y, 0) = \frac{M}{h}\delta(x) \tag{4.85}$$

in which M is the total number of particles released into the flow.

Furthermore, we write

$$\overline{u}(y) = U_m(1 + \chi(y)), \text{ and } \epsilon(y) = D_m\psi(y) \tag{4.86}$$

in which U_m and D_m are the cross-sectional average velocity and the cross-sectional average diffusion coefficient, respectively. We shall return to these quantities and the nondimensional functions $\chi(y)$ and $\psi(y)$ later in the section.

Now, define the pth moment of concentration

$$C_p = \int_{-\infty}^{\infty} \xi^p C d\xi \tag{4.87}$$

in which ξ is the normalized streamwise distance defined by

$$\xi = \frac{x - U_s t}{h} \tag{4.88}$$

in which U_s is the mean particle velocity, and C is the normalized concentration defined by

$$C = \frac{\overline{c}}{\frac{M}{h^2}} \tag{4.89}$$

Now, multiply the two sides of the above equations (Eqs. 4.83-4.85) by ξ^p, and integrate the equations from $-\infty$ to $+\infty$:

$$\frac{\partial C_p}{\partial \tau} - (\mu - \mu_s + \mu\chi)pC_{p-1} - \nu_s \frac{\partial C_p}{\partial \eta} = p(p-1)\psi C_{p-2} + \frac{\partial}{\partial \eta}(\psi \frac{\partial C_p}{\partial \eta}) \quad (4.90)$$

$$\eta = 0 \text{ and } 1: \qquad \psi \frac{\partial C_p}{\partial \eta} + \nu_s C_p = 0 \quad (4.91)$$

and

$$\tau = 0: \qquad C_p(\eta, 0) = 1 \text{ and } 0, \text{ respectively, for } p = 0 \text{ and } p > 0 \quad (4.92)$$

Here,

$$\eta = \frac{y}{h}, \ \tau = \frac{D_m t}{h^2} \quad (4.93)$$

are the normalized distance from the bottom of the channel and the normalized time, respectively. Also, μ, μ_s and ν_s are the normalized mean flow velocity, the normalized mean particle velocity and the normalized mean fall velocity, respectively:

$$\mu = \frac{U_m h}{D_m}, \ \mu_s = \frac{U_s h}{D_m}, \ \nu_s = \frac{wh}{D_m} \quad (4.94)$$

Regarding the flow velocity, $\overline{u}(y)$, and turbulent diffusion coefficient, $\epsilon(y)$, distributions across the depth, first of all, from Eq. 2.85,

$$\overline{u} - U_m = \frac{1}{\varkappa} U_f [\ln(\frac{y}{h}) + 1] \quad (4.95)$$

(the logarithmic law). The distribution of the turbulent diffusion coefficient, on the other hand, is found from the analogy between the momentum flux (Eq. 2.89) and the flux due to turbulent diffusion

$$\epsilon = \frac{-\Gamma}{\frac{d\overline{c}}{dy}} = \frac{-\rho\overline{u'v'}}{\rho\frac{d\overline{u}}{dy}} \quad (4.96)$$

Taking $-\rho\overline{u'v'} \simeq \rho U_f^2(1 - \frac{y}{h})$ (see Eq. 2.21), and using the above analogy (Eq. 4.96), the diffusion coefficient

$$\epsilon(y) = \varkappa U_f \ y(1 - \frac{y}{h}) \quad (4.97)$$

and D_m is

$$D_m = \frac{1}{h}\int_0^h \epsilon(y)\ dy = \frac{1}{6}\varkappa h U_f \tag{4.98}$$

The functions $\chi(y)$ and $\psi(y)$ in Eqs. 4.86 are then

$$\mu\chi = \frac{6}{\varkappa^2}(1+\ln\eta),\ \text{and}\ \psi = 6\eta(1-\eta) \tag{4.99}$$

4.3.2 Zeroth moment of concentration

For $p = 0$, the solution to the Eqs. 4.90-4.92 is found to be as follows

$$C_0 = \frac{\sin(\pi\beta)}{\pi\beta}(\frac{1-\eta}{\eta})^\beta + \sum_{K=1}^{\infty} a_K(\frac{1-\eta}{\eta})^\beta F(-K, 1+K; 1-\beta; \eta)\exp\{-6(K^2+K)\tau\} \tag{4.100}$$

in which a_K

$$a_K = \frac{(2K+1)\ \Gamma(K+1-\beta)}{\Gamma^2(1-\beta)\ \Gamma(K+1+\beta)}\ {}_3F_2(-K, K+1, 1; 1-\beta, 2; 1) \tag{4.101}$$

F is a hypergeometric function, ${}_3F_2$ is a generalized hypergeometric series, and Γ is the Gamma function (Gradshteyn and Ryzhik, 1965). The quantity β here is the fall velocity parameter defined by

$$\beta = \frac{\nu_s}{6} = \frac{w}{\varkappa U_f} \tag{4.102}$$

and the solution is found for $\beta \neq 0$, $\beta < 1$.

Fig. 4.9 displays $C_0(\eta, \tau)$ for two values of β. Note that the physical meaning of C_0 is that C_0 is identical to the p.d.f. of the particle position across the depth. As seen from the figure, the larger the value of β, the more weighted the distributions towards the bottom, as expected.

From Eq. 4.100

$$C_0(\eta) = \frac{\sin(\pi\beta)}{\pi\beta}(\frac{1-\eta}{\eta})^\beta \qquad \text{as} \qquad \tau \to \infty \tag{4.103}$$

Sumer (1974) argues that, for the case of neutrally buoyant particles ($\beta = 0$), C_0 should go to unity, $C_0 \to 1$. Indeed the above equation reveals this.

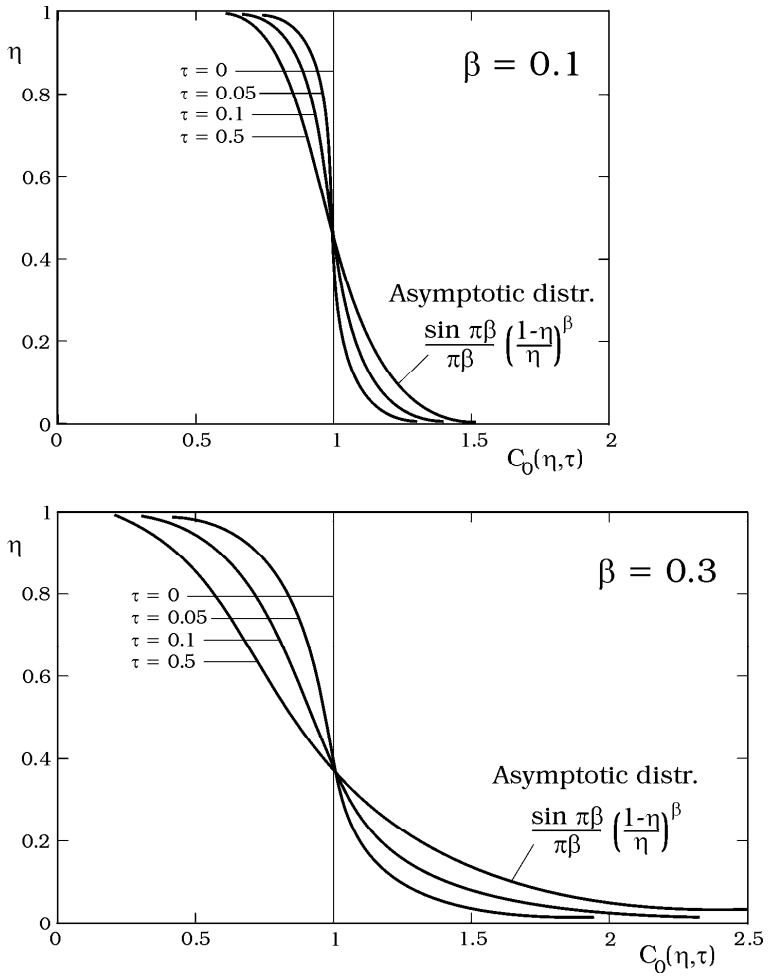

Figure 4.9: $C_0(\eta, \tau)$ for two different sediment with (a): $\beta = \frac{w}{\kappa U_f} = 0.1$, and (b): $\beta = \frac{w}{\kappa U_f} = 0.3$. Sumer (1974).

4.3.3 Mean particle velocity

For this, we define

$$m_p = \int_0^1 C_p \, d\eta \tag{4.104}$$

Now, integrate Eqs. 4.90 and 4.92 from $\eta = 0$ to 1, and using the boundary conditions (Eq. 4.91),

$$\frac{dm_p}{d\tau} - p \int_0^1 (\mu - \mu_s + \mu\chi) C_{p-1} \, d\eta - p(p-1) \int_0^1 \psi C_{p-2} \, d\eta = 0 \tag{4.105}$$

$$\tau = 0: \qquad m_p(0) = 1 \text{ and } 0, \text{ respectively, for } p = 0 \text{ and } p > 0 \tag{4.106}$$

Now, the preceding two equations for $p = 1$

$$\frac{dm_1}{d\tau} - \int_0^1 (\mu - \mu_s + \mu\chi) C_0 \, d\eta = 0 \tag{4.107}$$

and

$$m_1(0) = 0 \text{ at } \tau = 0 \tag{4.108}$$

Note that m_1 represents the mean particle displacement relative to the ξ axis, and $\frac{dm_1}{d\tau}$ represents the mean particle velocity relative to this axis. Since this axis moves with the mean particle velocity (Eq. 4.88), then $\frac{dm_1}{d\tau} \to 0$ as time $\tau \to \infty$. Hence, from Eq. 4.107, for large times

$$- \int_0^1 (\mu - \mu_s + \mu\chi) C_0(\eta, \infty) \, d\eta = 0$$

or, from Eq. 4.103,

$$\mu_s - \mu = \int_0^1 \mu\chi \; C_0(\eta, \infty) \, d\eta = \int_0^1 \mu\chi \frac{\sin(\pi\beta)}{\pi\beta} \left(\frac{1-\eta}{\eta}\right)^\beta d\eta \tag{4.109}$$

This is the mean particle velocity relative to the mean flow velocity. Fig. 4.10 illustrates how the mean particle velocity varies with the fall velocity parameter. Note that for $\beta = 0$, the case of neutrally-buoyant particles, obviously this velocity must be equal to the mean flow velocity, meaning that $\mu_s - \mu$ must be zero, as revealed by the figure.

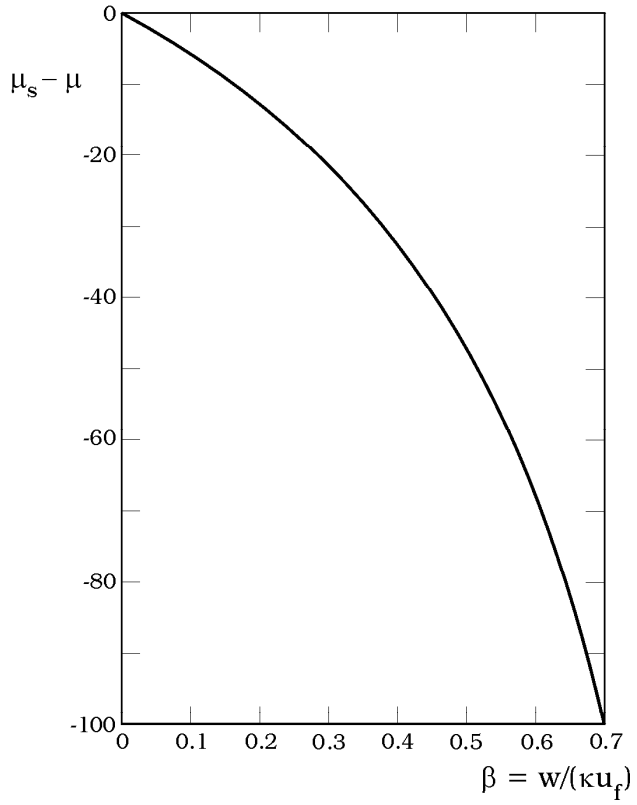

Figure 4.10: Mean velocity of heavy particles relative to the mean flow velocity. Sumer (1974).

4.3.4 Longitudinal dispersion coefficient

The longitudinal dispersion coefficient can be written in the normalized form as

$$\frac{D_1}{hU_f} = \frac{\varkappa}{6}(\frac{1}{2}\frac{dm_2}{d\tau})_{\tau\to\infty} \tag{4.110}$$

(see Eqs. 4.87 and 4.104).

From Eq. 4.105,

$$\frac{1}{2}\frac{dm_2}{d\tau} = 6\int_0^1 \eta(1-\eta)C_0\ d\eta + \int_0^1 (\mu - \mu_s + \mu\chi)C_1\ d\eta \tag{4.111}$$

in which C_1 is found from Eqs. 4.90-4.92, setting $p = 1$

$$C_1 = \phi(\eta) + \sum_{K=1}^{\infty} a_K f_K(\eta) \exp\{-6(K^2+K)\tau\} + \sum_{K=1}^{\infty} d_K (\frac{1-\eta}{\eta})^{\beta} F(-K, 1+K; 1-\beta; \eta) \exp\{-6(K^2+K)\tau\} \quad (4.112)$$

in which

$$\phi = A_\phi (\frac{1-\eta}{\eta})^{\beta} - \frac{\sin(\pi\beta)}{\pi\beta} (\frac{1-\eta}{\eta})^{\beta} \int_0^{\eta} (\frac{1-\eta}{\eta})^{-\beta} \frac{1}{6\eta(1-\eta)} d\eta \times \int_0^{\eta} (\mu - \mu_s + \mu\chi)(\frac{1-\eta}{\eta})^{\beta} d\eta \quad (4.113)$$

in which $\beta < 1$. It may be noted that $C_1 \to \phi$ as $\tau \to \infty$.

Now, from Eqs. 4.111, 4.113 and 4.103, the dispersion coefficient is obtained as

$$\frac{D_1}{hU_f} = \frac{\varkappa}{6}(1-\beta^2) - \frac{\varkappa}{36} \frac{\sin(\pi\beta)}{\pi\beta} \int_0^1 [(\mu - \mu_s) + \mu\chi](\frac{1-\eta}{\eta})^{\beta} d\eta \times \int_0^{\eta} (\frac{1-\eta}{\eta})^{-\beta} \frac{1}{\eta(1-\eta)} d\eta \int_0^{\eta} [(\mu - \mu_s) + \mu\chi](\frac{1-\eta}{\eta})^{\beta} d\eta \quad (4.114)$$

in which $\beta < 1$.

For the case of *neutrally buoyant particles/dispersant*, putting $\beta = 0$, one gets

$$\frac{D_1}{hU_f} = \frac{\varkappa}{6} - \frac{\varkappa}{36} \int_0^1 \mu\chi d\eta \int_0^{\eta} \frac{1}{\eta(1-\eta)} d\eta \int_0^{\eta} \mu\chi d\eta \quad (4.115)$$

The expression in Eq. 4.115 was first obtained by Elder (1959). The integral can be calculated numerically. The result is (taking $\varkappa$, the von Karman constant, 0.41)

$$\frac{D_1}{hU_f} = 0.07 + 5.86 = 5.93 \quad (4.116)$$

As seen from Eq. 4.115, the dispersion coefficient consists of two terms; the first term on the right hand side of the equation, $\frac{\varkappa}{6}$, (the numerical value of which is 0.07, Eq. 4.116) represents the effect of the turbulent diffusion in the streamwise direction; it stems from the first term on the right hand side of Eq. 4.83. The second term is actually the main portion of the longitudinal

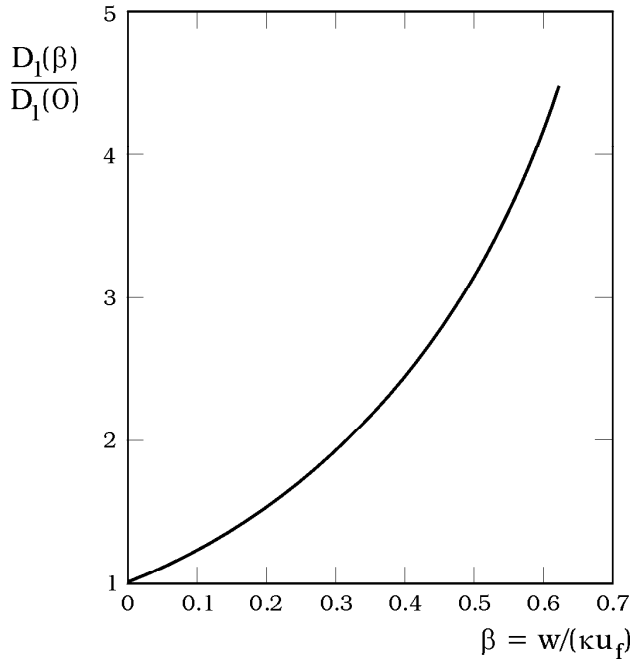

Figure 4.11: Ratio of the longitudinal dispersion coefficient of heavy particles to that of neutrally-buoyant particles. Sumer (1974).

dispersion coefficient, and induced by the combined action of the turbulent diffusion across the depth y and the variation of the flow velocity in the $y-$ direction.

Returning to the case of *heavy particles,* the dispersion coefficient is plotted in Fig. 4.11. The figure shows that the dispersion coefficient increases with increasing β, the fall velocity parameter. This can be explained as follows. A heavy particle spends most of the time near the bottom where the velocity gradient is largest. On the other hand, the larger the velocity gradient, the larger the dispersion coefficient. Therefore, a heavier particle (i.e., with larger β) should have a larger dispersion coefficient.

4.4 Longitudinal dispersion in rivers

In the previous section, the longitudinal dispersion coefficient has been calculated for an open-channel flow, and found to be $\frac{D_l}{hU_f} \simeq 6$. Field experiments in

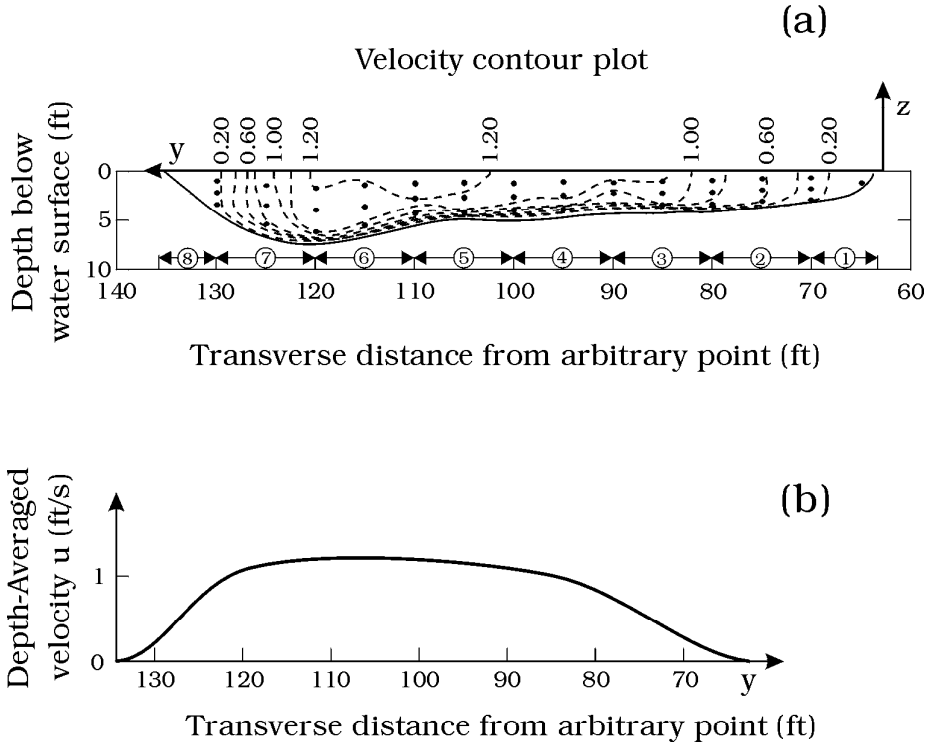

Figure 4.12: (a): The cross-sectional velocity distribution at Renton Junction in the Green-Duwamish River, Washington. Contours are lines of constant velocity, in increment of 0.2 ft/s; (b): The transverse profile of the depth-averaged velocity corresponding to the velocity distribution shown in (a). Taken from Fischer et al. (1979).

rivers show, however, that $\frac{D_1}{hU_f}$ takes values much larger than 6. The largest value reported in Fischer et al. (1979) is $\frac{D_1}{hU_f} \simeq 7500$ in the Missouri river. This evidence makes it clear that the value obtained for the case of the open channel, namely $\frac{D_1}{hU_f} \simeq 6$, cannot apply to real streams. The reason why $\frac{D_1}{hU_f} \simeq 6$ value does not apply was studied by Fischer (1966, 1967). It was shown that, in the case of real streams, although the velocity distribution satisfies the logarithmic law in the vertical direction, the variation of the velocity across the river width apparently plays the major role.

A quantitative estimate of the dispersion coefficient in a real stream can be obtained by neglecting the vertical profile completely, but instead, by taking

the transverse velocity profile, i.e., the velocity profile across the river width. (Fig. 4.12 displays an example illustrating the transverse velocity variation in a river, the velocity isolines at a measurement section in the Green-Duwamish River in Washington, and the corresponding transverse velocity profile).

Fisher obtained the following expression for the longitudinal dispersion coefficient

$$D_1 = -\frac{1}{A}\int_0^W (u(y) - U_m)\ d(y)\ dy \int_0^y \frac{1}{\epsilon_t d(y)}\ dy \int_0^y (u(y) - U_m)\ d(y)\ dy \tag{4.117}$$

in which A is the cross-sectional area of the river, W width at the surface, U_m mean flow velocity, y the transverse distance measured from one bank of the river (Fig. 4.12) (not to be confused with the vertical distance used in the previous section), $d(y)$ the depth (the depth is a function of y, Fig. 4.12), ϵ_t is the turbulent diffusion coefficient in the transverse direction (it may or may not be a function of y), and $u(y)$ is the depth-averaged velocity defined by (Fig. 4.12) :

$$u(y) = \frac{1}{d(y)}\int_{-d(y)}^{0} \overline{u}(y,z)\ dz \tag{4.118}$$

Returning to the expression obtained for the case of the open-channel flow in the previous section, Eq. 4.115, (omitting the first term on the right hand side of the equation)

$$\frac{D_1}{hU_f} = -\frac{\varkappa}{36}\int_0^1 \mu\chi d\eta \int_0^\eta \frac{1}{\eta(1-\eta)} d\eta \int_0^\eta \mu\chi d\eta$$

This is actually in terms of dimensional quantities

$$\frac{D_1}{hU_f} = -\frac{1}{h}\int_0^h (\overline{u}(y) - U_m)dy \int_0^y \frac{1}{\epsilon(y)} dy \int_0^y (\overline{u}(y) - U_m)dy$$

or alternatively

$$\frac{D_1}{hU_f} = -\frac{1}{h^2}\int_0^h (\overline{u}(y) - U_m)hdy \int_0^y \frac{1}{\epsilon(y)h} dy \int_0^y (\overline{u}(y) - U_m)hdy \tag{4.119}$$

As seen, this expression is quite similar to that obtained by Fischer (1966, 1967), Eq. 4.117. The only difference is that, in the case of the river dispersion, y is the transverse distance, while, in the case of the open-channel dispersion, y is the vertical distance.

Fischer et al. (1979) give a numerical example to illustrate how to use Eq. 4.117 in a field application.

Finally, it may be noted that real streams may have irregularities such as bends, sandbars, side pockets, pools, riffles, bridge piers, man-made revetments, and even occasional junked car, or sunken barges. Every irregularity contributes to dispersion. (Fischer et al., 1979, and Pedersen, 1977). Empirical expressions have been given for the longitudinal dispersion coefficient in terms of gross flow characteristics of the river (Fischer et al., 1979, p. 136). These can be used to make first assessments of the dispersion coefficient.

4.5 References

1. Aris, R. (1956): "On the dispersion of a solute in a fluid flowing through a tube". Proc. Roy. Soc., vol. A235, p. 67.

2. Batchelor, G.K. (1949): "Diffusion in a field of homogenous turbulence". Australian J. Sci. Res., vol. A2, No. 4, p.473.

3. Batchelor, G.K. and Townsend, A.A. (1956):"Turbulent diffusion". In: Surveys in Mechanics (ed. G.K. Batchelor and R. M Davies), Cambridge University Press, p.352.

4. Elder, J. (1959): "The dispersion of marked fluid in turbulent shear flow". J. Fluid Mech.., vol. 5, p. 544.

5. Fischer, H.B. (1966): Longitudinal Dispersion in Laboratory and Natural Streams. Tech. Report KH-R-12, California Institute of Technology, Pasadena, California.

6. Fischer, H.B. (1967): "The mechanics of dispersion in natural streams". J. Hydraul. Div., Proc. ASCE, vol. 93, p. 187.

7. Fischer, H.B., List, E.J., Koh, R.C.Y., Imberger, J. and Brooks, N.H. (1979): Mixing in Inland and Coastal Waters. Academic Press, Inc.

8. Monin, A.M. and Yaglom, A.S. (1973): Statistical Fluid Mechanics: Mechanics of Turbulence, vol. 1, MIT Press. Cambridge, Mass.

9. Pedersen, F.B. (1977): Prediction of Longitudinal Dispersion in Natural Streams. Series Paper No. 14, Technical University of Denmark, Institute of Hydrodyn. and Hyd. Eng. (ISVA).

10. Sayre, W.W. (1968): Hydraulic Papers, No. 3, Colorado State University, Fort Collins.

11. Sumer, B.M. (1974): "Mean velocity and longitudinal dispersion of heavy particles in turbulent open-channel flow". J. Fluid Mech., vol. 65, p.11.

12. Taylor, G.I. (1921): "Diffusion by continuous movements". Proc. London Math. Soc., vol. 20, p. 196.

13. Taylor, G.I. (1953): "Dispersion of soluble matter in solvent flowing slowly through a tube". Proc. Roy. Soc. London, A, vol. CCXIX, p.186.

14. Taylor, G.I. (1954): "The dispersion of matter in turbulent flow through a pipe". Proc. Roy. Soc. London, vol. A223, p.446.

Chapter 5

Wave boundary layers

In shallow waters, the orbital motion of water particles under a progressive wave degenerates into a bottom-parallel, straight line, oscillatory motion at the seabed (Fig. 5.1). For each half cycle of this oscillatory motion at the bed, a "new" time-dependent boundary layer develops. This cyclic boundary layer is called the *wave boundary layer*.

The wave boundary layers are of great importance for several processes: Turbulent mixing of mass and momentum takes place in the wave boundary layers; Likewise, frictional dissipation takes place in the wave boundary layers; The wave boundary layers are one of the key components of the sediment transport processes; Exchanges of chemicals and organisms between seabed and the main body of the water take place in the wave boundary layers. Therefore, understanding of wave-boundary layers is essential to develop predictive tools and capabilities for the previously mentioned processes.

Fredsøe and Deigaard (1992, Chapters 2 and 3) can be consulted for a detailed treatment of the subject including the mathematical modelling.

The flow in the wave boundary layers may be in the laminar regime, it may be in the transitional, or it may be in the turbulent regime.

We will start off with the laminar-regime wave boundary layers, and then we will focus on the turbulent wave boundary layers. The latter will be mainly based on the work of Jensen et al. (1989), an extensive experimental work conducted in an oscillating water tunnel, covering both smooth- and rough-boundary flows, with very broad range of the Reynolds number including very high Reynolds numbers.

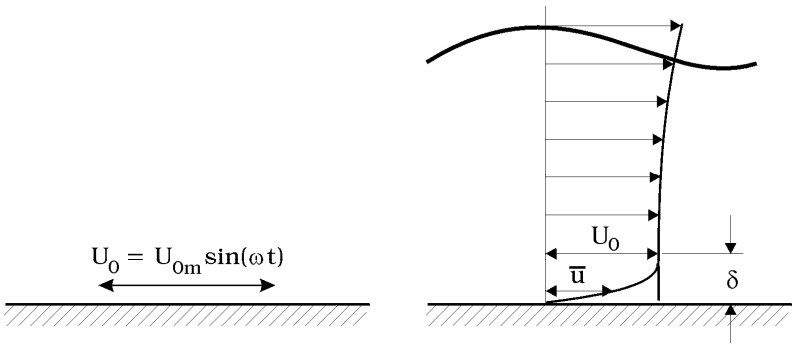

Figure 5.1: Definition sketch.

5.1 Laminar wave boundary layers

5.1.1 Velocity distribution across the boundary layer depth

The streamwise component of the N.-S. equation (Eqs. 1.8 and 1.9) in the boundary layer (Fig. 5.2):

$$\frac{\partial u}{\partial t} + u\frac{\partial u}{\partial x} + v\frac{\partial u}{\partial y} = -\frac{1}{\rho}\frac{\partial p}{\partial x} + \frac{1}{\rho}\frac{\partial \tau}{\partial y} \tag{5.1}$$

First of all, v in the boundary layer is practically zero, therefore, the third term on the left hand side of the equation drops out. Secondly, the x distances are large compared to the y distances (the wave length in the laboratory $L = O$(2-3 m) while the boundary layer thickness $\delta = O(1\text{ mm}) - O(1\text{ cm})$; the same is also true for the turbulent wave boundary layers in the sea, $L = O(100\text{ m})$ while the boundary layer thickness $\delta = O(10\text{ cm})$); therefore, the $x-$ dependence in the above equation can be neglected, hence the second term on the right hand side of the equation also drops out. Therefore, Eq. 5.1:

$$\frac{\partial u}{\partial t} = -\frac{1}{\rho}\frac{\partial p}{\partial x} + \frac{1}{\rho}\frac{\partial \tau}{\partial y} \tag{5.2}$$

Now, the boundary layer is actually driven by the pressure gradient $\frac{\partial p}{\partial x}$. This term can be calculated from the equation of motion outside the boundary layer (in the free-stream region). This equation, by setting $\tau = 0$ in the

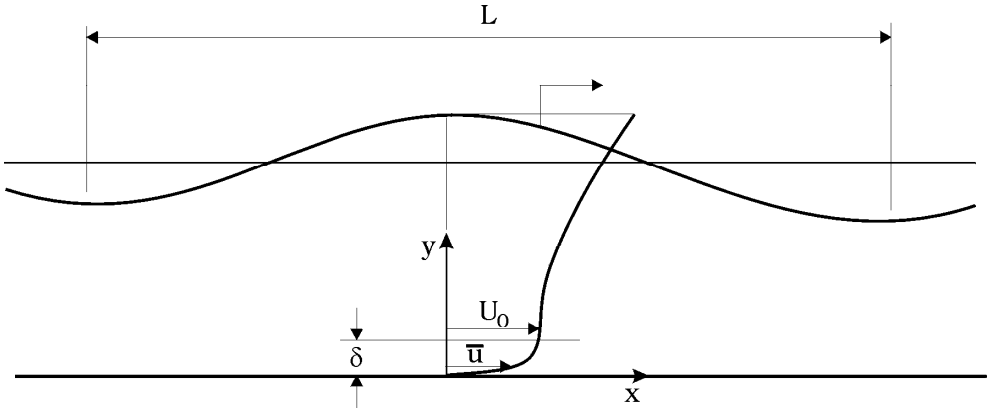

Figure 5.2: The boundary-layer thickness, δ, is small compared with the wave length, L.

above equation,

$$\frac{\partial U_0}{\partial t} = -\frac{1}{\rho}\frac{\partial p}{\partial x} \tag{5.3}$$

in which U_0 is given as

$$U_0 = U_{0m}\sin(\omega t) \tag{5.4}$$

in which ω is the angular frequency of the wave ($\omega = \frac{2\pi}{T}$), T being the wave period.

From Eqs. 5.2 and 5.3, one gets

$$\frac{\partial u}{\partial t} = \frac{\partial U_0}{\partial t} + \frac{1}{\rho}\frac{\partial \tau}{\partial y} \tag{5.5}$$

in which τ is the shear stress

$$\tau = \mu\frac{\partial u}{\partial y} \tag{5.6}$$

Therefore Eq. 5.5

$$\frac{\partial u}{\partial t} = \frac{\partial}{\partial t}(U_{0m}\sin(\omega t)) + \nu\frac{\partial^2 u}{\partial y^2} \tag{5.7}$$

The boundary conditions

$$y \to \infty: \qquad u \to U_{0m}\sin(\omega t) \tag{5.8}$$

and

$$y = 0: \qquad u = 0 \tag{5.9}$$

The solution to Eq. 5.7 with the preceding boundary conditions is

$$u(y,t) = U_{0m}\sin(\omega t) - U_{0m}\exp(-\frac{y}{\delta_1})\sin(\omega t - \frac{y}{\delta_1}) \tag{5.10}$$

in which δ_1

$$\delta_1 = (\frac{2\nu}{\omega})^{\frac{1}{2}} \tag{5.11}$$

representing the thickness of the boundary layer, called the Stokes length.

The time development of the velocity distribution is plotted from Eq. 5.10 in Fig. 5.3. In the figure, δ is the boundary layer thickness, slightly different from that in Eq. 5.11; namely, δ is the distance from the bed where the velocity becomes maximum at the phase value $\omega t = 90^0$; this distance is found from the above solution as

$$\delta = \frac{3\pi}{4}(\frac{2\nu}{\omega})^{\frac{1}{2}} \tag{5.12}$$

or, in terms of the Reynolds number, *Re,*

$$\frac{\delta}{a} = \frac{3\pi}{4}(\frac{2}{Re})^{\frac{1}{2}} \tag{5.13}$$

in which

$$Re \ = \frac{aU_{0m}}{\nu} \tag{5.14}$$

in which a is the amplitude of the orbital motion of water particles at the bed,

$$a = \frac{U_{0m}}{\omega} \tag{5.15}$$

As seen from Fig. 5.3, the flow near the bed leads over the flow in the free stream region. (As a result, the near-bed flow reverses earlier).

This is related to the driving pressure gradient. From Eqs. 5.3 and 5.4, it can readily be seen that $\frac{\partial p}{\partial x} > 0$ after $\omega t = 90^0$ in the half period of the motion. This means that the boundary layer will experience an *adverse pressure gradient* during this phase of the half period (Fig. 5.4). This pressure gradient dictates the boundary-layer flow to reverse. However, for the flow to respond, it will have to "dissipate" its momentum. Clearly, the near-bed flow dissipates its momentum earlier than the outer flow, meaning that it will

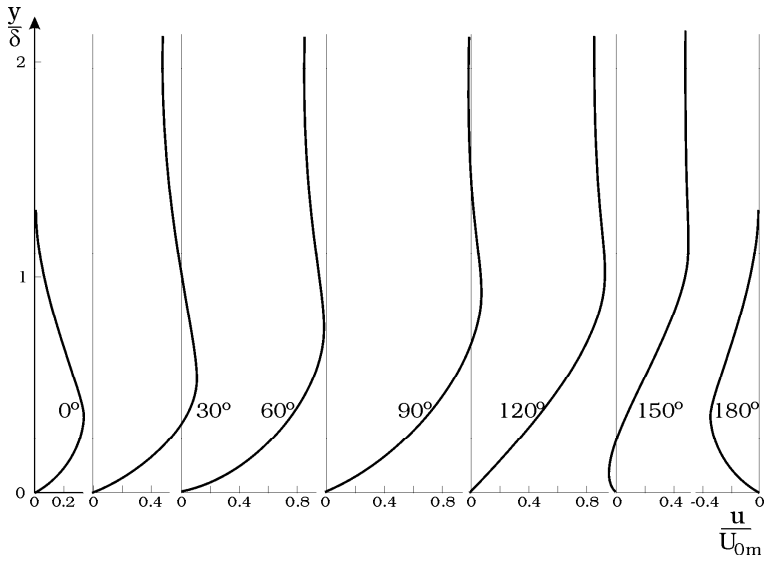

Figure 5.3: Time development of velocity profiles in laminar wave boundary layer.

respond to the pressure gradient earlier, therefore will reverse earlier than the outer flow, as revealed by the velocity profiles in Fig. 5.3.

It may be noted that the preceding description may also explain the overshooting exhibited by the plotted velocity profiles in Fig. 5.3.

5.1.2 Flow resistance

The bed shear stress,

$$\tau_0 = \mu(\frac{\partial u}{\partial y})_{y=0} = \frac{\mu U_{0m}}{\delta_1}[\sin(\omega t) + \cos(\omega t)] \tag{5.16}$$

or

$$\tau_0 = \frac{\sqrt{2}\mu U_{0m}}{\delta_1}[\sin(\omega t + \frac{\pi}{4})] \tag{5.17}$$

This equation shows that the bed shear stress leads over the free-stream flow with a phase difference (cf. Eq. 5.4)

$$\Phi = 45^0 \tag{5.18}$$

This also implies that the flow at the bed reverses $\Phi = 45^0$ earlier than the free stream.

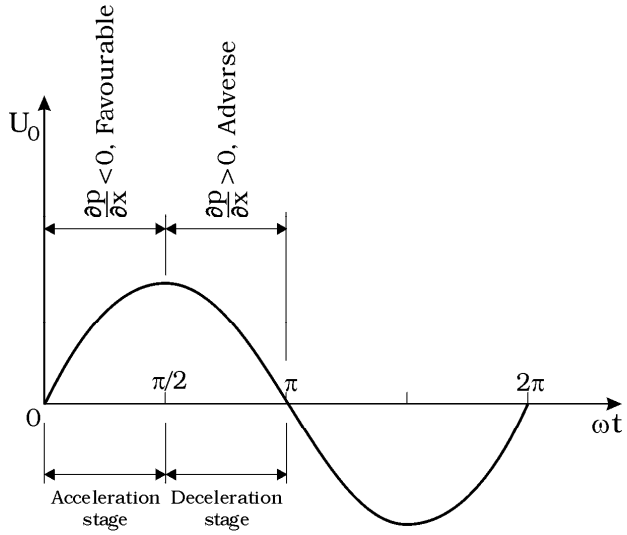

Figure 5.4: Two different pressure gradients over one half cycle.

Finally, the friction coefficient in wave boundary layers is defined by

$$f_w = \frac{2\tau_{0m}/\rho}{U_{0m}^2} \tag{5.19}$$

or

$$U_{fm} = \sqrt{\frac{f_w}{2}} U_{0m} \tag{5.20}$$

in which f_w is the wave friction coefficient (cf. Eq. 2.128), and U_{fm} is the maximum value of the friction velocity defined by

$$U_{fm} = \sqrt{\frac{\tau_{0m}}{\rho}} \tag{5.21}$$

Here τ_{0m} is the maximum value of the bed shear stress. From Eqs. 5.16 and 5.20, f_w

$$f_w = \frac{2}{\sqrt{Re}} \tag{5.22}$$

5.2 Laminar-to-turbulent transition

One way of illustrating the laminar-to-turbulent transition is to plot the friction factor as a function the Reynolds number. Fig. 5.5 a shows this.

The figure also includes, for convenience, the phase difference (lead) between the bed shear stress and the free-stream velocity (Fig. 5.5 b) plotted versus the Reynolds number.

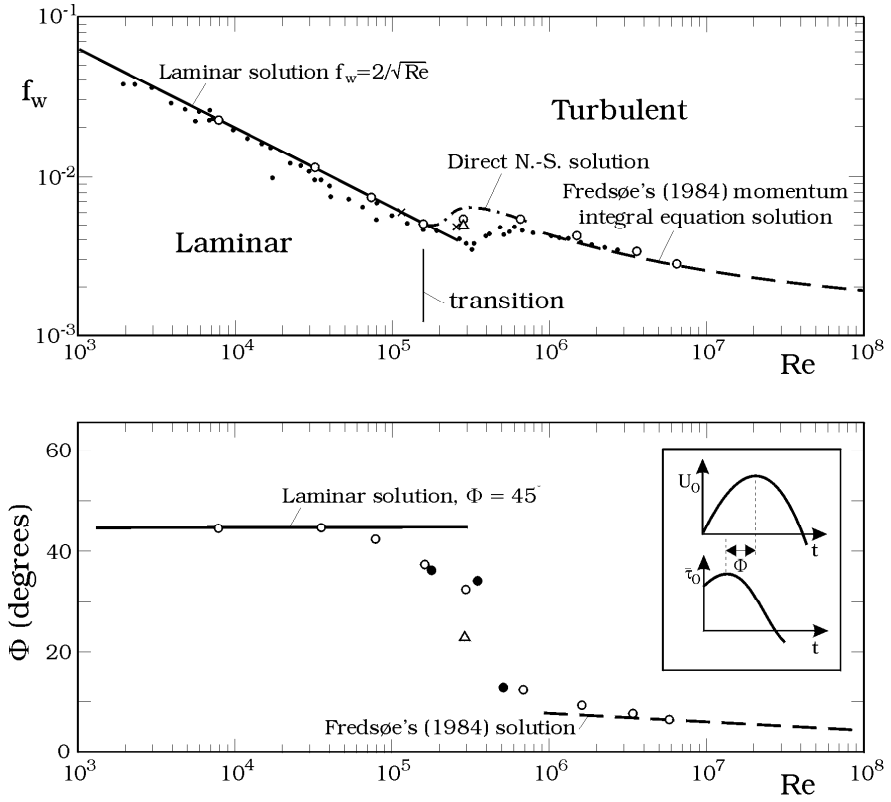

Figure 5.5: (a): Wave friction coefficient, and (b): phase difference. Jensen et al. (1989).

1. The transition to turbulence occurs at $Re \simeq 1.5 \times 10^5$. The bed shear stress measurements of Jensen et al. (1989) showed that the bed shear stress signal is disturbed first at $Re = 1.6 \times 10^5$. Hydrodynamic instability calculations apparently seem to capture this critical value of Re (see Sleath, 1984).

2. The data for both the friction coefficient and the phase difference agrees well with the theoretical results for the laminar-flow case, depicted in Eqs. 5.22 and 5.18.

3. The phase lead Φ decreases with the transition. This can be explained as follows. In the transitional/turbulent flows, the momentum exchange between the layers of fluid will be enhanced. Therefore, the near-bed flow will be supplied with the new, momentum-rich fluid from the upper layers of the boundary layer, and as a result, it will dissipate its momentum not as fast as in the case of the laminar flow. Hence, its response to the adverse pressure gradient will be delayed, leading to the decrease in the phase lead, as indicated in Fig. 5.5 b. In the fully-developed turbulent case (very large Re), the phase lead is only about 5^0.

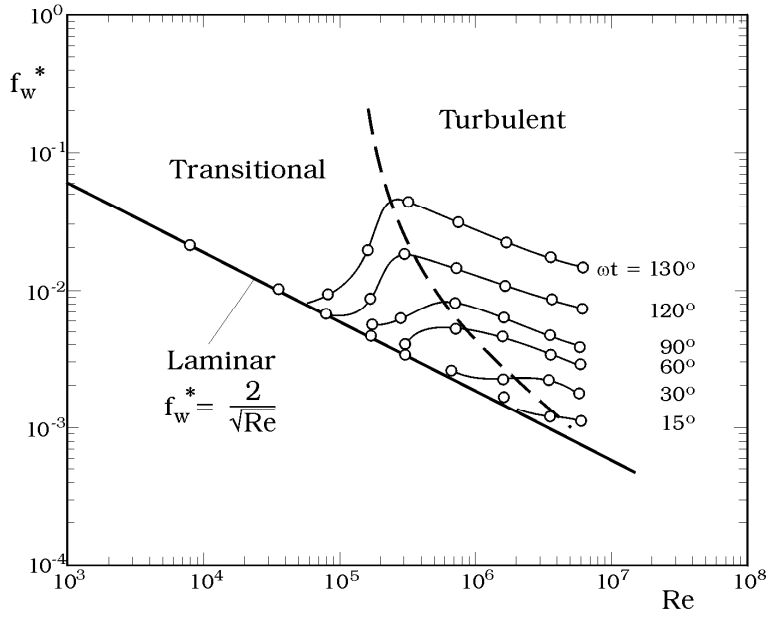

Figure 5.6: Normalized friction coefficient at different phase values. Jensen et al. (1989).

Fig. 5.6 offers another way of illustrating the transition to turbulence. Here, the friction coefficient is defined in a way slightly different from that in Eq. 5.19, namely

$$f_w^\star = \frac{2\tau_0/\rho}{U_{0m}^2 \sin(\omega t + \frac{\pi}{4})} \tag{5.23}$$

Note that the bed shear stress above is not the maximum value of the shear stress, but rather the phase-resolved bed shear stress, $\tau_0 = f(\omega t)$. The advantage of this representation is that, when divided by $\cos(\omega t - \frac{\pi}{4})$, the bed shear stress will be independent of the phase ωt in the case of the laminar flow (from Eq. 5.17):

$$\tau_0 = \frac{\rho U_{0m}^2}{Re^{\frac{1}{2}}} \sin(\omega t + \frac{\pi}{4}) \tag{5.24}$$

but will depend only on *Re:*

$$f_w^\star = \frac{2}{Re^{\frac{1}{2}}} \tag{5.25}$$

which represents a straight line when plotted on a log-log paper.

Now, this enables us to identify the flow regime in the following way.

1. Measure the bed shear stress, $\tau_0 = f(\omega t)$.
2. Calculate the friction coefficient $f_w^\star$ from Eq. 5.23.
3. Plot the latter quantity versus Re on a log-log paper, with ωt as a parameter.
4. If $f_w^\star$ versus Re on this plot collapses on the straight line representing
$$f_w^\star = \frac{2}{Re^{\frac{1}{2}}}$$
then the flow will be in the laminar regime; otherwise it will be either in the transitional regime, or in the turbulent regime.

Jensen et al. (1989) did this exercise. Their results are depicted in Fig. 5.6.

This figure is an important figure. It implies that, even for very large *Re,* the flow regime may remain laminar for quite some period of time during the boundary layer development in the half cycle. For example, for $Re = 5 \times 10^5$, the flow remains laminar until $\omega t \simeq 40^0$, while for $Re = 10^6$, this figure is $\omega t \simeq 20^0 - 25^0$.

Fig. 5.6 also suggests the following. The pattern of the variation of $f_w^\star$ with Re is not the same outside the laminar line; apparently there are two distinct patterns, implying a change in the flow regime. These two regions are interpreted by Jensen et al. as the transitional and fully developed turbulent regimes. From the figure, it can be seen that, even for Re as high as 10^6, the flow becomes a fully developed turbulent flow only after the phase value $\omega t \simeq 60^0$.

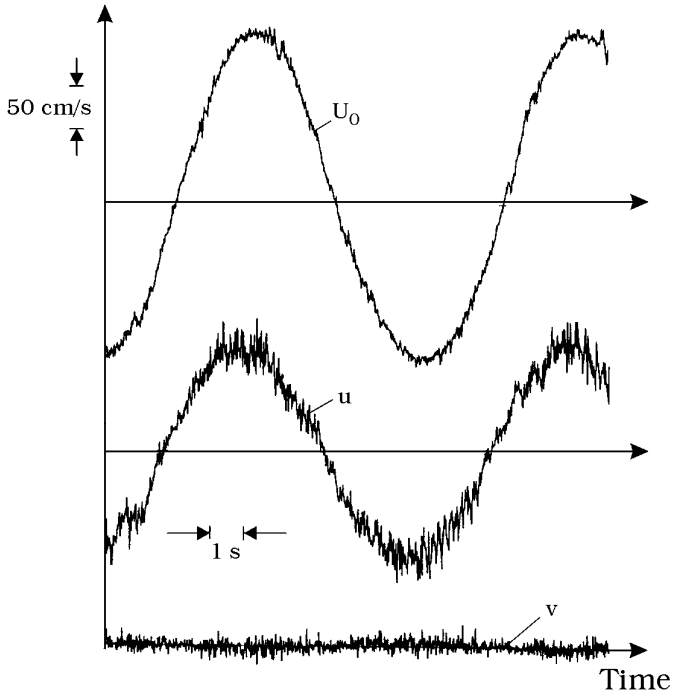

Figure 5.7: Sample velocity records. Re $= 6 \times 10^6$. U_0 was measured at $y = 140$ mm, and u and v at $y = 1$ mm. Jensen et al. (1989).

5.3 Turbulent wave boundary layers

5.3.1 Ensemble averaging

Fig. 5.7 displays time series of the horizontal and vertical velocity components of the velocity in the boundary layer (the bottom two time series). The top time series is the free-stream velocity. This is from an experiment with $Re = 6 \times 10^6$.

The so-called ensemble averaging is used to calculate the mean values:

$$\overline{u}(y, \omega t) = \frac{1}{N} \sum_{j=1}^{N} u[y,\ \omega(t + (j-1)T)] \tag{5.26}$$

Likewise, for example, the root-mean-square (r.m.s.) value of the fluctuating

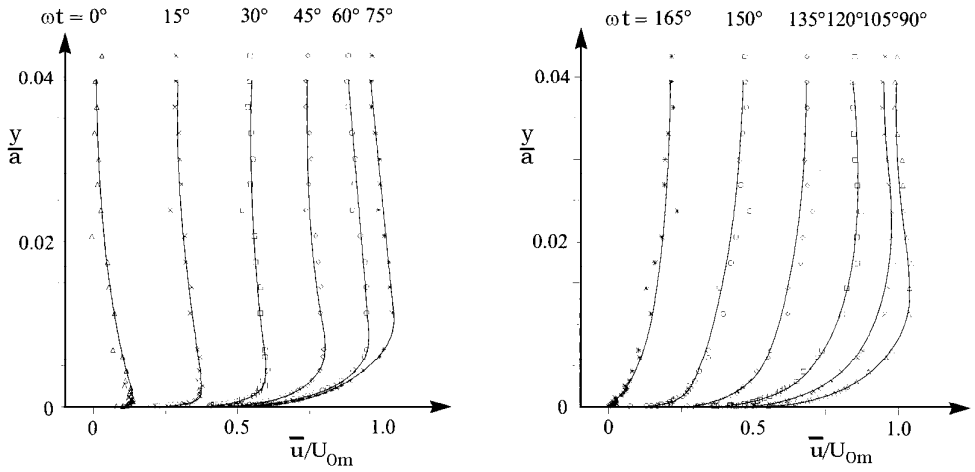

Figure 5.8: Mean velocity distributions. Smooth bed. Re = 6×10^6. Jensen et al. (1989).

velocity $u' = u - \overline{u}$,

$$\sqrt{\overline{u'^2}}(y,\omega t) = \left\{ \frac{1}{N-1} \sum_{j=1}^{N} [u[y,\ \omega(t+(j-1)T)] - \overline{u}(y,\omega t)]^2 \right\}^{\frac{1}{2}} \qquad (5.27)$$

5.3.2 Mean flow velocity

Fig. 5.8 shows the time development of the velocity profiles for $Re = 6 \times 10^6$. The way in which the velocity profiles evolve with time is similar to that in the case of the laminar wave boundary layer (Fig. 5.3). Features such as the early reversal of the flow near the bed, and the overshooting in the velocity profiles are observed here, too.

The velocity profiles in the previous figure are plotted in wall units on semi-logarithmic plots in Fig. 5.9. The figure also includes the van Driest profile (Eq. 2.97, the velocity profile obtained for steady boundary layers) as a reference line in each panel. Note that U_f used in the normalized quantities $y^+ = \frac{yU_f}{\nu}$ and $\frac{\overline{u}}{U_f}$ is the temporal value (the phase resolved value) of the friction velocity. Recall that the van Driest profile tends to the logarithmic

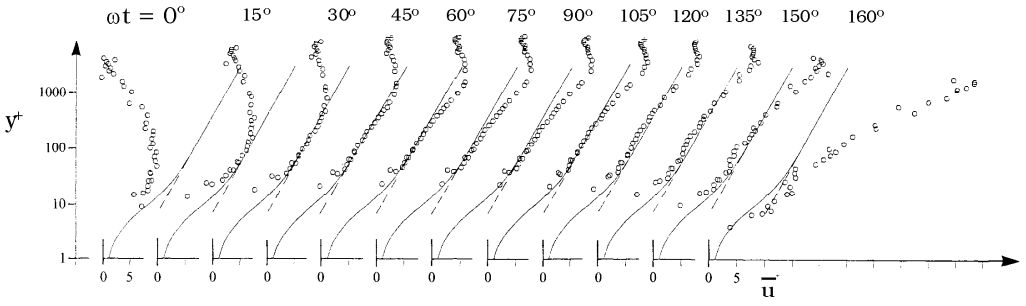

Figure 5.9: Mean velocity distributions in semi-log plot. Smooth bed. Re = 6×10^6. Solid curve: van Driest profile. Dashed lines: log law. Jensen et al. (1989).

distribution for large values of y^+ (Eqs. 2.97 and 2.99)

$$\overline{u} = U_f \ (A \ln y^+ + B) \tag{5.28}$$

Fig. 5.9 shows the following.

1. The oscillatory-flow velocity distributions agree remarkably well with the steady-flow ones in the range of $\omega t = 70^0 - 110^0$ where the flow experiences almost zero pressure gradient.

2. The logarithmic layer exists already at $\omega t = 15^0$ and is maintained throughout the ωt range from $\omega t \simeq 15^0$ up to almost 160^0.

3. At earlier phases, the logarithmic layer does not exist, however. This is because the boundary layer at these stages is not thick enough to house the logarithmic layer in it.

4. It may be noted that the velocity profiles in the early phases of the acceleration stage (where the pressure gradient is favourable) resemble quite closely those obtained in favourable pressure-gradient steady boundary layers, and likewise, those in the later phases of the deceleration stage (where the pressure gradient is adverse) resemble, again, quite closely the velocity distributions obtained in adverse pressure-gradient steady boundary layers (Coles, 1956).

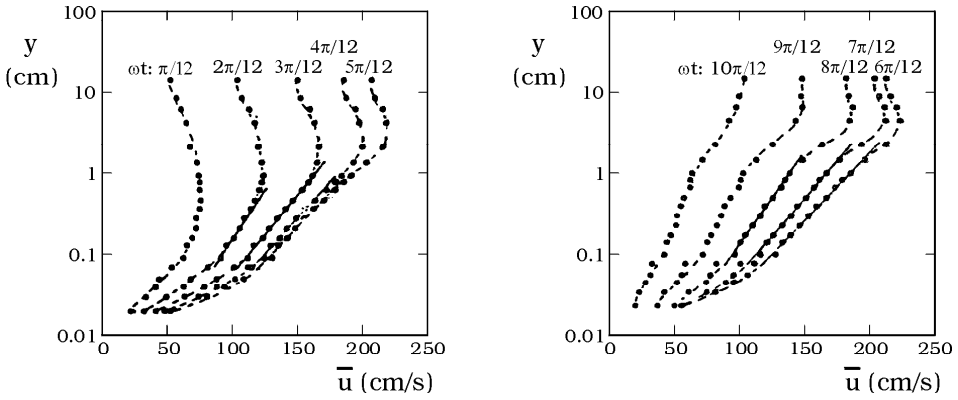

Figure 5.10: Mean velocity distributions. Sumer et al. (1987).

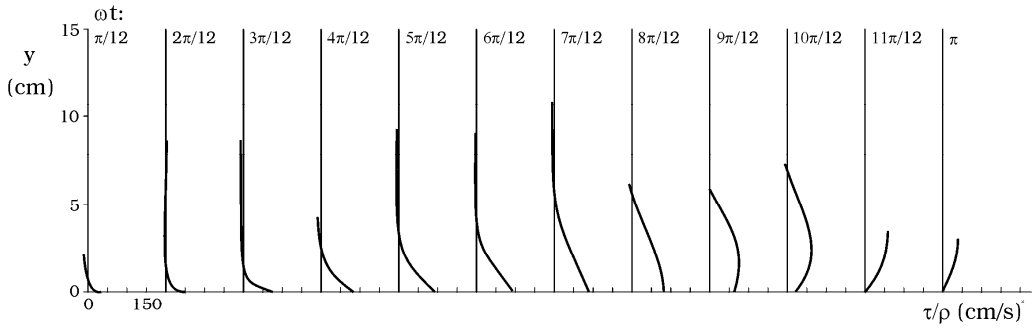

Figure 5.11: Shear stress distributions, corresponding to the velocity distributions in the previous figure. Sumer et al. (1987).

Finally, note the following. Fig. 5.10 shows the semi-log plots of the velocity distributions obtained in another research (Sumer et al., 1987), while Fig. 5.11 shows the corresponding shear stress distributions. As seen from Fig. 5.11, the constant stress layer is displaced to higher elevations in the later phases (starting from $\omega t = \frac{9\pi}{12}$) of the deceleration stage. This means that the logarithmic layer should also be displaced to these higher elevations. The velocity distributions may still be represented by the logarithmic law. However, U_f in such a representation cannot be the wall shear velocity, but a velocity defined by $(\frac{\tau}{\rho})^{\frac{1}{2}}$ where τ is the shear stress occurring at these elevations rather than at the wall.

5.3.3 Flow resistance

The friction coefficient, defined by Eq. 5.19 or Eq. 5.20, has been determined from experiments in oscillatory flows and plotted in Fig. 5.5 for both transitional and fully developed turbulent oscillatory boundary layers.

The variation of the friction coefficient with Re in Fig. 5.5 in the fully developed turbulent regime ($Re \gtrsim 10^6$) can be approximated by (Fredsøe and Deigaard, 1992, p. 29)

$$f_w = \frac{0.035}{Re^{0.16}} \tag{5.29}$$

5.3.4 Turbulence quantities

Fig. 5.12 and 5.13 presents the turbulence data in terms of

$$\frac{\sqrt{\overline{u'^2}}}{U_f}\ , \quad \frac{\sqrt{\overline{v'^2}}}{U_f}\ , \quad \frac{\sqrt{\overline{w'^2}}}{U_f}, \quad \frac{-\overline{u'v'}}{U_f^2} \tag{5.30}$$

versus y^+. Also plotted in the figures are the corresponding steady boundary-layer distributions (see, for example, Fig. 2.7).

Except at very early phases of the acceleration stage, and also late phases of the deceleration stage, the oscillatory-flow profiles appear to be in reasonable accord with the steady boundary-layer distributions throughout the phase space. See Jensen et al. (1989) for further details.

5.3.5 Effect of Reynolds number

Fig. 5.14 gives the mean velocity profiles for different Reynolds number.

The characteristic features of the time development of the velocity profiles shown in the preceding figure are as follows.

1. The velocity profile eventually reaches a state where the logarithmic layer comes into existence.

2. This logarithmic layer grows in thickness, as one proceeds further in the phase space ωt.

3. This continues to be the case until practically the point of reversal near the bed is reached.

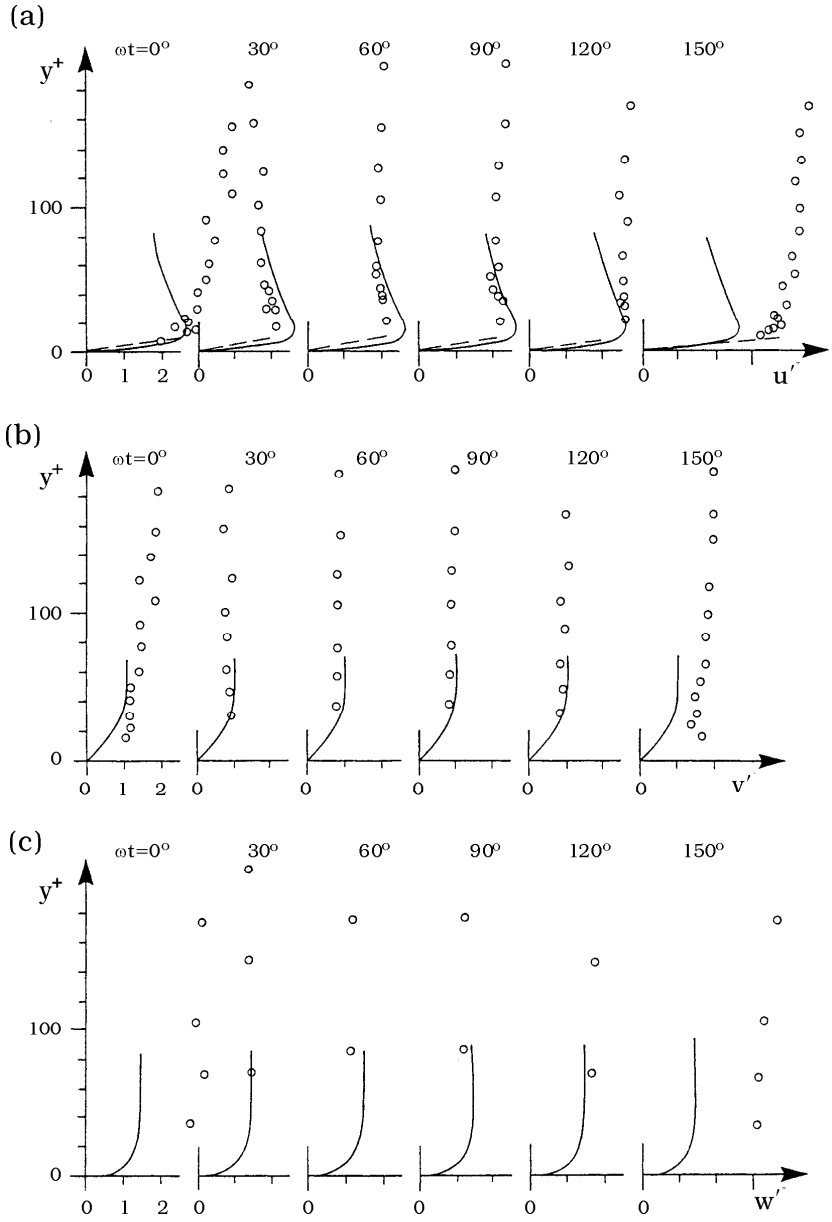

Figure 5.12: R.m.s. values of u', v' and w'. Smooth bed. Re $= 6 \times 10^6$. Jensen et al. (1989).

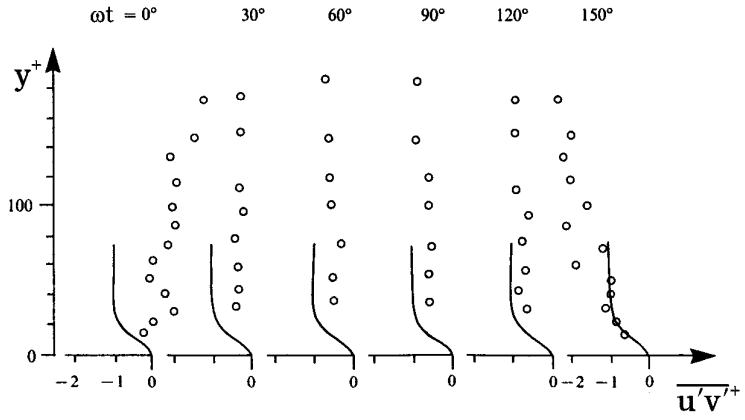

Figure 5.13: Reynolds stresses. Smooth bed. Re = 6 $\times 10^6$. Jensen et al. (1989).

From the figure, it is seen that the higher *Re*, the earlier the logarithmic layer comes into existence. This can be explained by reference to Fig. 5.6; From the latter figure, it is seen that, for the establishment of the logarithmic layer, the flow has to reach the fully developed turbulent state.

Jensen et al. (1989) also give the effect of *Re* on the turbulence quantities.

5.3.6 Boundary layer thickness

Fig. 5.15 presents the normalized boundary-layer thickness $\frac{\delta}{a}$ plotted against *Re.* Here δ is the distance from the bed where the velocity becomes maximum at the phase value $\omega t = 90^0$. The laminar flow solution has already been given in Eq. 5.12; in terms of *Re:*

$$\frac{\delta}{a} = \frac{3\pi}{4}(\frac{2}{Re})^{\frac{1}{2}} \tag{5.31}$$

From the figure, the boundary-layer thickness for storm conditions (very large *Re)*

$$\frac{\delta}{a} = O(0.01) \tag{5.32}$$

This corresponds to a boundary-layer thickness of $\delta = O(10$ cm).

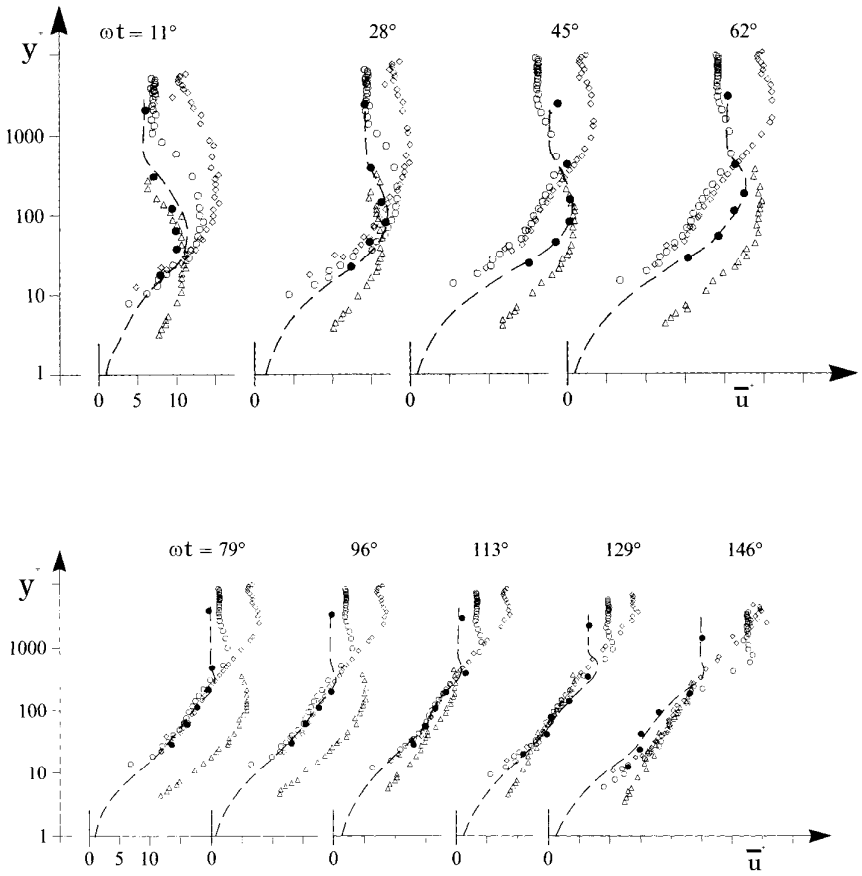

Figure 5.14: Mean velocity distributions. Smooth bed. Diamonds: Re $= 6 \times 10^6$. Jensen et al. (1989). Empty circles: Re $= 1.6 \times 10^6$. Filled circles: Re $= 5 \times 10^5$. Dashed lines: Re $= 5 \times 10^5$, Spalart and Baldwin's (1987) direct N.-S. simulation. Triangles: Re $= 2.8 \times 10^5$, Hino et al. (1983). From Jensen et al. (1989).

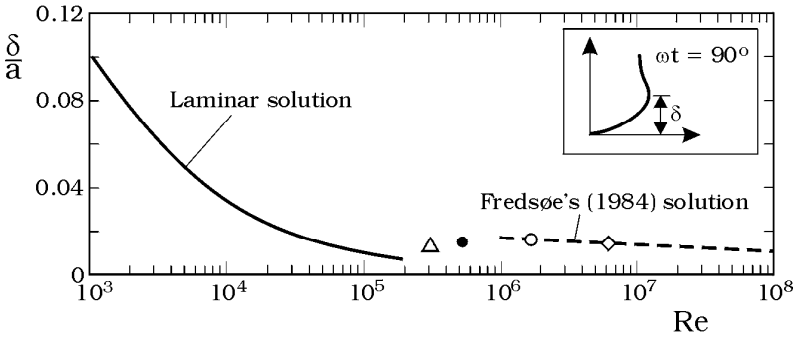

Figure 5.15: Boundary-layer thickness. Smooth bed. Jensen et al. (1989).

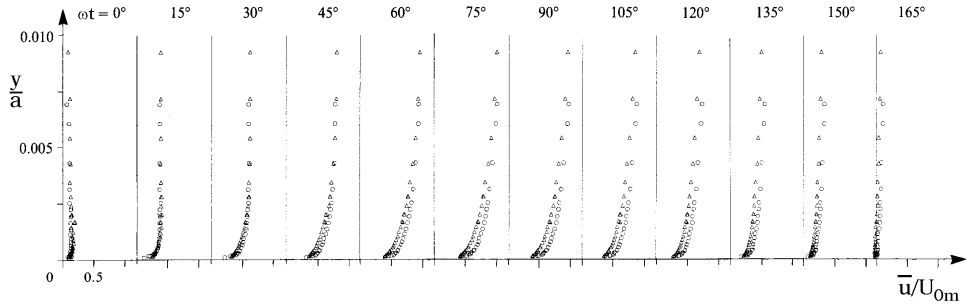

Figure 5.16: Mean velocity $\overline{u}$. Circles: Smooth bed. Triangles: Rough bed. Re $= 6 \times 10^6$. Jensen et al. (1989).

5.3.7 Turbulent wave boundary layers over rough walls

Figs. 5.16-5.19 compare the rough-bed results with the corresponding smooth-bed ones in the tests of Jensen et al. (1989). $Re = 6 \times 10^6$ and $k_s^+ = 84$ in which $k_s^+ = \frac{k_s U_{fm}}{\nu}$ where k_s is Nikuradse's equivalent sand roughness. The parameter $\frac{a}{k_s}$, on the other hand, is 3700.

From these figures, the following points appear to be noteworthy.

1. The description given in the preceding paragraphs of how the flow and turbulence evolve during one half-cycle is qualitatively the same for the rough-bed flows, too.

2. The introduction of the roughness, however, results in a decrease in the

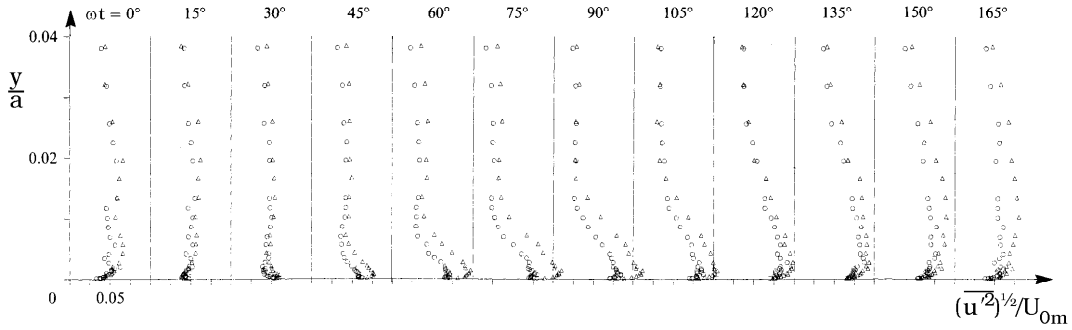

Figure 5.17: R.m.s. value of u'. Circles: Smooth bed. Triangles: Rough bed. Re $= 6 \times 10^6$. Jensen et al. (1989).

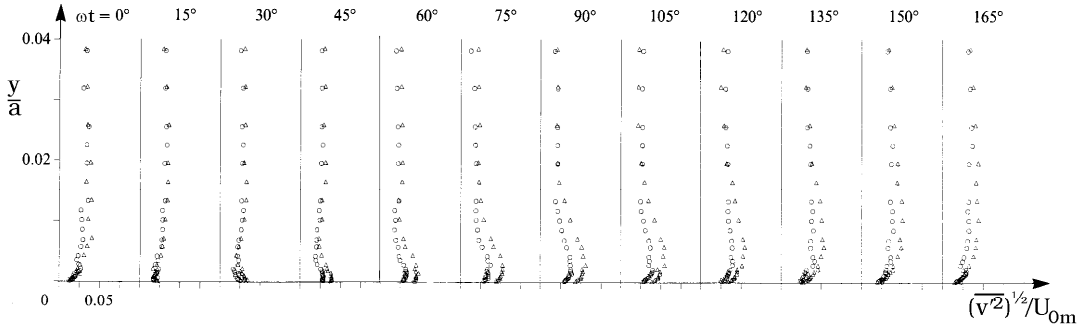

Figure 5.18: R.m.s. value of v'. Circles: Smooth bed. Triangles: Rough bed. Re $= 6 \times 10^6$. Jensen et al. (1989).

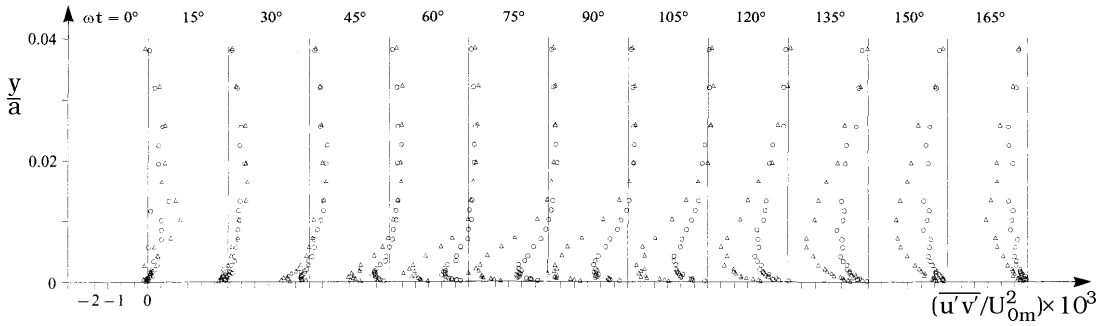

Figure 5.19: Reynolds stress $\overline{u'v'}$. Circles: Smooth bed. Triangles: Rough bed. Re $= 6 \times 10^6$. Jensen et al. (1989).

mean flow velocity and an increase in the turbulence quantities.

3. However, this effect tends to disappear with the distance from the bed; the mean flow velocity is practically the same for the two cases for distances $\frac{y}{a} \gtrsim 0.01$. The same is also true for the turbulence quantities, although this time the effect of roughness disappears at somewhat larger distances from the bed, namely for $\frac{y}{a} \gtrsim 0.03$. The decrease in the mean velocity is due to the retarding effect of the rough boundary while the increase in the turbulence quantities is due to the enhancement of the momentum transfer by the presence of the roughness elements..

4. The flow begins to feel the effect of the roughness only after ωt reaches the value of about 15^0. This is because the temporal value of the roughness Reynolds number is still far too small for these phases for the bed to act as a completely rough boundary and, as a result, the flow quantities for this short interval of time remain practically unchanged, regardless of the boundary category.

The rough turbulent boundary layers are governed solely by the parameter $\frac{a}{k_s}$. This parameter plays a similar role to that of Re in the case of the smooth turbulent wave boundary layers. Jensen et al. (1989) discussed the effect of this parameter on the mean and turbulence flow quantities.

The *friction coefficient* in the case of the rough bed can be represented by the following empirical expressions (Fredsøe and Deigaard, 1992, p. 25

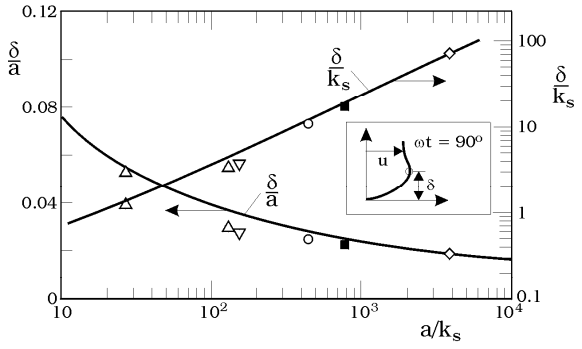

Figure 5.20: Boundary-layer thickness. Rough bed. Jensen et al. (1989).

and 26):

$$f_w = 0.04(\frac{a}{k_s})^{-\frac{1}{4}} \qquad \text{when } \frac{a}{k_s} > 50 \tag{5.33}$$

$$f_w = 0.4(\frac{a}{k_s})^{-\frac{3}{4}} \qquad \text{when } \frac{a}{k_s} < 50 \tag{5.34}$$

The latter expression is due to Kamphuis (1975) (Fredsøe and Deigaard, 1992, p. 26).

In the case of the transitional-category-bed wave boundary layers, the friction coefficient can be obtained from Kamphuis' (1975) empirical diagrams. Also consult Fredsøe and Deigaard (1992, p. 33).

Finally, Fig. 5.20 depicts the boundary-layer thickness. The figure shows that, the boundary-layer thickness for storm conditions (very large $\frac{a}{k_s}$)

$$\frac{\delta}{a} = O(0.02) \tag{5.35}$$

which corresponds to a boundary-layer thickness of $\delta = O(20 \text{ cm})$.

5.4 Other aspects

Several other aspects of wave boundary layers have been studied in recent years. The following is a partial list of these studies undertaken at ISVA.

Fredsøe, Sumer, Laursen and Pedersen (1993) have studied the non-uniform wave boundary layers, where the non-uniformity is due to a sudden change in the bed roughness, while Sumer, Laursen and Fredsøe (1993) have

studied the non-uniform wave boundary layers, where the non-uniformity is due to the convergent/divergent geometry of the flow environment.

Lodahl, Sumer and Fredsøe (1998) have investigated the combined oscillatory boundary layer and current in a circular pipe. The circular pipe has been selected in favour of a rectangular-section tunnel, to achieve a "-clean" flow environment (to avoid secondary currents, and more importantly to achieve a 2-D flow environment).

Arnskov, Fredsøe and Sumer (1993) have studied combined wave and current boundary-layer flow in a basin. In this study, the waves were propagating at an angle to the current, including the normally incident waves.

Tanaka, Sumer and Lodahl (1998) have studied the effect of cnoidal waves on laminar wave boundary layers.

Fredsøe, Andersen and Sumer (1999) have studied combined wave and current boundary-layer flows over a ripple-covered bed.

Fredsøe, Sumer, Kozakiewicz, Chua and Deigaard (2003) have studied the effect of externally-generated turbulence on wave boundary layers.

5.5 References

1. Arnskov, M. M., Fredsøe, J. and Sumer, B. M. (1993): "Bed shear stress measurements over a smooth bed in three-dimensional wave-current motion". Coastal Engineering, Vol. 20, pp. 277- 316.

2. Coles, D. (1956): "The law of the wake in a turbulent boundary layer". J. Fluid Mech., vol. 1, p. 191.

3. Fredsøe, J. (1984): "Turbulent boundary layer in wave-current motion". J. Hydraul. Eng. ASCE. 110, p. 1103.

4. Fredsøe, J., Andersen, K. H. and Sumer, B. M. (1999): "Wave plus current over ripple-covered bed", Coastal Engineering, vol. 38, 177-221.

5. Fredsøe, J. and Deigaard, R. (1992). Mechanic of Coastal Sediment Transport. Advanced Series on Ocean Engineering., Vol. 3, World Scientific.

6. Fredsøe, J., Sumer, B.M., Laursen, T. S.and Pedersen, C. (1993): "Experimental investigations of wave boundary layers with a sudden change in roughness". Journal of Fluid Mechanics, Vol. 252, pp.117-145.

7. Fredsøe, J., Sumer, B.M., Kozakkiewicz, A., Chua, L. H. C. and Deigaard, R. (2003): "Effect of externally generated turbulence on wave boundary layer". Coastal Engineering, vol. 49, pp. 155-183.

8. Jensen, B. L., Sumer, B. M. and Fredsøe, J.: "Turbulent oscillatory boundary layers at high Reynolds numbers". Journal of Fluid Mechanics, Vol. 206, p. 265, 1989.

9. Kamphuis, J. W. (1975): "Friction factor under oscillatory waves". J. Waterways, Port, Coastal and Ocean Eng. Div., ASCE, Vol. 101 (WW2), pp. 135-144.

10. Lodahl, C. R., Sumer, B. M. and Fredsøe, J. (1998): "Turbulent combined oscillatory flow and current in a pipe", J. Fluid Mech., vol. 373, 313-348.

11. Sleath, J. F. A. (1984): Sea Bed Mechanics, John Wiley & Sons.

12. Sumer, B. M., Jensen, B. L. and Fredsøe, J: "Turbulence in oscillatory boundary layers". Advances in Turbulence. Proc. 1st European Conference, Lyon, France, published by Springer, p. 556, 1987.

13. Sumer, B. M., Laursen, T. S. and Fredsøe, J. (1993): "Wave boundary layers in a convergent tunnel". Coastal Engineering, Vol. 20, pp. 317-342.

14. Tanaka, H., Sumer, B. M. and Lodahl, C. (1998): "Theoretical and experimental investigation on laminar boundary layers under cnoidal wave motion", Coastal Engineering Journal, vol. 40, No. 1, 81-98.

Chapter 6

Turbulence modelling

6.1 The closure problem

We have derived the basic equations of turbulent flows in Chapter 1. These equations are the continuity equation (Eq. 1.6) and the Reynolds equations (the equations of motion) (Eq. 1.14), respectively:

$$\frac{\partial \overline{u_i}}{\partial x_i} = 0 \tag{6.1}$$

$$\rho(\frac{\partial \overline{u}_i}{\partial t} + \overline{u}_j \frac{\partial \overline{u}_i}{\partial x_j}) = \rho \overline{g}_i + \frac{\partial}{\partial x_j}(\overline{\sigma}_{ij} - \rho \overline{u'_i u'_j}) \tag{6.2}$$

with the quantity σ_{ij}, the stress on the fluid

$$\overline{\sigma}_{ij} = -\overline{p}\delta_{ij} + \mu(\frac{\partial \overline{u}_i}{\partial x_j} + \frac{\partial \overline{u}_j}{\partial x_i}) \tag{6.3}$$

and the Reynolds stress tensor

$$-\rho \overline{u'_i u'_j} = \begin{bmatrix} -\rho \overline{u'_1 u'_1} & -\rho \overline{u'_1 u'_2} & -\rho \overline{u'_1 u'_3} \\ -\rho \overline{u'_2 u'_1} & -\rho \overline{u'_2 u'_2} & -\rho \overline{u'_2 u'_3} \\ -\rho \overline{u'_3 u'_1} & -\rho \overline{u'_3 u'_2} & -\rho \overline{u'_3 u'_3} \end{bmatrix} \tag{6.4}$$

in which there are, due to symmetry, six independent Reynolds stresses (three diagonal components and three off-diagonal ones).

As has already been discussed (Chapter 1), there are four equations for the mean flow, i.e., the continuity equation (Eq. 1.6) and the three Reynolds

equations (Eq. 1.14) whereas there are ten unknowns (namely, three components of the velocity, $\overline{u}_i$, and the pressure, $\overline{p}$, and six components of the Reynolds stress, $-\rho\overline{u_i'u_j'}$), hence the system is not closed. This problem is known as the *closure problem of turbulence*.

To close the system, we must find enough number of equations to solve for the unknowns. We do this through turbulence modelling.

(In the case of laminar flow, there are four unknowns (namely, three components of the velocity, u_i, and the pressure, p), and four equations, i.e., the continuity equation (Eq. 1.4) and three N.-S. equation (Eqs. 1.8 and 1.9). Therefore, the system is closed.)

6.2 Turbulence models

There are several kinds of turbulence models the most important of which are

1. Algebraic models;
2. Turbulence-energy equation models; and
3. Simulation models such as Direct Numerical Simulation (DNS), Large Eddy Simulation (LES) and Detached Eddy Simulation (DES).

Algebraic models, also known as the zero-equation models, are the simplest of all turbulent models. Here, (1) the Reynolds stress is expressed as the product of a turbulence viscosity (eddy viscosity) and the mean strain rate, the so-called Boussinesq eddy-viscosity approximation, and (2) the turbulence viscosity, in turn, is often computed in terms of a mixing length. Of the algebraic models, the mixing-length model is the simplest and the most "popular" one. This model will be described in the next section.

Turbulence-energy equation models are advanced models. Here, too, the Reynolds stress is expressed as the product of a turbulence viscosity (eddy viscosity) and the mean strain rate. However, the turbulence viscosity is not computed in terms of a mixing length, but rather in terms of the turbulence kinetic energy, $k = \frac{1}{2}(\overline{u_i'u_i'})$. There are two kinds of turbulence-energy equation models: (1) One-equation models, and (2) Two-equations models. As an example, the so-called $k-\omega$ model, a two-equations model, will be described in the following paragraphs.

Simulation models are most advanced models. These models directly address the turbulence process itself, and therefore they do not involve the afore mentioned closure problem. In a DNS study, a complete time-dependent solution of the Navier-Stokes equations and the continuity equation is sought. Therefore the solution furnishes the time series of (1) the three components of the velocity and (2) the pressure in 3-D space. Up until now, only low Reynolds number-flows are calculated with the DNS method. For large Reynolds numbers, the scales of the dissipative part of turbulence motion are so small that this kind of small scale motion can not be resolved in a numerical calculation (the number of grid points required to resolve this motion increases approximately with Re^3, Rodi, 1992). However, the upper limit of the Reynolds number range is pushed to higher and higher values as more and more computer power becomes available. Rogallo and Moin (1984) gives a review of the DNS method where the principal/early publications are cited. Regarding the LES model, here the large eddies (large-scale motions) are computed while the smallest eddies are modelled. The details of the LES model along with an application example are given in the chapter.

Wilcox's (1994) book can be consulted for a detailed account of turbulence models.

6.3 Mixing-length model

The mixing-length model is an algebraic model. We will describe this model with reference to the steady boundary-layer flow close to a smooth or rough wall (i.e., in the constant stress layer, see Section 2.1).

6.3.1 Turbulent transport of momentum

Under this subsection, we will focus on the turbulent transport of momentum. We need this piece of information to develop the mixing-length theory/model. The treatment will be quite general, not necessarily limited to the flow close to a wall.

For this, we refer to Fig. 6.1, and we consider a small fluid element (a fluid parcel) adjacent to the unit area indicated in Fig. 6.1, A (Fig. 6.2), at time t. This fluid parcel will be transported to the other side of the area during the time interval Δt (B, Fig. 6.2), and this is due to the turbulent motion. (No such transportation would occur if the flow was in the laminar

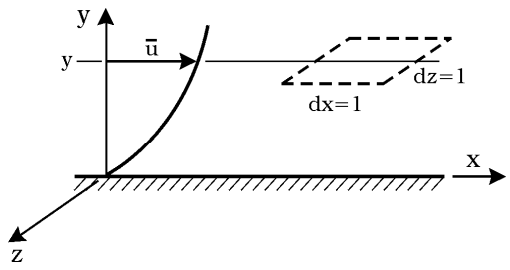

Figure 6.1: Definition sketch.

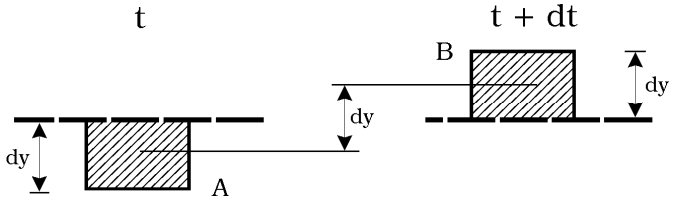

Figure 6.2: Travel of fluid element A from one side of the area (dx,dz) considered in the previous figure to the other side.

regime.)

The mass of the fluid transported from one side of the unit area to the other is

$$\rho(1 \times 1 \times dy)$$

and therefore the momentum transported in the $y-$direction from one side of the unit area to the other ($x-$ component):

$$x - \text{component of momentum transported: } \rho(1 \times 1 \times dy) \times u$$

or, inserting $u = \overline{u} + u'$

$$x - \text{component of momentum transported: } \rho(1 \times 1 \times dy) \times (\overline{u} + u')$$

and, similarly, the $y-$component:

$$y - \text{component of momentum transported: } \rho(1 \times 1 \times dy) \times v$$

Now, Newton's second law (for the $x-$direction)

$$\begin{aligned} F_x &= \frac{d}{dt}\left[x - \text{component of momentum transported}\right] \\ &= \frac{d}{dt}\left[\rho(1 \times 1 \times dy) \times (\overline{u} + u')\right] \\ &= \rho\frac{d(dy)}{dt}(\overline{u} + u') \end{aligned}$$

in which F_x is the force generated by this momentum transport. Here, $\frac{d(dy)}{dt} = \frac{d}{dt}(\text{Vertical distance travelled by fluid}) = v = v'$, and therefore

$$F_x = \rho v'(\overline{u} + u')$$

and by time averaging

$$\overline{F_x} = \rho\overline{v'(\overline{u} + u')} = \rho\overline{v'\overline{u}} + \rho\overline{u'v'}) = 0 + \rho\overline{u'v'} = \rho\overline{u'v'} \tag{6.5}$$

Likewise, Newton's second law for the $y-$direction gives

$$\overline{F_y} = \rho\overline{v'v'} \tag{6.6}$$

These forces, $\overline{F_x}$ and $\overline{F_y}$, are exerted on the unit area indicated in Fig. 6.1, and therefore they are, respectively, the shear and normal stresses. (Notice that these stresses are induced by turbulence (Fig. 6.3.) So the above analysis demonstrates that

1. The turbulent transport of momentum in the $y-$direction generates stresses in the fluid;

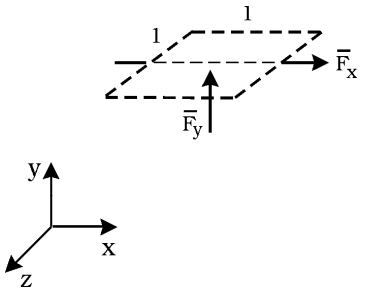

Figure 6.3: Forces (stresses) induced by turbulence.

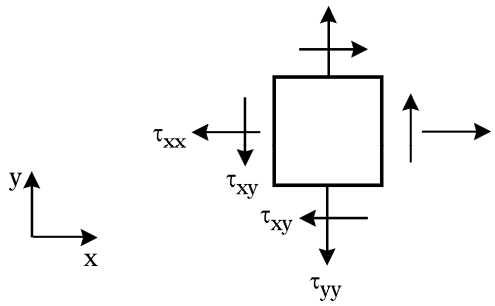

Figure 6.4: Stresses generated by turbulence.

2. The transport corresponding to the $x-$component of the momentum generates a shear stress, equal to $-\rho\overline{u'v'}$, considering the sign convention adopted in Chapter 1 (the positive shear stress is in the direction opposite to the $x-$direction); and

3. The transport corresponding to the $y-$component of the momentum generates a normal stress, equal to $-\rho\overline{v'v'}$ (again, considering the positive normal stress is in the direction opposite to the $y-$direction).

Hence the stresses generated by turbulence are

$$\begin{bmatrix} \tau_{xx} & \tau_{xy} \\ \tau_{xy} & \tau_{yy} \end{bmatrix} = \begin{bmatrix} -\rho\overline{u'^2} & -\rho\overline{u'v'} \\ -\rho\overline{u'v'} & -\rho\overline{v'^2} \end{bmatrix} \tag{6.7}$$

(see Fig. 6.4).

These are the Reynolds stresses introduced already in Chapter 1. We obtained the Reynolds stresses in Chapter 1 by time averaging the Navier-Stokes equations. Here, we have obtained the Reynolds stresses in a different way, in a way which will prove useful when developing the mixing-length model/theory in the next sub-section.

6.3.2 Mixing length

1) Reynolds shear stress in terms of the mixing length

Consider a fluid parcel, A, at location I (Fig. 6.5). Suppose that this fluid parcel has just been formed as a new coherent entity at Location I, and

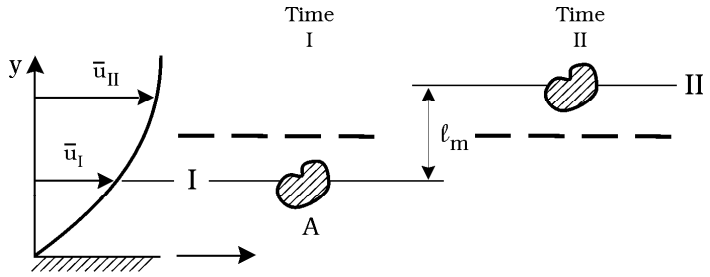

Figure 6.5: A fluid parcel travelling from Level I to Level II.

suppose that it starts to move upwards. Now, from Level I, the fluid parcel will travel a distance ℓ_m, called mixing length, and subsequently mix with the surrounding fluid at Level II. (We expect that ℓ_m is much the same as the Lagrangian macro length scale, or the Eulerian macro length scale in the $y-$direction, see Chapter 3).

With the upward motion of the fluid parcel,

1. Momentum will be transported over the distance ℓ_m, from Level I to Level II;

2. This momentum transport will generate a shear stress, equal to $-\rho\overline{u'v'}$; and

3. Newton's second law implies that the change in the momentum over the time from I to II should be equal to the shear stress $-\rho\overline{u'v'}$, i.e.,

$$-\rho\overline{u'v'} = \text{Momentum II} - \text{Momentum I} \tag{6.8}$$

The right-hand-side of the preceding equation is the momentum gained with the travel of the fluid parcel from I to II.

With the travel of the fluid parcel from I to II, the $x-$component of the fluid velocity will increase from u_I to u_{II} , and therefore the gained velocity will be

$$\overline{u}_{II} - \overline{u}_I \cong \ell_m \frac{d\overline{u}}{dy} \tag{6.9}$$

The gained momentum ($x-$component) will then be, Fig. 6.6:

$$\text{Momentum II} - \text{Momentum I} = (\rho q)(\ell_m \frac{d\overline{u}}{dy}) \tag{6.10}$$

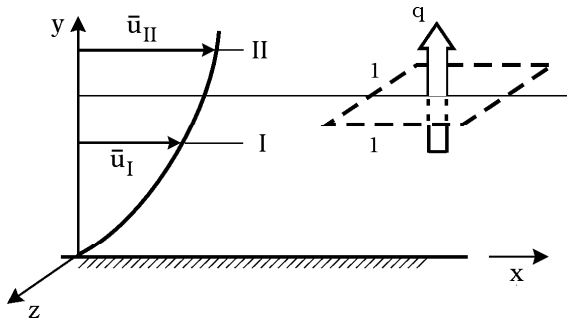

Figure 6.6: Volume associated with Fluid Parcel A passing through per unit area.

in which q is the volume associated with the fluid parcel (Fig. 6.5) passing through *per unit area per unit time* (Fig. 6.6). The quantity q is

$$q = V_t(1 \times 1) = V_t$$

and therefore the gained momentum ($x-$component) will be

$$\text{Momentum II} - \text{Momentum I} = \rho V_t \ell_m \frac{d\overline{u}}{dy} \tag{6.11}$$

in which V_t is the fluid velocity in the vertical direction, an average velocity representing the vertical velocity of the fluid parcel over the travelled distance ℓ_m. From Eqs. 6.8 and 6.11:

$$-\rho\overline{u'v'} = \text{Momentum II} - \text{Momentum I} = \tag{6.12}$$

$$= \rho V_t \ell_m \frac{d\overline{u}}{dy} \tag{6.13}$$

2) Boussinesq eddy-viscosity approximation and Prandtl's mixing length hypothesis

Now, drawing an analogy to Newton's friction law

$$\tau = \mu \frac{du}{dy} \tag{6.14}$$

the turbulence shear stress can be written as (as was first suggested by Boussinesq in 1877)

$$-\rho\overline{u'v'} = \mu_t \frac{d\overline{u}}{dy} \tag{6.15}$$

in which μ_t is called turbulence viscosity (or eddy viscosity). Hence, from Eqs. 6.13 and 6.15, the turbulence viscosity is

$$\mu_t = \rho \ell_m V_t \tag{6.16}$$

The hypothesis leading to Eq. 6.16 is known as *Prandtl's mixing-length hypothesis*.

(It may be noted that, in a recent publication, Nielsen and Teakle, 2004, develop a theory of turbulent diffusion of momentum and suspended particles, a finite-mixing-length theory, in which the turbulence viscosity is expressed as $\mu_t = \rho \ell_m V_t (1 + O(\ell_m/L)^2)$. Here L is the scale of the velocity distribution $\overline{u}(y)$. It may also be noted that different diffusivities exhibited by different "species", like density, heat and salinity, in turbulent flows may be qualitatively explained in terms of Nielsen and Teakle's theory. See also Absi, 2005, in relation to the latter publication.)

To sum up at this point: (1) The Reynolds shear stress is expressed as the product of a turbulence viscosity (eddy viscosity), μ_t, and the mean strain rate, $\frac{d\overline{u}}{dy}$ (Eq. 6.15), the so-called Boussinesq eddy-viscosity approximation; and (2) The turbulence (eddy) viscosity, in turn, is computed in terms of the mixing length (Eq. 6.16).

3) Prandtl's second hypothesis

The question is, however: What is V_t? To assess and therefore model this, we consider the control volume in Fig. 6.7. The motion associated with the fluid parcel A in Fig. 6.5 is from the left bottom corner of the control volume to the right top corner, and involves three kinds of velocities:

1. The vertical velocity V_t at the instant I (It is important to notice that there is no vertical velocity at the instant II because the fluid parcel mixes with the surrounding fluid at II; Recall the definition of the mixing length ℓ_m.);

2. The horizontal velocity at the instant I; and

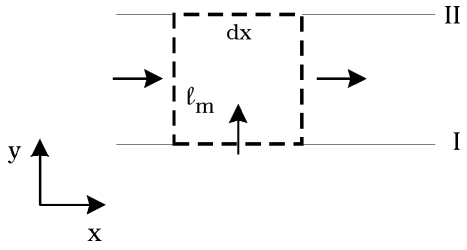

Figure 6.7: Control volume.

3. The horizontal velocity at the instant II.

The amount of fluid entering the control volume in the vertical direction (associated with this motion) per unit time is then:

$$V_t \times dx \tag{6.17}$$

while the amount of fluid entering the control volume in the horizontal direction per unit time at the instant I:

$$\overline{u}_I \times \ell_m \tag{6.18}$$

and that leaving the control volume in the horizontal direction per unit time at the instant II:

$$\overline{u}_{II} \times \ell_m \tag{6.19}$$

Continuity requires:

$$V_t \times dx + \overline{u}_I \times \ell_m = \overline{u}_{II} \times \ell_m$$

and therefore

$$V_t = (\overline{u}_{II} - \overline{u}_I)\frac{\ell_m}{dx}$$

and since $O(\ell_m) = O(dx)$ (small), then

$$V_t \cong \overline{u}_{II} - \overline{u}_I$$

or from Eq. 6.9:

$$V_t \cong \ell_m \frac{d\overline{u}}{dy}$$

We write the term $\frac{d\overline{u}}{dy}$ in terms of its absolute value to ensure that the amount of fluid passing through the unit area, i.e., $q(= v)$ is always positive (Fig. 6.5):

$$V_t = \ell_m \left| \frac{d\overline{u}}{dy} \right| \tag{6.20}$$

This is known as *Prandtl's second hypothesis.*

With the latter hypothesis (Eq. 6.20), the turbulence (eddy) viscosity from Eq. 6.16 is expressed as

$$\mu_t = \rho \ell_m^2 \left| \frac{d\overline{u}}{dy} \right| \tag{6.21}$$

4) van Driest mixing length

The fourth step is to determine the mixing length in the preceding equation. Until now the analysis is given for the general case, and therefore it can be implemented for any distance y from the wall. However, from now on, we will restrict our attention to the region close to the wall, the layer called constant stress layer. (See Chapter 2). So, y is so small that we are in the constant stress layer, $\tau \simeq \tau_0$, and for this

$$y \ll h$$

in which h is the flow depth in the case of an open channel flow, or it is the radius in the case of a pipe flow, or the boundary-layer thickness in the case of a boundary layer over a wall. (See discussion in Section 2.1.2);

On the other hand, y should be sufficiently large, so large that the transport of momentum is due to turbulence. (Viscosity is neglected in the transport of momentum; This is for the case of the smooth wall. The rough-wall case will be treated later.) We require that the transport of momentum is due to turbulence because the previously described mixing length (Section 1.3.2) is essentially based on the turbulent transport of momentum. This last condition requires that y^+ should be

$$y^+ > 30 - 70$$

in which $y^+ = \frac{yU_f}{\nu}$, U_f being the wall shear stress (friction) velocity (Chapter 2).

Now, we should expect that the mixing length (for y values in the range $y \ll h$ and $y^+ > 30 - 70$) increases with increasing distance from the wall, and the simplest form of this dependence is

$$\ell_m = \varkappa y \tag{6.22}$$

in which $\varkappa$ is a constant. From the solution for the velocity (Eq. 6.28), $\varkappa$ turns out to be the von Karman constant ($\varkappa = \frac{1}{A} = 0.4$) introduced in Chapter 2. Eq. 6.22 is valid for the ranges $30 - 70 < y^+$, and $y \ll h$.

van Driest (1956) revised Eq. 6.22 so as to accommodate the influence of viscosity in the transport of momentum. This led to

$$\ell_m = \varkappa y[1 - \exp(-\frac{y^+}{A_d})] \tag{6.23}$$

in which A_d is called the damping coefficient, and taken as 25, and this equation for the mixing length is valid for the range $0 \leq y \ll h$. From Eq. 6.23, it is seen that

$$\ell_m \to \varkappa y, \text{ for large values of } y^+ \tag{6.24}$$

while

$$\ell_m \to 0, \text{ as } y^+ \to 0 \tag{6.25}$$

The latter implies that there will be no turbulent transport of momentum as the wall is approached. Note that, for rough-wall flows, the mixing-length will inevitably change. We shall consider the transitional and rough-wall situations later.

5) Summary of the model equations and solution

Eqs. 6.15, 6.21 and 6.23 are the model equations:

$$-\rho\overline{u'v'} = \mu_t \frac{d\overline{u}}{dy}$$

$$\mu_t = \rho\ell_m^2 \left|\frac{d\overline{u}}{dy}\right|$$

$$\ell_m = \varkappa y[1 - \exp(-\frac{y^+}{A_d})]$$

So, for the problem we consider, i.e., the steady boundary-layer flow close to a smooth wall (in the constant stress layer, see Section 2.1), there are three model equations (the preceding equations), and one Reynolds equation, Eq. 2.87, i.e., altogether four equations, and four unknowns, namely, $\overline{u}$, $-\rho\overline{u'v'}$, μ_t, and ℓ_m. Hence, the system is closed. Therefore the unknowns can be determined. Of particular interest is the velocity, $\overline{u}$. The solution for the latter quantity is obtained in Section 2.3.1 (Eq. 2.97):

$$\overline{u} = 2U_f \int_0^{y^+} \frac{dy^+}{1 + \left\{1 + 4\varkappa^2 y^{+2}[1 - \exp(-\frac{y^+}{A_d})]^2\right\}^{1/2}} \tag{6.26}$$

(the *van Driest* velocity distribution, Fig. 2.20). This equation is valid in the constant stress layer, namely for the range $0 \leq y \ll h$.)

For small values of y^+, the van Driest profile reduces to the linear velocity distribution in the viscous sublayer (Eq. 2.20),

$$\frac{\overline{u}}{U_f} = y^+ \tag{6.27}$$

while, for large values of y^+, it reduces to the logarithmic velocity distribution in the logarithmic layer (Eq. 2.20),

$$\overline{u} = U_f \ (A \ln y^+ + B) \tag{6.28}$$

It is seen from Fig. 2.20 that the van Driest profile agrees remarkably well with the experiment.

6) Mixing length in the case of transitional and rough walls and solution

In this case, the mixing length may be given as (Cebeci and Chang, 1978)

$$\ell_m = \varkappa(y + \Delta y)[1 - \exp(-\frac{(y^+ + \Delta y^+)}{A_d})] \tag{6.29}$$

y in the above equation is measured from the level where the velocity $\overline{u}$ is zero. This level lies almost at the top of the roughness elements, as discussed in Section 2.3.1 (y here should not be confused with the distance measured from the theoretical wall. $y+\Delta y$ is the distance measured from the theoretical wall. See the detailed discussion in Section 2.3.1).

Δy is the so-called coordinate displacement, or the coordinate shift (see Example 5 in Section 2.3.1), and given by Cebeci and Chang (1978)

$$\Delta y^+ = 0.9[\sqrt{k_s^+} - k_s^+ \ \exp(-\frac{k_s^+}{6})]; \qquad 5 < k_s^+ < 2000 \tag{6.30}$$

in which k_s^+ is the roughness Reynolds number (k_s being Nikuradse's equivalent sand roughness):

$$k_s^+ = \frac{k_s U_f}{\nu} \tag{6.31}$$

Here the distance from the wall y should be in the interval $0 \leq y \ll h$ where the upper boundary ensures that the y levels lie in the constant stress layer.

The solution for $\overline{u}$ for the set of the model equations along with the Reynolds equation is obtained in Section 2.3.1 (Eq. 2.103):

$$\overline{u} = 2U_f \int_0^{y^+} \frac{dy^+}{1 + \left\{1 + 4\varkappa^2(y^+ + \Delta y^+)^2[1 - \exp(-\frac{(y^+ + \Delta y^+)}{A_d})]^2\right\}^{1/2}} \tag{6.32}$$

Fig. 2.21 displays the velocity profiles obtained from the preceding equation including the smooth-wall profile. In Fig. 2.21, a represents the linear profile in the viscous sublayer (Eq. 6.27), b the logarithmic profile (Eq. 6.28) in the case of the hydraulically smooth wall, and c the logarithmic profile in the case of the completely rough wall (Eq. 2.65), namely, by putting $z = y + \Delta y$,

$$\overline{u} = AU_f \ \ln(\frac{30z}{k_s}) \tag{6.33}$$

z being measured from the theoretical wall.

7) Turbulence quantities

The turbulence quantities, namely the Reynolds stresses, $-\rho\overline{u'^2}$, $-\rho\overline{v'^2}$, $-\rho\overline{w'^2}$ and $-\rho\overline{u'v'}$, also are unknowns. The Reynolds shear stress, $-\rho\overline{u'v'}$, can be determined, using the model equation $-\rho\overline{u'v'} = \mu_t \frac{d\overline{u}}{dy}$, once the velocity $\overline{u}$ is computed. The mixing-length model is "designed" only to be able to handle the velocity $\overline{u}$, (and from the latter, the Reynolds stress $-\rho\overline{u'v'}$). It does not offer solutions for the other three unknowns, the turbulence quantities $-\rho\overline{u'^2}$, $-\rho\overline{v'^2}$ and $-\rho\overline{w'^2}$.

6.4 k-omega model

This model is a turbulence-energy equation model. As mentioned in the preceding paragraphs, there are two kinds of turbulence-energy equation model, one-equation model and two-equations model. The $k-\omega$ model is a two-equations model.

There are three versions of the $k-\omega$ model in the literature: (1) the original $k-\omega$ model, which is due to Wilcox (1994), (2) the $k-\omega$, BSL (baseline) model, and (3) the $k-\omega$, SST (shear-stress transport) model. The latter two models were developed by Menter (1993) to improve Wilcox's original model so that an even higher sensitivity could be obtained for adverse-pressure-gradient flows. In this section, we will describe the $k-\omega$, SST model.

Incidentally, the following note is worth mentioning. Menter (1993) made an extensive comparison between (1) the classic $k-\varepsilon$ model; (2) the original $k-\omega$ model; (3) the $k-\omega$, BSL model; and (4) the $k-\omega$, SST model for various well documented flows. The tested flows were, among others, two kinds of *adverse pressure gradient flow* (one having a very strong adverse pressure gradient, so strong that separation occurs); the backward-facing-step flow; and the flow past a NACA 4412 airfoil at an angle of attack near maximum lift condition. The latter two flows also have substantial *adverse pressure gradient* effects. The main conclusion from this inter-comparison exercise was that the $k-\omega$, SST model gave the most accurate results while the $k-\varepsilon$ model did not yield as accurate results as the other three for the tested adverse-pressure-gradient flow cases.

6.4.1 Model equations

There are two basic equations in the $k-\omega$ model: one equation for k, and the other equation for ω in which k is the turbulent kinetic energy (Eq. 1.31 or Eq. 6.36) and ω the specific dissipation of turbulent kinetic energy (Eq. 6.37). (We will use the symbol k for turbulent energy in favour of K_t, to be consistent with the usual notation used in the literature in conjunction with turbulence modelling.)

The equation for k:

$$\frac{\partial \rho k}{\partial t} + \frac{\partial \rho \overline{u}_j k}{\partial x_j} - \frac{\partial}{\partial x_j}\left[(\mu + \sigma_k \mu_t)\frac{\partial k}{\partial x_j}\right] = \tau_{ij}\frac{\partial \overline{u}_i}{\partial x_j} - \beta^* \rho k \omega \tag{6.34}$$

(It should be noted that this equation is in a form slightly different from that

given in Chapter 1 (Eq. 1.30). The derivation of this equation is given in Wilcox (1994, pp. 74-76). This reference also includes a detailed discussion on the $k-\omega$ model.)

Now, the second equation, the equation for ω:

$$\frac{\partial \rho\omega}{\partial t} + \frac{\partial \rho\overline{u}_j\omega}{\partial x_j} - \frac{\partial}{\partial x_j}\left[(\mu + \sigma_\omega \mu_t)\frac{\partial \omega}{\partial x_j}\right] = \frac{\gamma}{\nu_t}\tau_{ij}\frac{\partial \overline{u}_i}{\partial x_j} - \beta\rho\omega^2$$

$$+2\rho\,(1-F_1)\,\frac{\sigma_{\omega 2}}{\omega}\frac{\partial k}{\partial x_j}\frac{\partial \omega}{\partial x_j} \tag{6.35}$$

Above, k is:

$$k = \frac{1}{2}\overline{u_i' u_i'} \tag{6.36}$$

and ω:

$$\omega = \frac{\varepsilon}{k\beta^*} \tag{6.37}$$

in which ε is the dissipation of turbulent kinetic energy

$$\varepsilon = \nu\overline{\frac{\partial u_i'}{\partial x_k}\frac{\partial u_i'}{\partial x_k}} \tag{6.38}$$

In the preceding equations, τ_{ij} is the Reynolds stresses ($= -\rho\overline{u_i' u_j'}$),

$$\tau_{ij} = -\rho\overline{u_i' u_j'} = \mu_t\left(\frac{\partial \overline{u}_i}{\partial x_j} + \frac{\partial \overline{u}_j}{\partial x_i}\right) - \frac{2}{3}\rho k\delta_{ij} \tag{6.39}$$

u_i' is the fluctuating components of the velocity, δ_{ij} is the Kronecker delta ($\delta_{ij} = 1$ for $i = j$ and $\delta_{ij} = 0$ for $i \neq j$), and ν_t is kinematic eddy viscosity, $\nu_t = \mu_t/\rho$, and β^* is one of the model closure constants.

As seen from Eq. 6.39, this model, too, assumes the Boussinesq eddy-viscosity approximation where the Reynolds stress is related to the rate of mean strain. Note that we need the second term on the right-hand-side of Eq. 6.39 so that, when contracting (that is, when i is set equal to j), Eq. 6.39 gives $k = \frac{1}{2}\overline{u_i' u_i'}$, compatible with Eq. 6.36 (Wilcox, 1994, p. 75).

Now, σ_k in Eq. 6.34 and σ_ω, γ and β in Eq. 6.35 are given as

$$\sigma_k = F_1\sigma_{k1} + (1-F_1)\sigma_{k2} \tag{6.40}$$

$$\sigma_\omega = F_1\sigma_{\omega 1} + (1-F_1)\sigma_{\omega 2} \tag{6.41}$$

$$\gamma = F_1\gamma_1 + (1 - F_1)\gamma_2 \tag{6.42}$$

$$\beta = F_1\beta_1 + (1 - F_1)\beta_2 \tag{6.43}$$

in which σ_{k1}, σ_{k2}, $\sigma_{\omega1}$, $\sigma_{\omega2}$, γ_1, γ_2, β_1 and β_2, the model constants, are combined as a function of the distance z to the nearest wall with the so-called blending function , F_1.

6.4.2 Model constants

The model constants for inner (wall) region are:

β_1	β^*	$\gamma_1(=\frac{\beta_1}{\beta^*} - \frac{\sigma_{\omega1}\varkappa^2}{\sqrt{\beta^*}})$	σ_{k1}	$\sigma_{\omega1}$
0.0750	0.09	0.567	0.85	0.5

and for the outer region ($\varkappa$ in the tables is the von Karman constant):

β_2	β^*	$\gamma_2(=\frac{\beta_2}{\beta^*} - \frac{\sigma_{\omega2}\varkappa^2}{\sqrt{\beta^*}})$	σ_{k2}	$\sigma_{\omega2}$
0.0828	0.09	0.463	1.0	0.856

6.4.3 Blending function $\mathbf{F}_1$

The blending function F_1 is

$$F_1 = tanh\left(arg_1^4\right) \tag{6.44}$$

and

$$arg_1 = min\left[max\left(\frac{\sqrt{k}}{0.09\omega z}; \frac{500\nu}{z^2\omega}\right); \frac{4\rho k\sigma_{\omega2}}{(CD_{k\omega})z^2}\right] \tag{6.45}$$

with

$$(CD_{k\omega}) = max\left(2\rho\frac{\sigma_{\omega2}}{\omega}\frac{\partial k}{\partial x_j}\frac{\partial \omega}{\partial x_j}; 10^{-20}\right) \tag{6.46}$$

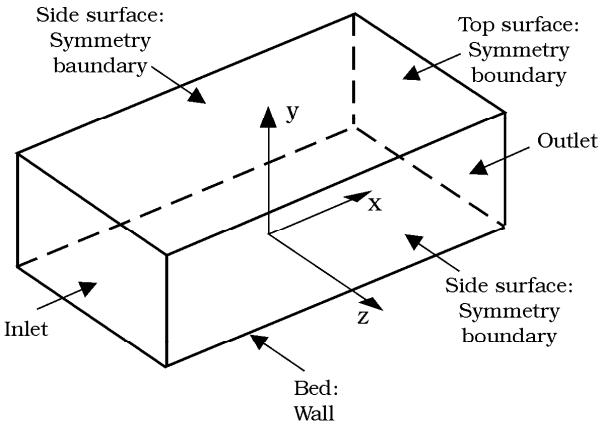

Figure 6.8: Computation domain.

6.4.4 Eddy viscosity and Blending function $\mathbf{F_2}$

In the $k-\omega, SST$ model, the eddy viscosity is calculated from

$$\mu_t = \rho \frac{0.3k}{max\left(0.3\omega; \Omega F_2\right)} \tag{6.47}$$

where Ω is the absolute value of the vorticity. The function F_2 in Eq. 6.47 is another blending function, defined by

$$F_2 = tanh\left(arg_2^2\right) \tag{6.48}$$

in which

$$arg_2 = max\left(2\frac{\sqrt{k}}{0.09\omega z}; \frac{500\nu}{z^2\omega}\right) \tag{6.49}$$

Both F_1 and F_2 take the value unity at the wall and gradually decrease and approach to zero as the distance from the wall is increased.

6.4.5 Boundary conditions

The boundaries of the computational domain (Fig. 6.8) are (1) Inlet, (2) Outlet, (3) Symmetry Boundaries and (4) Walls (e.g., the bed in the example

given in Fig. 6.8 and the surface of a rigid body present in the computational domain, if any).

1) Inlet and outlet boundary conditions

At the inlet, zero transverse, and vertical velocities are specified. At the outlet, zero-gradient conditions ($\partial/\partial n = 0$), Neumann conditions, are applied for all quantities.

2) Symmetry boundaries

At the symmetry boundaries , Neumann conditions are applied for k and ω and for the three components of the velocity (u, v and w). This is (1) at the sides and (2) at the top surface of the computational domain where a "lid" is placed in the case when the model cannot handle the free surface, Fig. 6.8).

3) Walls (e.g., the bed and/or the surface of a rigid body)

1. Zero velocity is specified for u , v and w.

2. Zero turbulent energy is specified for k when the wall is smooth, while the Neumann condition is applied when the wall is rough and transitional. Regarding the latter condition, experiments reveal that the Neumann condition is satisfied ($\partial k/\partial n = 0$) at the wall for rough boundaries, n being the direction normal to the wall (Nezu, 1977, Sumer et al., 2001 and 2003). A validation exercise for the case of a steady boundary layer in an open channel flow revealed a much better agreement with the experiments (Nezu, 1977, and Sumer et al., 2001) when the boundary condition was taken in the form of the Neumann condition (Roulund, 2000, p. 25).

3. The Dirichlet condition is applied for ω, namely

$$\omega = S_r \frac{U_f^2}{\nu} \quad \text{at the wall} \tag{6.50}$$

where $U_f = \sqrt{\tau_o/\rho}$ is the friction velocity based on the wall shear stress τ_o. The quantity S_r is a tuning parameter, and it is used to account for the bed roughness:

$$S_r = \begin{cases} \left(\frac{40}{k_s^+}\right)^3 & , \quad k_s^+ < 20.2 \\ \frac{100}{\left(k_s^+\right)^{0.85}} & , \quad k_s^+ > 20.2 \end{cases} \tag{6.51}$$

where $k_s^+ = (k_s U_f)/\nu$ is the wall roughness in wall units, and k_s is Nikuradse's equivalent sand roughness. Wilcox (1994) was the first to introduce the boundary condition in Eq. 6.50. The tuning parameter S_r was given by Wilcox (1994) as in Eq. 6.51, but with constants slightly different from those in Eq. 6.51 due to the special implementation of the velocity boundary conditions. With the present constants (Eq. 6.51), the friction velocity determined for a wide range of velocities for the case of the undisturbed flow was found to agree rather well with that obtained from the classic Colebrook and White equation (the difference being less than 6%, depending on the wall roughness, Roulund, 2000, p. 23).

4. For the implementation of the preceding boundary condition, the wall shear stress, $\tau_0 (= \rho U_f^2)$, is needed. Traditionally, τ_0 is calculated from $\tau_0 = (\mu + \mu_t)(\frac{\partial \overline{u}_i}{\partial x_j} + \frac{\partial \overline{u}_j}{\partial x_i})_{Wall}$. However, it may also be calculated from the van Driest (1956) velocity profile (Eq. 6.32):

$$\frac{\overline{u}}{U_f} = 2 \int_0^{y^+} \frac{dy^+}{1 + \sqrt{1 + 4\kappa^2 \left(y^+ + \Delta y^+\right)^2 \left[1 - \exp\left(-\frac{y^+ + \Delta y^+}{A}\right)\right]^2}} \tag{6.52}$$

This improves the stability of the model and allows a coarser mesh resolution at the bed, as was revealed by the work of Roulund et al. (2005). In the implementation of Eq. 6.52, $\overline{u}$ is taken as the tangential velocity in the cell adjacent to the wall.

Similar implementation of the bed shear stress in the wall boundary conditions is reported in Sørensen (1995) for the $k - \varepsilon$ model.

As a final remark in conjunction with the previous description, it may be emphasized that the $k - \omega$ model is a well tested model and has been used successfully in various contents in computational fluid dynamics (Wilcox, 1994, Menter, 1993). The only change made in the present implementation is the values of the constants in Eq. 6.51 which are slightly different from those originally given by Wilcox (1994) (item 3 above), plus the way in which the wall shear stress is calculated is through the van Driest equation (item 4 above).

6.4.6 Numerical computation

To sum up, the set of equations which needs to be solved consists of

1. The continuity equation, Eq. 6.1;

2. The Reynolds equations, Eqs. 6.2-6.4; and

3. The model equations, Eqs. 6.34-6.35.

With the solution, the three velocity components, the pressure, the turbulent kinetic energy and the specific dissipation of turbulent kinetic energy are calculated.

Unlike the mixing-length model, this set of equations is too complex for one to seek analytical solutions. Instead, the equations are solved numerically. To this end, one resorts to a CFD (Computational-Fluid-Dynamic) code coupled with a turbulence model (e.g., the $k-\omega$ model in the present case) which is incorporated into the code. CFD codes may also offer various turbulence-modelling options. In these codes, the momentum, continuity and turbulence-model equations are typically transformed into curvilinear coordinates, and they may be linearized and decoupled. The equations are discretized, using a computational mesh (e.g., the latter can be based on a multi-block structure with each block containing N^3 computational cells where N is the number of cells in each spatial direction.)

The $k-\omega$ model was implemented in a Ph.D. study to calculate flow around a vertical cylinder (a bridge pier or a pile) in relation to numerical modelling of scour around such structures (Roulund, 2000, and Roulund et al., 2005). More information about the model, boundary conditions, numerical computation, etc. with regard to the previously mentioned application can be found in the latter publications.

6.4.7 An application example

Under this subsection, we will present the results of a small study where the $k-\omega$ model was employed.

The CFD code used in this study, **EllipSys3D,** is a three-dimensional general purpose flow solver (an incompressible general purpose Navier-Stokes solver). It is a multiblock finite-volume numerical model that solves the incompressible Reynolds equations (Eqs. 6.2-6.2). The $k-\omega, SST$ model is used as the turbulence closure. EllipSys3D has been developed at the Risø National Laboratory, Denmark and at the Technical University of Denmark, Department of Fluid Mechanics. The code offers a variety of turbulence-model options, including the $k-\omega, SST$ model. The basic principles of the model are described in Michelsen (1992) and Sørensen (1995).

The problem studied in this example is a steady boundary layer flow in an open channel with a smooth, or alternatively, a rough bed. The flow domain is the same as that depicted in Fig. 6.8. As the model does not have the free-surface facility, a lid is placed at the top surface of the computational domain. The boundary conditions are exactly the same as described above under the heading *Boundary conditions*. The study is a part of the Ph.D. project of Dixen (2007).

Figs. 6.9 and 6.10 compare the velocity distributions obtained in this study with the experimental data, in linear and semi-logarithmic plots, respectively. (The Reynolds number is $Re(=\frac{hV}{\nu}) = 1.9 \times 10^4$, V being the depth-average velocity.) The agreement between the model prediction and the experiment is very good. (It may be noted that the experimental data agree very well with the van Driest velocity profile, not shown here for reasons of space.)

Figs. 6.11 and 6.12 present the kinetic energy of turbulence, k, obtained by the model, Fig. 6.11 in y/h, and 6.12 in y^+ (the latter figure gives a close-up picture near the bed). The figures also present data from experiments. $k = \frac{1}{2}(\overline{u'^2} + \overline{v'^2} + \overline{w'^2})$ is obtained in the experiments by measuring the three components of the velocity. The model prediction is not as good as that regarding the mean velocity. It underpredicts the turbulent energy by about 30% near the bed. Wilcox (1994, pp. 132-135) also reports similar behaviour for channel- and pipe-flow applications.

Next we give the results obtained for a *rough bed*. Nikuradse's equivalent sand roughness, $k_s^+(= \frac{k_s U_f}{\nu})$, is 200. The Reynolds number, $Re(=\frac{hV}{\nu})$, is 1.4×10^4. Similar to the smooth-bed case, Figs. 6.13 and 6.14 compare the velocity distributions with the experimental data, in linear and semi-logarithmic plots, respectively. The agreement between the model results and the experiment is generally good although the model underpredicts the velocity by slightly less than 20% near the free surface (at the lid in the computational domain). The model prediction captures the velocity quite well in the logarithmic region and in the buffer zone.

Finally, Figs. 6.15 and 6.16 present the kinetic energy of turbulence, k, obtained by the model, Fig. 6.15 in $y^+(= \frac{yU_f}{\nu})$, and 6.16 in $\frac{y}{k_s}$. The agreement between the model prediction and the experiment is quite good.

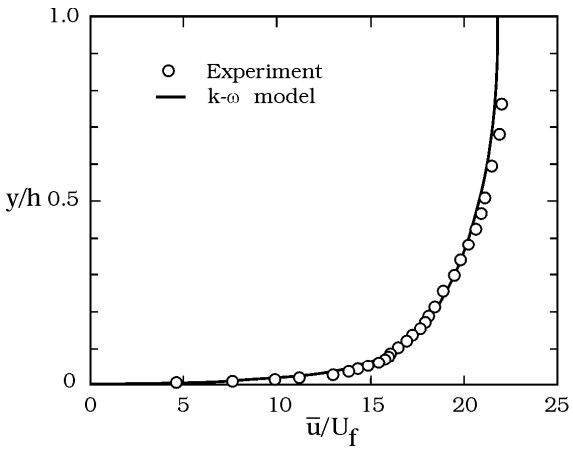

Figure 6.9: Velocity profile. Smooth wall.

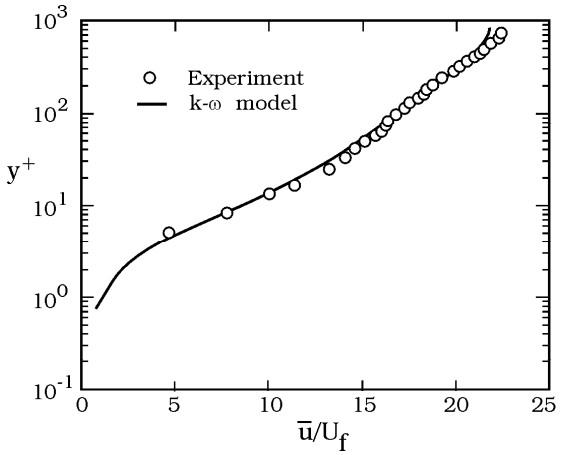

Figure 6.10: Velocity profile. Smooth wall. Semi-log plot.

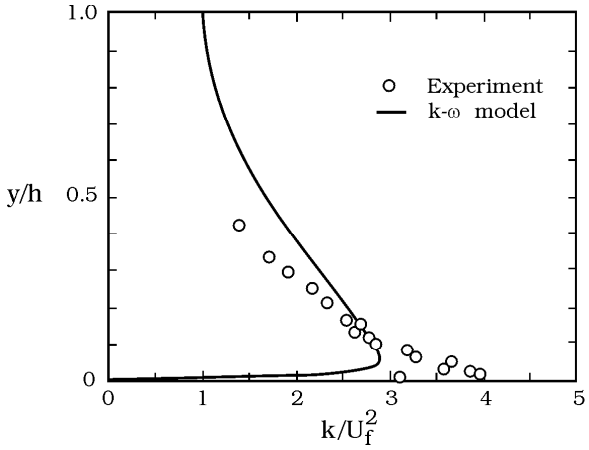

Figure 6.11: Turbulence kinetic energy versus distance from the wall. Smooth wall.

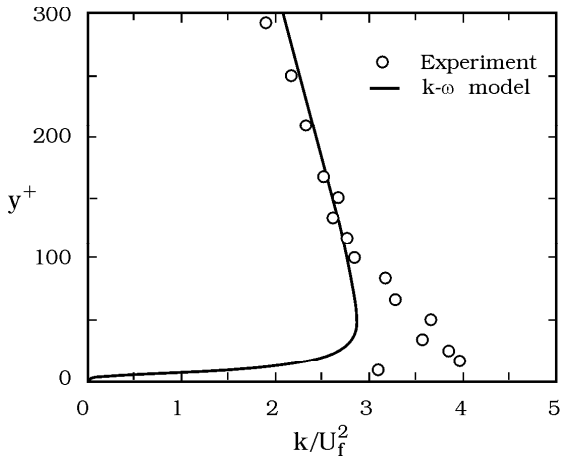

Figure 6.12: Turbulence kinetik energy versus distance from the wall, in terms of inner flow parameters. Smooth wall.

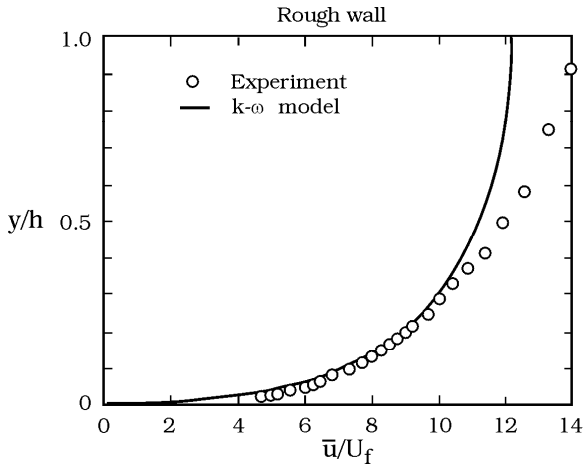

Figure 6.13: Velocity profile. Rough wall.

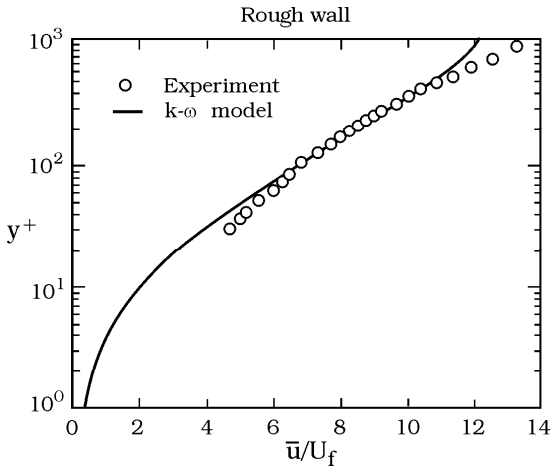

Figure 6.14: Velocity profile. Rough wall. Semi-log plot.

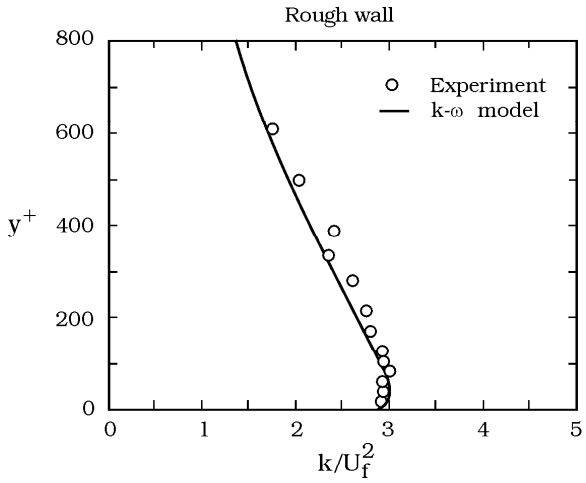

Figure 6.15: Turbulence kinetic energy in terms of inner flow parameters. Rough wall.

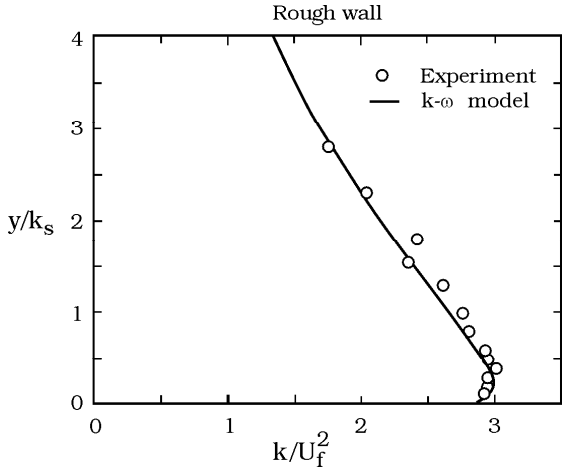

Figure 6.16: Turbulence kinetic energy in terms of inner flow parameters where the length scale is taken as ks. Rough wall.

6.5 Large Eddy Simulation (LES)

6.5.1 Model equations

The principal idea in the method of LES is to average the N.-S. equations over a small volume of space. (Recall that the N.-S. equations are averaged over time to obtain the Reynolds equations, i.e., Eqs. 6.1 and 6.2). Normally, the size of the averaging volume is chosen such that the small-scale component of turbulence is, for convenience, not resolved. The aforementioned space-averaging gives the following set of equations: (1) the continuity equation,

$$\frac{\partial u_i}{\partial x_i} = 0 \tag{6.53}$$

and (2) the equation of motion

$$\frac{\partial u_i}{\partial t} + u_j \frac{\partial u_i}{\partial x_j} = -\frac{1}{\rho}\frac{\partial p}{\partial x_i} + \nu \frac{\partial}{\partial x_j}\left(\frac{\partial u_i}{\partial x_j} + \frac{\partial u_j}{\partial x_i}\right) - \frac{\partial \overline{u_i' u_j'}}{\partial x_j} \tag{6.54}$$

in which u_i = the space-averaged (the resolved) component of the velocity; p = the space-averaged (the resolved) component of the pressure; and u_i' = the fluctuating component of the velocity over the averaging volume (called the subgrid-scale component of the velocity, to differentiate it from the term "fluctuation" in the conventional Reynolds decomposition), and $\overline{u_i' u_j'}$ = the subgrid-scale stresses, analogous to the Reynolds stresses in the case of the Reynolds decomposition.

The subgrid-scale stresses (SGS) are written (by analogy to the Boussinesq approximation)

$$\overline{u_i' u_j'} = \nu_t \left(\frac{\partial u_i}{\partial x_j} + \frac{\partial u_j}{\partial x_i}\right) \tag{6.55}$$

in which ν_t = the turbulence viscosity associated with the unresolved component of turbulence. (Note that the subgrid-scale stresses in the above equation are the off-diagonal part of the subgrid-scale stress tensor. The diagonal part is automatically included in the pressure term.) Hence, Eq. 6.54 will be

$$\frac{\partial u_i}{\partial t} + u_j \frac{\partial u_i}{\partial x_j} = -\frac{1}{\rho}\frac{\partial p}{\partial x_i} + \frac{\partial}{\partial x_j}\left[(\nu + \nu_t)\left(\frac{\partial u_i}{\partial x_j} + \frac{\partial u_j}{\partial x_i}\right)\right] \tag{6.56}$$

(It may be noted that the turbulence viscosity ν_t here is different from that in the $k - \omega$ model defined in the previous section. As emphasized in the

present definition, Eq. 6.55, ν_t is associated with the unresolved small-scale turbulence averaged over the "averaging" volume, while ν_t defined in conjunction with the $k-\omega$ model is associated with the turbulence over the entire spectrum).

On dimensional grounds, the turbulence viscosity is written as

$$\nu_t = C_s^2 \Delta^2 s \tag{6.57}$$

in which Δ is a length scale and C_s is a nondimensional constant. (By making an analogy to Prandtl's mixing-length hypothesis, it may be seen that s must be a quantity like $\partial u/\partial y$). We shall return to this point later.

Clearly, the resolved quantities, $u_i(x_i,t)$, $p(x_i,t)$ and $\nu_t(x_i,t)$ in Eqs. 6.55-6.57 should be dependent on the size of the averaging volume. The smaller the size of this volume, the better the resolution (both in space and time), and therefore the more information on space and time variations of $u_i(x_i,t)$, $p(x_i,t)$ and $\nu_t(x_i,t)$, implying that these quantities are dependent on the size of the averaging volume. This feature in LES is handled through ν_t as follows.

As seen in Eq. 6.57, ν_t involves a length scale, Δ. This quantity is taken as the length scale representing the size of the averaging volume

$$\Delta = (\Delta x_1 \Delta x_2 \Delta x_3)^{1/3} \tag{6.58}$$

in which Δx_1, Δx_2, Δx_3 are the grid sizes in the x_1-, x_2-, x_3- directions, respectively. (The averaging volume being considered to be $\Delta x_1 \Delta x_2 \Delta x_3$). Furthermore, the quantity s in Eq. 6.57 is taken as

$$s = (2 S_{ij} S_{ij})^{1/2} \tag{6.59}$$

in which S_{ij}

$$S_{ij} = \frac{1}{2}\left(\frac{\partial u_i}{\partial x_j} + \frac{\partial u_j}{\partial x_i}\right) \tag{6.60}$$

It is easy to see that s can also be written in the following form

$$s = \left[\left(\frac{\partial u_i}{\partial x_j} + \frac{\partial u_j}{\partial x_i}\right)\frac{\partial u_i}{\partial x_j}\right]^{1/2} \tag{6.61}$$

The above model (Eqs. 6.53-6.59) is known as the Smagorinsky (1963) model for LES. As seen, only one "closure" coefficient is required, namely

C_s, the Smagorinsky constant. The value of the Smagorinsky constant is determined from experiments.

To sum up, the solution of the above set of equations, namely Eqs. 6.53-6.55, and Eqs. 6.57-6.60, basically gives the time series of the hydrodynamic quantities (the velocity components and the pressure) in space, similar to the time series obtained in a laboratory experiment using, for example, the Laser Doppler Anemometer (LDA), or the Particle Image Velocimetry (PIV) techniques. Once we obtain this raw data, then we process the data in terms of statistical quantities such as the mean, the variance, other statistical moments, and even correlations and spectra, in exactly the same fashion as we process data from experiments. (It should be added that, clearly, the time series obtained through the LES "experiments" are resolved with a resolution equal to the grid size selected in the simulation, just as the experimentally obtained time series are resolved with a resolution equal to the size of the measurement volume of the measuring instrument, e.g. to the size of the measurement volume of the LDA probe.)

A detailed account of turbulence models for LES has been given in a review paper by Meneveau and Katz (2000).

6.5.2 An application example

In this subsection, we will present the results of a study where the LES model was used to simulate the wave boundary layer in a U-shaped oscillating tunnel (Fig. 6.17); The study is essentially a part of a Ph.D. work conducted at the Technical University of Denmark, Lohmann et al. (2006). The CFD code employed in the study, called NS3, a 3-D numerical flow solver, was made available by DHI Water and Environment.

The Smagorinski subgrid-scale model was used in the calculations. Regarding the value chosen for the Smagorinski constant,C_s, experience shows that C_s equals 0.2 in isotropic turbulence and 0.1 in channel flow. In Lohmann et al.'s (2006) study, the latter value was found to be most appropriate, based on comparison with experimental data. The van Driest damping function $f = 1 - \exp(-\frac{y^+}{A_d})$ (see Eq. 6.23) is generally used as a standard part of the Smagorinski subgrid-scale formation; it was also used in the study of Lohmann et al. (2006) (see p. 3 of the latter publication).

Note that the free-stream velocity varies according to

$$U_0 = U_{0m} \sin(\omega t)$$

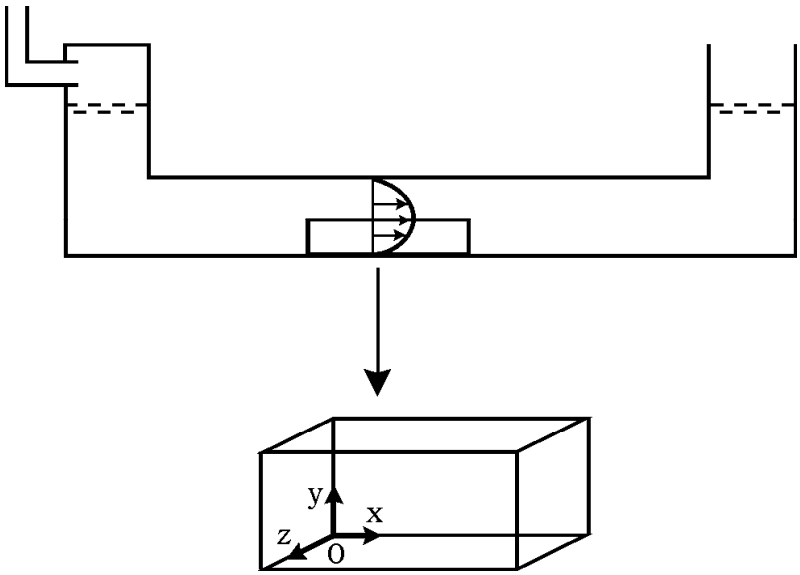

Figure 6.17: U-shaped oscillating tunnel.

in which ω is the angular frequency of the motion, $\omega = \frac{2\pi}{T}$, T being the period. (See Chapter 5 for a detailed discussion of wave boundary layers.)

Fig. 6.18 presents the raw time series of the three components of the resolved velocity at three different values of the distance y from the bed. As seen from Fig. 6.18, the time series is, qualitatively, no different from the ones obtained experimentally using LDA (c.f. Fig. 5.7 in Chapter 5).

Ensemble averaging is used to calculate the mean value of the resolved velocity, e.g.,

$$\overline{u}(y,\omega t) = \frac{1}{N}\sum_{j=1}^{N} u[y,\ \omega(t+(j-1)T)] \tag{6.62}$$

and the root-mean-square (r.m.s.) value of the subgrid-scale component of the velocity, e.g., $u' = u - \overline{u}$,

$$\sqrt{\overline{u'^2}}(y,\omega t) = \left\{ \frac{1}{N-1}\sum_{j=1}^{N} [u[y,\ \omega(t+(j-1)T)] - \overline{u}(y,\omega t)]^2 \right\}^{\frac{1}{2}} \tag{6.63}$$

Lohmann et al. (2006) found that, for the chosen phase values, averaging

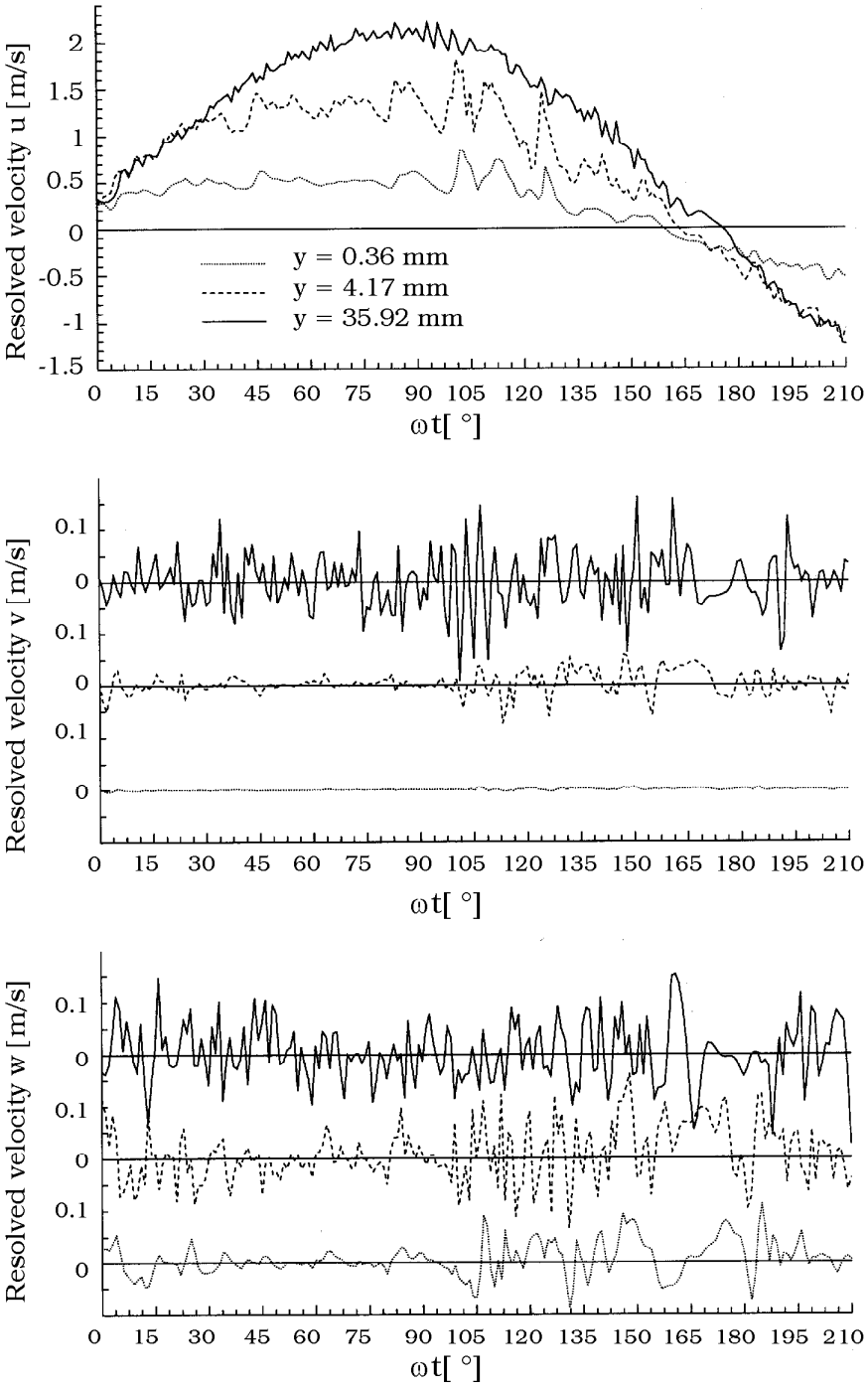

Figure 6.18: Time series of velocity components.

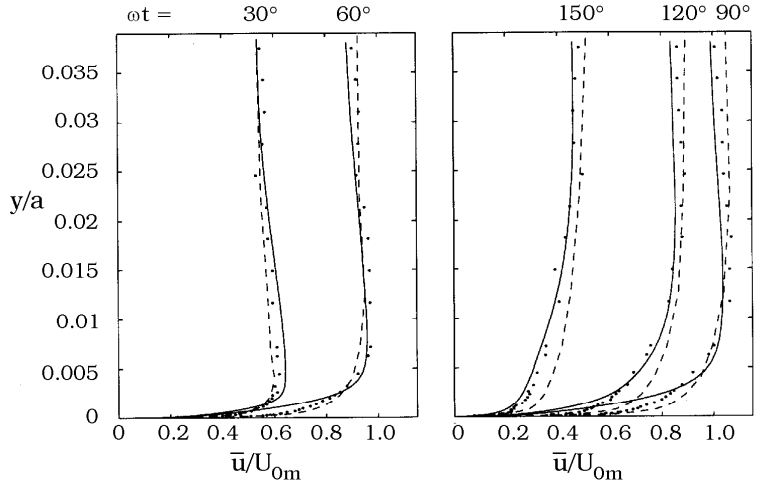

Figure 6.19: Sequence of velocity profiles over half period of the motion.

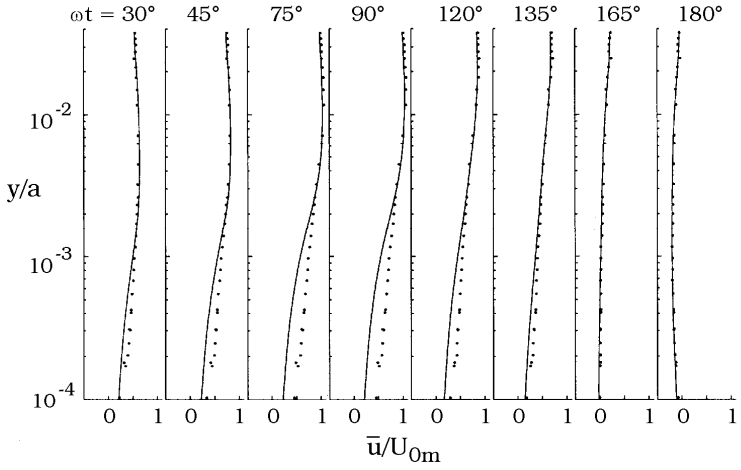

Figure 6.20: Sequence of velocity profiles over half period of the motion. Semi-log plot.

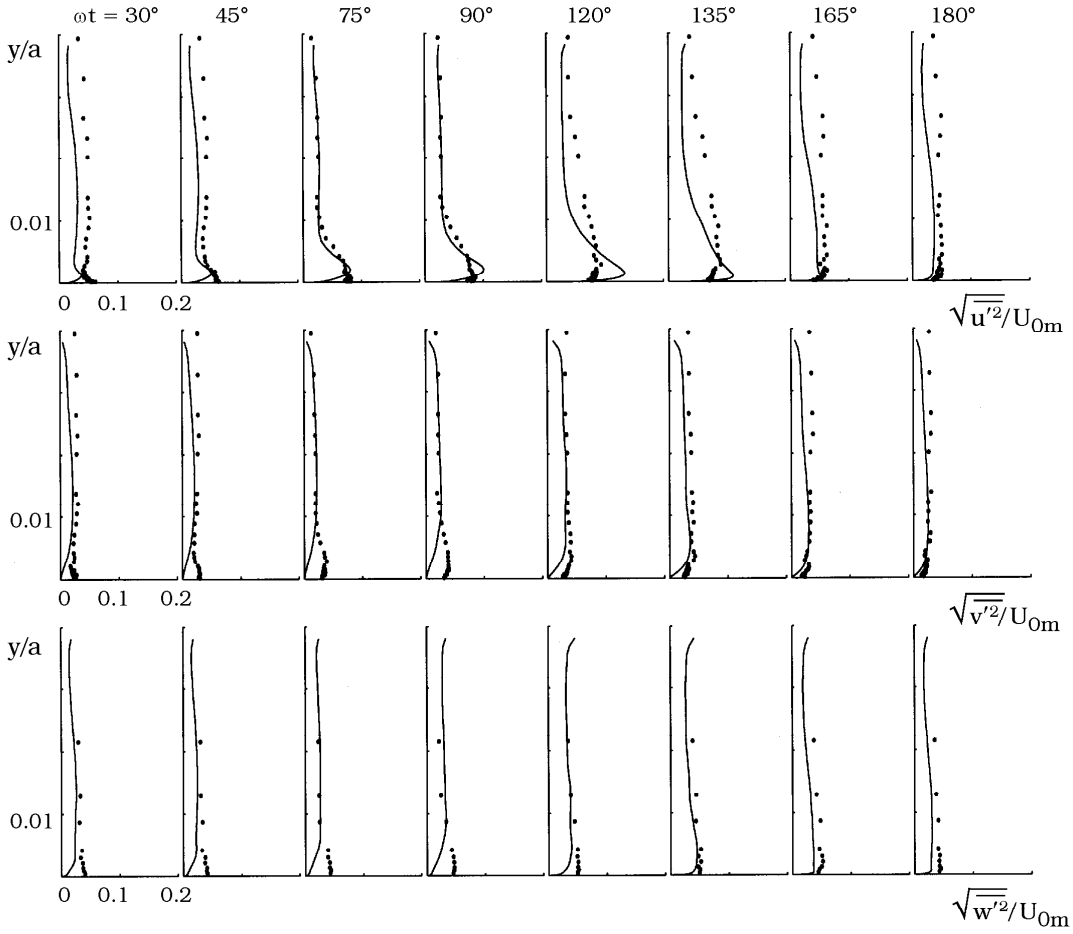

Figure 6.21: Sequence of turbulence profiles.

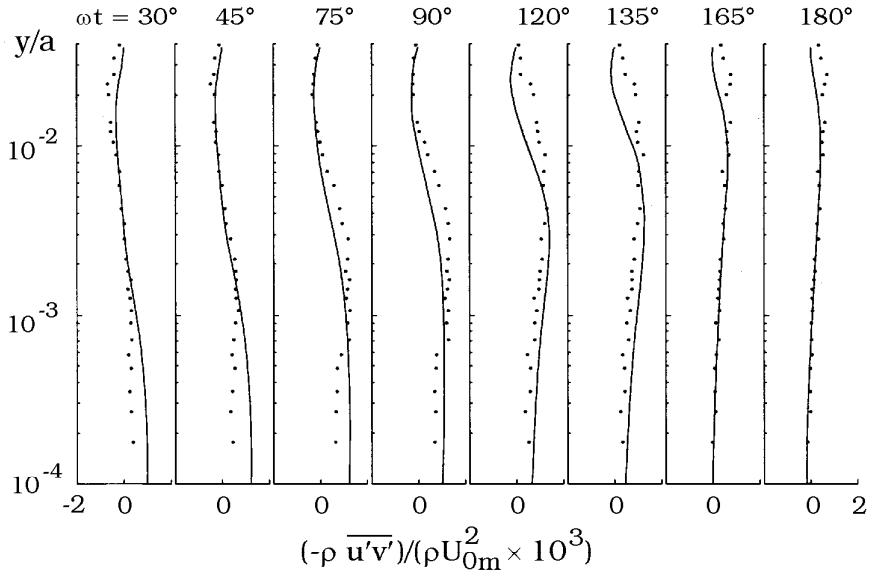

Figure 6.22: Shear stress profiles.

first over the $x-z$ plane at a given $y-$location, and then over 3 periods was sufficient to achieve reliable ensemble averages.

Fig. 6.19 gives a sequence of velocity profiles at different phase values ωt over one half period of the motion. The distance from the wall is normalized by the amplitude of the free-stream motion, $a(=\frac{U_{0m}T}{2\pi})$. The figure also gives two sets of other data: one from the numerical study of Justesen (1988) where a turbulence-energy equation model, namely the $k-\varepsilon$ model, was used; and the second from the experimental work of Jensen et al. (1989); the latter has been described in greater detail in Chapter 5. Fig. 6.19 shows that the LES model does a better job than the $k-\varepsilon$ model. In Fig. 6.20, the velocity information is plotted on a semi-logarithmic graph. The figure illustrates how the LES solution behaves for small values of the distance from the bed in relation to the experimental data. From the figure, although superior to the $k-\varepsilon$ model, the LES model underpredicts the velocities for small y values.

Figs. 6.21 and 6.22 present the turbulence data obtained by the LES model along with the experimental data. Although there are discrepancies between the model prediction and the experiment, the model predicts the

turbulence fairly well. Yet, one must note that the model near the bed fails to some extent to predict the turbulence accurately. This may be a major shortcoming when processes (to be studied by the model) have significant elements related to the turbulence near the bed, particularly related to the $y-$ and $z-$components of turbulence.

6.6 References

1. Absi, R. (2005): "Comment on 'Turbulent diffusion of momentum and suspended particles: A finite-mixing-length theory' (Physics of Fluids, 16, 2342 (2004))". Physics of Fluids, vol. 17, 079101-079102.

2. Cebeci, T. and Chang, K.C. (1978): "Calculation of incompressible rough-wall boundary-layer flows". AIAA Journal, vol. 16, No. 7, p.730.

3. Dixen, M. (2007): Ph.D. Study. Technical University of Denmark, MEK, Coastal, Maritime and Structural Engineering Section. Ph.D. study is in progress, and undertaken under the supervision of B. M. Sumer and J. Fredsøe.

4. Jensen, B. L., Sumer, B. M. and Fredsøe, J.: "Turbulent oscillatory boundary layers at high Reynolds numbers". Journal of Fluid Mechanics, Vol. 206, p. 265, 1989.

5. Justesen, P. (1988): Turbulent wave boundary layers. Series Papers 43, Institute of Hydrodynamics and Hydraulic Engineering, Lyngby, Denmark. A Ph.D. study supervised by J. Fredsøe and B.M. Sumer.

6. Lohmann, I.P., Fredsøe, J., Sumer, B.M. and Christensen, E.D. (2006): "Large eddy simulation of the ventilated wave boundary layer", J. Geophysical Research, vol. 111, C06036, doi:10.1029/2005JC002946, 1-21.

7. Meneveau, C. and Katz, J. (2000): Scale-Invariance and turbulence models for Large-Eddy Simulation. In: Annual Rev. Fluid Mech., vol. 32, 1-32.

8. Menter, F. R. 1993 Zonal two equation k-ω turbulence models for aerodynamic flows. Paper AIAA-93-2906, AIAA 24th Fluid Dynamic Conference, July 6-9, 1993, Orlando, Florida.

9. Michelsen, J. A. 1992 Basis3D - a platform for development of multiblock PDE solvers. Technical report, Dept. of Fluid Mechanics, Technical University of Denmark, AFM 92-05, ISSN 0590-8809.

10. Nezu, I. 1977 Turbulent Structure in Open Channel Flows. Ph.D. thesis, Kyoto University, Japan.

11. Nielsen, P. and Teakle, A.L. (2004). "Turbulent diffusion of momentum and suspended particles: A finite-mixing-length theory". Physics of Fluids, vol. 16, Number 7, p. 2342.

12. Rodi, W. (1992): "On the simulation of turbulent flows past bluff bodies". J. Wind Eng., No. 52, August, pp.1-16.

13. Rogallo, R.S. and Moin, P. (1984): "Numerical simulation of turbulent flows". Annual Review of Fluid Mechanics, vol. 16, pp. 99-137.

14. Roulund, A. 2000 Three-dimensional modelling of flow around a bottom-mounted pile and its application to scour. Ph.D. thesis, Department of Hydrodynamics and Water Resources, Technical University of Denmark, Supervisors B.M. Sumer, and J. Fredsøe.

15. Roulund, A., Sumer, B.M., Fredsøe, J. and Michelsen, J.: "Numerical and experimental investigation of flow and scour around a circular pile". J. Fluid Mechanics, vol. 534, 351-401, 2005.

16. Sørensen, N. N. 1995 General purpose flow solver applied to flow over hills. Ph.D. thesis, Risø National Laboratory, Roskilde, Denmark, Risø-R-827(EN).

17. Sumer, B. M., Chua, L. H. C., Cheng N.-S. & Fredsøe, J. 2003 The influence of turbulence on bedload sediment transport, J. Hydraulic Engineering ASCE, 129, No. 8, August Issue.

18. Sumer, B. M., Cokgor, S., & Fredsøe, J. 2001 Suction removal of sediment from between armour blocks. Journal of Hydraulic Engineering, ASCE, 127, No. 4, pp. 293-306, 2001.

19. van Driest, E.R. (1956): "On turbulent flow near a wall". J. Aeronautical Sciences, vol. 23, p.1007.

20. Wilcox, D.C. (1994): Turbulence Modelling for CFD. DCW Industries, Inc., La Canada, California, 460 p.

.